IFT - UNESP
INSTITUTO DE FÍSICA TEÓRICA

MASTER'S THESIS IFT–D.010/22

# Two-body problem in scalar gravity with self-interactions

Alan Müller

Supervisor

*Riccardo Sturani*

June 2022

Müller, Alan
M958t Two-body problem in scalar gravity with self-interactions / Alan Müller. – São Paulo, 2022
87 f.

Dissertação (mestrado) – Universidade Estadual Paulista (Unesp), Instituto de Física Teórica (IFT), São Paulo
Orientador: Riccardo Sturani

1. Teoria de campos escalares. 2. Ondas gravitacionais. 3. Relatividade geral (Física). I. Título

Sistema de geração automática de fichas catalográficas da Unesp. Biblioteca do Instituto de Física Teórica (IFT), São Paulo. Dados fornecidos pelo autor(a).

*To my parents.*

# Acknowledgements

Luck has mysterious ways of working things out. In my case, it had me born into a loving family, one which has always been supportive of me in every decision I have made. I will be forever in debt to my parents, Ricardo and Fabiana, who have during their lives gone through unspeakable efforts in order to provide for me and my sister Bruna, whose company and guidance throughout the years I am also thankful for. Besides my nuclear family, I would also like to express my gratitude towards my long gone grandparents, Aldina, Zé and Neusa, who have always helped and proven their devotion to us in every way imaginable. Their memory will always be kept alive in me.

Once luck did its work in giving me a wonderful family, it was my parents' dedication which ultimately enabled me to accomplish countless goals. Among these are my undergraduate education at IFUSP and my acceptance at IFT. In both these places, I have met many extraordinary people, one of them being my advisor Riccardo, without whose knowledge, attention and counseling this work would not have been possible. It was also at IFT that I was able to get a scholarship from CAPES, and I would like to acknowledge their support in my pursuit of a master's degree.

Speaking of extraordinary people, it is my wish to thank all teachers, professors, educators and researchers of the world, for the paramount role they play, and in particular those I had the good fortune of meeting. Special thanks should be given to Raul Abramo, from IFUSP, who first introduced me to general relativity in two of the courses I took, and who also recommended Riccardo as a supervisor. Without his suggestion, I would not be writing these words today.

It was also at IFUSP that I met my girlfriend Giulia. She means the world to me. She sheds light into my life, shares with me many moments and is always by my side. She is the one who gives me strength and keeps me going. Her parents, Carlos and Márcia, that to me are like a second family, have also been of supreme importance, especially during the COVID-19 pandemic.

Last, but not least, I want to thank all colleagues and friends of mine, some deserving special mention. Gabriel Lefundes, Gabriel Vidal and Matheus Cravo have helped me a lot during my time at IFT. Ian, whom I have met at IFUSP, has shared with me many moments of joy while we played RuneScape. Equally happy moments I have shared with many of my other friends, too many, fortunately, that I would inevitably be unfair if I tried to mention them. Du, Guto, Rafa and Felipe, however, are worthy of record. The moments we have spent together were as important to me as those in which I had to be productive.

I apologize to anyone I might have failed to mention. If you have been a part of my life in any way, then you have contributed to this moment. Thank you.

*"L'essentiel est invisible pour les yeux."*

Antoine de Saint-Exupéry, *Le Petit Prince*

# Resumo

É bem estabelecido que o Universo está expandindo de modo acelerado. E uma das possíveis causas é um grau de liberdade escalar leve. Campos escalares também são uma consequência inevitável de muitas tentativas de estender modelos padrões, como dimensões extras, supersimetria e teoria das cordas. É natural, portanto, perguntar-se o quão compatíveis eles são com a fenomenologia. Em particular, grande interesse teórico existe em saber se tais escalares levam a violações dos princípios fraco e forte da equivalência. Neste trabalho, no entanto, focamos em outro — embora relacionado — assunto. O fenômeno no qual estamos interessados é a fase inspiral de binárias compactas. Usando uma abordagem de teoria de campos efetiva, estudamos os efeitos nesses sistemas de várias autointerações que esse campo escalar pode apresentar, focando nas contribuições de ordem mais baixa das autointerações $\phi^3$, $\phi\left(\partial\phi\right)^2$ e $\phi^4$ ao potencial efetivo e à potência emitida pelo sistema. Encontramos divergências IR que indicam inconsistências nos modelos $\phi^3$ e $\phi^4$, e argumentamos sobre como essas inconsistências podem estar relacionadas à natureza não-perturbativa da autointeração $\phi^3$. A autointeração $\phi\left(\partial\phi\right)^2$ se comporta de maneira similar às autointerações cúbicas da relatividade geral. Como uma investigação adicional ao final de nosso trabalho, comparamos potência monopolar com potência dipolar em escalares, ambas na ordem mais baixa e na ausência de autointerações, e estimamos a excentricidade de uma órbita elíptica a partir da qual a potência monopolar passa a dominar. Também discutimos a contribuição ao potencial efetivo de autointerações sem derivadas em geral.

**Palavras Chaves**: Campos escalares; Autointerações; Divergências; Sistemas binários; Ondas gravitacionais.

**Áreas do conhecimento**: Física; Relatividade Geral; Teoria de Campos Efetiva.

# Abstract

It is well-established that the Universe is expanding at an accelerated rate. And one of the possible causes is a light scalar degree of freedom. Scalar fields are also an inevitable consequence in many attempts at extending standard models, such as extra dimensions, supersymmetry and string theory. It is only natural, then, to ask how compatible they are with phenomenology. In particular, great theoretical interest exists in knowing whether such scalars lead to violations of the weak and strong equivalence principles. In this work, however, we focus on another, albeit related, subject. The phenomenon we are interested in is the inspiral of compact binaries. Using an effective field theory approach, we study the effects on these systems of many self-interactions that this scalar field might present, focusing on the leading contributions from a $\phi^3$, a $\phi\,(\partial\phi)^2$ and a $\phi^4$ self-interaction to the effective potential and the emitted power. We encounter IR divergences which indicate inconsistencies in the $\phi^3$ and $\phi^4$ models, and argue as to how these inconsistencies are related to the non-perturbative nature of the $\phi^3$ self-interaction. The $\phi\,(\partial\phi)^2$ self-interaction is found to behave similarly to standard cubic self-interactions of general relativity. As an additional investigation at the end of our work, we compare leading monopolar power with leading dipolar power emitted in scalars, in the absence of self-interactions, and estimate the eccentricity of an elliptical orbit for which monopolar power begins to dominate. We also discuss the contributions to the effective potential of non-derivative self-interactions in general.

**Keywords**: Scalar fields; Self-interactions; Divergences; Binary systems; Gravitational waves.

**Fields of knowledge**: Physics; General relativity; Effective field theory.

# Contents

# Introduction

Contrary to what was expected from the attractive nature of gravity, the recently observed brightness of Type Ia Supernovae (SNIa) has shown that the Universe is expanding at an accelerated rate [1–4]. This has also been confirmed by other observations, such as the temperature anisotropies of the Cosmic Microwave Background (CMB) and the Baryon Acoustic Oscillations (BAO) [5–10]. In the standard framework of general relativity (GR), this phenomenon is accounted for as the effect of a new energy density component broadly referred to as *dark energy* (DE).

The simplest candidate for DE is a cosmological constant. And even though the observations are consistent with such a model, it is unsatisfactory from the theoretical point of view. Firstly, what *is* this constant energy density? And why is it constant? Furthermore, an attempt at explaining it as the more fundamental zero-point energy predicted by quantum field theory (QFT) has led to what has been described as ”the largest discrepancy between theory and experiment in all of science,” also known as the *cosmological constant problem* [11]. A constant vacuum energy density might not be the final answer after all.

Are there any other explanations, then, to account for the accelerated expansion of the Universe? Another valid yet bold approach is to simply claim that GR is wrong and that we have to modify it. However, the dynamics of a spin-2 field such as the gravitational field are tightly constrained on theoretical grounds, and our current understanding is that, in order to modify gravity, we need to introduce new degrees of freedom, the simplest of which being a scalar [12]. This leads to a broad class of alternative models called *scalar-tensor theories* [13, 14].

One big advantage of this approach is that the possible couplings of this extra scalar field to matter are much less constrained than those of a spin-2 field [12]. But more importantly, a scalar field is also a simple candidate for a dynamical DE that is backed by theory. The downside is that, in order for it to be able to mimic a constant energy density, this scalar needs to be light [13], resulting in a long-range, fifth force. In order to avoid this problem, as well as many others listed in [15], and make this light scalar phenomenologically viable, one needs to consider several screening mechanisms which are known in the literature. Among them are the following: the presence of matter drives the field to a region of weak coupling [15];

the *chameleon mechanism*, in which the scalar field becomes massive in the presence of matter, effectively escaping detection [16]; or the presence of matter induces the field to a region of zero coupling via symmetry restoration [17].

Of course, this extra degree of freedom (DOF) should also leave observable traces in other phenomena we know. And the emerging branch of gravitational-wave (GW) astronomy offers a new channel through which to observe these traces. In fact, recent GW detections have imposed serious constraints on several scalar-tensor theories, going as far as ruling some of them out [18–21]. These constraints are further discussed in [12].

Amongst the most important GW sources are compact binaries. During the inspiral phase, the components of a compact binary move at non-relativistic (NR) velocities, offering $v$ as an expansion parameter. Precisely because of this parameter, these systems are unique, in that they present a clear hierarchy of scales which justifies an effective field theory (EFT) approach to the problem, first introduced in [22]. And an effort has already been started in [12] at investigating the consequences of a light scalar in the dynamics of such systems. This work aims at extending this effort by considering different self-interactions that this scalar field might present.

We compute the leading contributions from a $\phi^3$, a $\phi\,(\partial\phi)^2$ and a $\phi^4$ self-interaction to both the effective potential and the emitted power of these systems, and encounter incurable IR divergences indicating inconsistencies in the conservative sector of the $\phi^3$ model and in the radiative sector of the $\phi^4$ model. We argue as to how these inconsistencies are related to each other, and could be ultimately traced back to the non-perturbative nature of the $\phi^3$ self-coupling. On the other hand, the $\phi\,(\partial\phi)^2$ self-interaction is found to behave in a way very similar to a simple cubic self-interaction predicted by GR, due to its two derivatives. As an additional endeavor, we use results from [12] to compare leading monopolar power with leading dipolar power emitted in scalars, in the absence of self-interactions. Looking at the particular case of an elliptical orbit, we show that the monopolar power starts to dominate only at high eccentricities. To conclude our work, we discuss in detail the contribution to the effective potential from a general non-derivative self-interaction $\phi^n$, focusing on its UV and IR behavior.

# Outline

The present work is divided into six chapters and an appendix. In Chapter 1, we briefly motivate the inspiral problem of compact binaries and its clear separation of scales. In Chapter 2, we explain the EFT approach used in our computations. In Chapter 3, we present the theory we will work with and explain how to apply the EFT formalism to it. In Chapters 4 and 5, we use this formalism to compute several contributions to both conservative and radiative sectors of the effective two-body Lagrangian. In Chapter 6, we discuss the results obtained. Finally, in the appendix, we present and prove several identities, integrals and action terms used in this work.

# Notation and conventions

- We borrow the notation of [23] and denote the *Lagrangian* (not the Lagrangian density) as $\mathcal{L}$ instead of $L$, i.e., $S = \int dt \mathcal{L}$;
- We work in $d+1$ spacetime dimensions, performing dimensional regularization on the spatial dimensions only;
- We denote the gravitational constant by $G_{\mathrm{N}}$;
- We work with units in which $\hbar = c = 1$, and denote units in powers of energy, e.g., $[G_{\mathrm{N}}] = -2$;
- The reduced Planck mass is given by $m_{\mathrm{Pl}} \equiv (32\pi G_{\mathrm{N}})^{-1/2}$;
- A dimensionally transmutated Planck mass valid in $d+1$ spacetime dimensions is defined as $\Lambda \equiv m_{\mathrm{Pl}} \mu^{\epsilon/2}$, where $\mu$ is an arbitrary energy scale and $\epsilon \equiv d-3$;
- We use the Einstein convention, in which repeated indices are summed over;
- Greek letters denote covariant indices ranging from 0 to $d$;
- Latin letters denote spatial indices ranging from 1 to $d$;
- Sometimes we denote $t \equiv x^0$;
- Sometimes we omit the time dependence of a time-dependent function (e.g., $\mathcal{I} \equiv \mathcal{I}(t)$);

- We denote the time average of a time-dependent quantity $\mathcal{I}$ by $\langle \mathcal{I} \rangle \equiv \frac{1}{T}\int_0^T dt \mathcal{I}$;
- A dot denotes a time derivative (e.g., $\dot{\mathcal{I}} \equiv d\mathcal{I}/dt$);
- We use boldface to denote spatial vectors (e.g., $\boldsymbol{x} \equiv \vec{x}$);
- Sometimes we refer to the order of magnitude, or *scaling*, of a vector quantity without explicitly showing that we are actually talking about its magnitude, i.e., $\boldsymbol{k} \sim 1/r$ instead of $|\boldsymbol{k}| \sim 1/r$;
- We put hats above unit vectors (e.g., $\hat{\boldsymbol{x}}$);
- Sometimes we refer to spacetime vectors without writing their Greek indices explicitly (e.g., $x \equiv x^\mu$), especially when they are inside the argument of some function (e.g., $\phi(x) \equiv \phi(x^\mu)$);
- Sometimes, when the argument of a function is understood, we omit it (e.g., $\phi \equiv \phi(x)$);
- The spacetime metric is denoted by $g_{\mu\nu}$;
- We work with a *mostly plus* metric signature, in which the Minkowski metric is then given by $\eta_{\mu\nu} \equiv \mathrm{diag}(-1, 1, 1, 1)$;
- The norm squared of a spacetime vector $k \equiv (\omega, \boldsymbol{k})$ in Minkowski spacetime is denoted as $k^2 \equiv \eta_{\mu\nu} k^\mu k^\nu = -\omega^2 + \boldsymbol{k}^2$;
- The trace of a quantity $h_{\mu\nu}$ in Minkowski spacetime is denoted as $h \equiv \eta^{\mu\nu} h_{\mu\nu}$, without the indices. But we also use $h$ in the argument of functionals to refer to $h_{\mu\nu}$;
- We denote proper time by $\tau$ (e.g., $d\tau^2 = -g_{\mu\nu} dx^\mu dx^\nu$);
- *Partial derivatives* are denoted by $\partial_\mu$ and *covariant derivatives* are denoted by $\nabla_\mu$. The covariant derivative $\nabla_\mu \phi$ of a scalar $\phi$ will sometimes be denoted by $\phi_\mu$;
- We use the shorthand notation $\int_{\boldsymbol{k}, \cdots, \boldsymbol{q}} \equiv \int \frac{d^d \boldsymbol{k}}{(2\pi)^d} \cdots \frac{d^d \boldsymbol{q}}{(2\pi)^d}$;
- We use a multi-index notation introduced by Blanchet and Damour [24], defined in the following way: $\boldsymbol{x}^L \equiv \boldsymbol{x}^{i_1} \cdots \boldsymbol{x}^{i_\ell}$ for a spatial vector $\boldsymbol{x}$; and $\mathcal{I}^L \equiv \mathcal{I}^{i_1 \cdots i_\ell}$ for a spatial tensor of $\ell$ indices;

- We denote the *symmetric trace-free* part of a spatial tensor of $\ell$ indices, say $\boldsymbol{x}^L$, as $\boldsymbol{x}^L_{\mathrm{STF}}$;
- The Fourier transform of a function $h_{\mu\nu}$ and its inverse are respectively given by

$$h_{\mu\nu}(\omega, \boldsymbol{k}) = \int dt d^d \boldsymbol{x} h_{\mu\nu}(t, \boldsymbol{x})\, e^{i\omega t - i\boldsymbol{k}\cdot\boldsymbol{x}},$$
$$h_{\mu\nu}(t, \boldsymbol{x}) = \int_{\boldsymbol{k}} \frac{d\omega}{2\pi} h_{\mu\nu}(\omega, \boldsymbol{k})\, e^{-i\omega t + i\boldsymbol{k}\cdot\boldsymbol{x}}.$$

  Since we will always show explicitly the frequency dependence of functions in Fourier space, there is no ambiguity in omitting the usual $\sim$ above these functions.

# Chapter 1

# The inspiral problem

In this chapter we briefly motivate the hierarchy of scales characteristic of the inspiral problem of compact binaries. We do this in four main steps. Firstly, in Section 1.1, we introduce the simple separation of scales involved in general GW sources. Secondly, in Section 1.2, we take our system to be gravitationally-bound, adding an extra separation of scales. In Section 1.3, we specialize to the case of compact binaries, revealing that one of the scales is actually that of the typical size of a constituent. Finally, in Section 1.4, we consider a compact binary during its inspiral phase, in which it can be treated as a Post-Newtonian source.

## 1.1 Gravitational-wave sources

Let us consider a system which sources GWs. If the typical internal velocities of this system are $\sim v$ and the typical size of the system is $\sim r$, then by dimensional analysis arguments one can see that the typical frequency of motion is

$$\omega \sim v/r. \tag{1.1}$$

This is also the frequency of the GWs emitted, since the latter is inherited from the former via the wave equation [25]. Since GWs travel at the speed of light, their wavelength can be written in terms of their frequency as

$$\lambda \sim \omega^{-1}. \tag{1.2}$$

Substituting relation (1.2) into (1.1), we find that

$$r \sim \lambda v. \tag{1.3}$$

Since $v < 1$, we see here that the simple assumption that a system sources GWs already suggests the separation of two scales: one characterized by the typical size

$r$ of the system as a whole; and another characterized by the wavelength $\lambda$ of the GWs emitted. Of course, if the internal velocities are relativistic, $v \sim 1$, and these two scales might not be so different from each other. But nevertheless we still have $r \lesssim \lambda$.

## 1.2 Gravitationally-bound systems

Suppose that the system under consideration, besides generating GWs, is also a *gravitationally-bound system*. This means that it is held together mainly by gravitational forces, so that, at leading order, the virial theorem reads

$$R_{\mathrm{S}} \sim r v^2, \tag{1.4}$$

where $R_{\mathrm{S}}$ is the Schwarzschild radius of the system [25]. Examples of self-gravitating systems are binary systems and neutron stars, while an example of a system which is *not* gravitationally-bound is a beam of charged particles [25]. Putting (1.3) and (1.4) together, we can write

$$R_{\mathrm{S}} \sim r v^2 \sim \lambda v^3. \tag{1.5}$$

Therefore, now we have three main scales in the problem: that of the Schwarzschild radius $R_{\mathrm{S}}$ of the system; that of the typical size $r$ of the system; and that of the wavelength $\lambda$ of the GWs emitted.

## 1.3 Compact binaries

A *binary system* is a gravitationally-bound system of two bodies. And an object is said to be *compact* if its typical size is of order of its Schwarzschild radius, e.g., a black hole (BH) or a neutron star (NS). But this can lead to some confusion, since, from these two definitions alone, one might think that a compact binary is a binary system which is also compact. Instead, a *compact binary* is a binary system whose *constituents* are compact.

With this definition in hands, let us suppose that the system we are considering is not only a gravitationally-bound source of GWs, but, more specifically, a compact binary. Let us remember that the Schwarzschild radius of an object of mass $m$ is given by $2G_{\mathrm{N}}m$. Since the mass of a binary is equal to the sum of the masses of its constituents, then the Schwarzschild radius of the composite system will be the sum of the Schwarzschild radii of the two bodies. But the objects, being compact, have Schwarzschild radii of order of their typical sizes, which we will call $r_{\mathrm{s}}$. Thus, since a compact binary only has two objects, its Schwarzschild radius will also be of order of the typical size of a component,

$$R_{\mathrm{S}} \sim r_{\mathrm{s}}. \tag{1.6}$$

Using (1.6) into (1.5), we find

$$r_{\mathrm{s}} \sim r v^2 \sim \lambda v^3. \tag{1.7}$$

Hence, a compact binary still has three characteristic scales. But now the scale of the Schwarzschild radius of the system can be identified with the small scale of the typical size of the objects.

In the discussion that follows, it might be useful to know how a compact binary evolves. A short description is given in [26] and reproduced here for completeness of our discussion. There are *three* main phases. First, there is the *inspiral*, in which the constituents move at NR velocities, slowly approaching each other. During the *merger*, on the other hand, the components reach relativistic velocities as their orbital separation falls below the innermost stable orbit of a BH, and the objects meet, combining into a compact body. Finally, in the case of BH binaries, there is the *ringdown*, in which the geometry becomes that of a Kerr spacetime.

## 1.4 Post-Newtonian sources

A *Post-Newtonian* (PN) system is a gravitationally-bound system with NR velocities. In this case, an expansion in the small parameter $v$ is connected to the weak-field limit via the virial theorem (1.4) [25]. Leading-order (LO) predictions in this scheme, i.e., *Newtonian* predictions, constitute 0PN, while $v^{2n}$ terms with respect to LO are referred to as $n$PN. One must, of course, take into account the scaling of all quantities involved in order to compute this. For instance, using the virial theorem, as well the Newtonian potential, one can see that corrections to the potential involving combinations of the type $G_{\mathrm{N}}^{n-j+1} v^{2j}$ should be regarded as $n$PN [27].

As we have briefly mentioned in Section 1.3, the components of a compact binary move slowly in the inspiral phase, and since a compact binary is a special type of self-gravitating system, it can be essentially treated as a PN source during this phase. Thus, substituting $v \ll 1$ in (1.7), we find that our system satisfies the following relation,

$$r_{\mathrm{s}} \ll r \ll \lambda. \tag{1.8}$$

This is the long-awaited *separation* or *hierarchy* of scales characterizing the *inspiral problem*. The importance of this clear separation of scales is that it invites an EFT approach to the problem, in which $v$ is the parameter separating the scales. Because $v$ is small, it also serves as an expansion parameter for computing several observables. One of particular interest is the time-varying phase of the emitted waves, given in terms of the mechanical energy and the emitted flux [22].[1]

Now that we have motivated an EFT approach, it might be a good idea to spend some time reviewing the subject of EFTs.

[1]We use the term *energy flux*, or simply *flux*, as a synonym for the emitted power.

# Chapter 2

# Effective Field Theory

In this chapter, we review the subject of EFTs by illustrating it with massless $\phi^3$ theory, taking great inspiration from the steps of [26]. First, in Section 2.1, we talk briefly about the characteristics of our initial theory, and take the first step of performing a decomposition into soft and hard modes. In Section 2.2, we show how to integrate out the hard modes and find an effective action for the soft component, by means of a diagrammatic expansion which starts from the generating functional of the theory. Later on, in Chapter 3, we will see how hard and soft modes can be interpreted, in the inspiral problem, as describing the physics of a near and a far region, respectively.

## 2.1 Hard and soft modes

Massless $\phi^3$ theory is given by

$$S[\phi] = \int d^4x \left( -\frac{1}{2}\eta^{\mu\nu}\partial_\mu\phi\partial_\nu\phi - \frac{\lambda_3}{3!}\phi^3 \right). \tag{2.1}$$

Let us suppose that the problem we want to consider presents two different length scales, which we will smartly call $r$ and $\lambda$, such that $r \ll \lambda$. Suppose, furthermore, that we are not interested in the high-energy physics happening at scale $r$. In the language of field theory, we say that we want to *integrate out* the DOFs with momenta $\sim 1/r$. Let us see how we do that.

First, we write $\phi$ in Fourier space,

$$\phi(x) = \int \frac{d^4k}{(2\pi)^4}\phi(k)\, e^{ik\cdot x}.$$

Then we define the *soft* modes $\bar{\varphi}(k)$ and the *hard* modes $\Phi(k)$, according to

$$\bar{\varphi}(k) \equiv \begin{cases} \phi(k), & |k| \sim 1/\lambda, \\ 0, & |k| \sim 1/r, \end{cases}$$
$$\Phi(k) \equiv \begin{cases} 0, & |k| \sim 1/\lambda, \\ \phi(k), & |k| \sim 1/r. \end{cases} \tag{2.2}$$

These modes allow us to decompose $\phi(k) = \Phi(k) + \bar{\varphi}(k)$ and consequently

$$\phi = \Phi + \bar{\varphi}, \tag{2.3}$$

where we have

$$\Phi(x) = \int \frac{d^4k}{(2\pi)^4} \Phi(k) e^{ik\cdot x},$$
$$\bar{\varphi}(x) = \int \frac{d^4k}{(2\pi)^4} \bar{\varphi}(k) e^{ik\cdot x}. \tag{2.4}$$

Here, $\Phi$ represents high-energy DOFs which we want to integrate out, while $\bar{\varphi}$ represents low-energy DOFs that will be left in the theory once we do that.

Substituting (2.3) into (2.1), we find

$$S[\Phi, \bar{\varphi}] = S_0[\Phi] + S[\bar{\varphi}] + S_{\text{int}}[\Phi, \bar{\varphi}], \tag{2.5}$$

where $S_0[\Phi]$ is the kinetic action for $\Phi$,

$$S_0[\Phi] = \int d^4x \left( -\frac{1}{2}\eta^{\mu\nu}\partial_\mu \Phi \partial_\nu \Phi \right),$$

while $S[\bar{\varphi}]$ looks exactly like (2.1), but with $\phi$ replaced by $\bar{\varphi}$, and $S_{\text{int}}[\Phi, \bar{\varphi}]$ is given by

$$S_{\text{int}}[\Phi, \bar{\varphi}] = \int d^4x \left( -\frac{\lambda_3}{3!}\Phi^3 - \frac{\lambda_3}{2}\Phi^2\bar{\varphi} - \frac{\lambda_3}{2}\Phi\bar{\varphi}^2 \right). \tag{2.6}$$

Notice how the kinetic action for $\phi$ naturally decomposes into those for $\Phi$ and $\bar{\varphi}$. This can be traced back to definitions (2.2), in which, whenever $\Phi(k)$ is zero, $\bar{\varphi}(k)$ is not, and vice versa.

## 2.2 Integrating out hard modes

With (2.5) in hands—an action for both $\Phi$ and $\bar{\varphi}$—all there is left to do is get rid of $\Phi$. We do this by *integrating out* $\Phi$, which formally means solving for $\Phi$ and then substituting back into (2.5), yielding an *effective field theory* for $\bar{\varphi}$. One way of doing this is via a *generating functional*,

$$Z[J] = \int \mathcal{D}\phi e^{iS[\phi]+i\int d^4x J\phi}. \tag{2.7}$$

Using decomposition (2.3) into (2.7), we are able to write

$$Z[J] = \int \mathcal{D}\bar{\varphi}\mathcal{D}\Phi e^{iS[\Phi,\bar{\varphi}]+i\int d^4x J\Phi + i\int d^4x J\bar{\varphi}}. \tag{2.8}$$

Now we require that this generating functional is also that of an effective action for $\bar{\varphi}$ and $J$,

$$Z[J] \equiv \int \mathcal{D}\bar{\varphi} e^{iS_{\text{eff}}[J,\bar{\varphi}]+i\int d^4x J\bar{\varphi}}. \tag{2.9}$$

Comparing (2.8) with (2.9), we can see that

$$e^{iS_{\text{eff}}[J,\bar{\varphi}]} = \int \mathcal{D}\Phi e^{iS[\Phi,\bar{\varphi}]+i\int d^4x J\Phi}. \tag{2.10}$$

Taking the logarithm of both sides of (2.10), one finds

$$iS_{\text{eff}}[J,\bar{\varphi}] = \log \int \mathcal{D}\Phi e^{iS[\Phi,\bar{\varphi}]+i\int d^4x J\Phi}. \tag{2.11}$$

This is the *effective action* for $\bar{\varphi}$ and $J$. Due to nonlinearities in $S[\Phi,\bar{\varphi}]$, the logarithm in (2.11) might not be so easy to compute in general.

One thing we can do is a perturbative expansion. Substitution of (2.5) into (2.11) yields

$$iS_{\text{eff}}[J,\bar{\varphi}] = iS[\bar{\varphi}] + \log \int \mathcal{D}\Phi e^{iS_{\text{int}}[\Phi,\bar{\varphi}]+i\int d^4x J\Phi} e^{iS_0[\Phi]}. \tag{2.12}$$

Expanding the first of the exponentials in (2.12), one is able to find

$$iS_{\text{eff}}[J,\bar{\varphi}] = iS[\bar{\varphi}] + \log\left(1 + \sum_{n=1}^{\infty}\frac{i^n}{n!}\int \mathcal{D}\Phi \left(S_{\text{int}}[\Phi,\bar{\varphi}] + \int d^4x J\Phi\right)^n e^{iS_0[\Phi]}\right), \tag{2.13}$$

where we have set $\int \mathcal{D}\Phi e^{iS_0[\Phi]} = 1$, as is also done in [28], in order to simplify our lives as much as possible.[1]

Note that a diagrammatic expansion is already at play in (2.13) with the appearance of

$$\sum_{n=1}^{\infty} \frac{i^n}{n!} \int \mathcal{D}\Phi \left( S_{\text{int}} \left[ \Phi, \bar{\varphi} \right] + \int d^4 x J \Phi \right)^n e^{iS_0[\Phi]}. \tag{2.14}$$

In order to see that, consider the following term present in (2.14),

$$-\frac{1}{2} \int d^4 x d^4 y J \left( x \right) \int \mathcal{D}\Phi \Phi \left( x \right) \Phi \left( y \right) e^{iS_0[\Phi]} J \left( y \right). \tag{2.15}$$

Notice the appearance of the propagator from QFT,

$$\int \mathcal{D}\Phi \Phi \left( x \right) \Phi \left( y \right) e^{iS_0[\Phi]} = \langle T \Phi \left( x \right) \Phi \left( y \right) \rangle , \tag{2.16}$$

which can be shown to write

$$\langle T \Phi \left( x \right) \Phi \left( y \right) \rangle = \int \frac{d^4 k}{\left( 2\pi \right)^4} \frac{-i}{k^2 - ia} e^{ik \cdot (x-y)},$$

where we emphasize that the Feynman prescription is forced upon us by the path integral formulation.[2]

Thus, (2.15) can also be properly understood as a Feynman diagram,

$$-\frac{1}{2} \int d^4 x d^4 y J \left( x \right) \langle T \Phi \left( x \right) \Phi \left( y \right) \rangle J \left( y \right) = \otimes \cdots\cdots \otimes ,$$

where crossed circles represent sources and dotted lines represent hard modes. Another term in (2.14) is as follows,

$$-\frac{\lambda_3^2}{8} \int d^4 x d^4 y \bar{\varphi} \left( x \right) \int \mathcal{D}\Phi \Phi^2 \left( x \right) \Phi^2 \left( y \right) e^{iS_0[\Phi]} \bar{\varphi} \left( y \right). \tag{2.17}$$

Note that $\bar{\varphi}\left( x \right)$ and $\bar{\varphi}\left( y \right)$ remain both unaffected by the integral over $\Phi$, as they

[1] We are cheating here a little. What we actually mean is that $\int \mathcal{D}\Phi e^{iS_0[\Phi]}$ is a normalization constant independent of $\Phi$, so for all practical purposes it can be treated as if equal to unity.

[2] Note that the correlation function as denoted in the way shown in (2.16)—i.e., with a time-ordering operator inside the angle brackets—is a mere notation inherited from QFT which does not mean much here. After all, we are treating the fields classically, i.e., they are not operators, so time-ordering is meaningless.

should. Now we need the help of good old *Wick's theorem* in order to proceed,

$$\int \mathcal{D}\Phi\Phi^2(x)\,\Phi^2(y)\,e^{iS_0[\Phi]} = 2\,\langle T\Phi(x)\,\Phi(y)\rangle^2 + \langle T\Phi(x)\,\Phi(x)\rangle\,\langle T\Phi(y)\,\Phi(y)\rangle\,. \tag{2.18}$$

Using (2.18) into (2.17), one sees the appearance of what can be interpreted as two Feynman diagrams,

$$-\frac{\lambda_3^2}{4}\int d^4x d^4y \bar{\varphi}(x)\,\langle T\Phi(x)\,\Phi(y)\rangle^2\,\bar{\varphi}(y) - \frac{\lambda_3^2}{8}\left(\int d^4x \bar{\varphi}(x)\,\langle T\Phi(x)\,\Phi(x)\rangle\right)^2$$

= 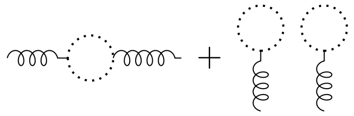 ,

(2.19)

where coil lines represent soft momenta modes. Notice how these never appear contracted, i.e., are always external. This was expected, since they are not being integrated out. Following similar steps for other terms, (2.14) becomes something like

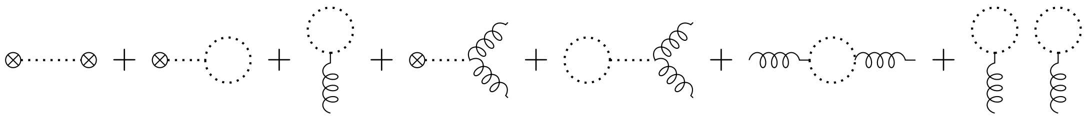

$+ \cdots,$

(2.20)

including connected *and* disconnected diagrams. However, (2.20) is not yet the final answer, because we still need to take the annoying logarithm in (2.13). In order to do so, we consider the following series representation,

$$\log(1+x) = \sum_{k=1}^{\infty} \frac{(-1)^{k+1}\,x^k}{k},$$

valid as long as $|x| < 1$. When applied to the logarithm in (2.13), all terms with $k \geq 2$ will involve disconnected diagrams, because they come from products of (2.14) with itself.[3] But the $k = 1$ term, which is nothing more than (2.14), also contains disconnected diagrams, as can be seen in (2.20). As it turns out, these exactly cancel out the $k \geq 2$ contributions, leaving us with connected diagrams

[3] All terms in (2.14) are diagrams and the product of two or more diagrams is by definition a disconnected diagram.

only.[4] For instance, the $k = 2$ term

$$\frac{\lambda_3^2}{8}\left(\int d^4x\bar{\varphi}\left(x\right)\left\langle T\Phi\left(x\right)\Phi\left(x\right)\right\rangle\right)^2$$

exactly cancels out the second term of (2.19). All in all, one finds

$$\log\left(1+\sum_{n=1}^{\infty}\frac{i^n}{n!}\int\mathcal{D}\Phi\left(S_{\text{int}}\left[\Phi,\bar{\varphi}\right]+\int d^4xJ\Phi\right)^n e^{iS_0[\Phi]}\right)$$

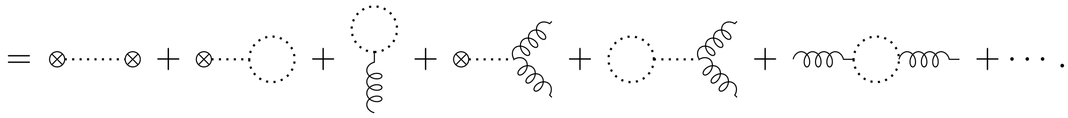

(2.21)

Substituting (2.21) back into (2.13), we finally find that

$$iS_{\text{eff}}\left[J,\bar{\varphi}\right] = iS\left[\bar{\varphi}\right]$$

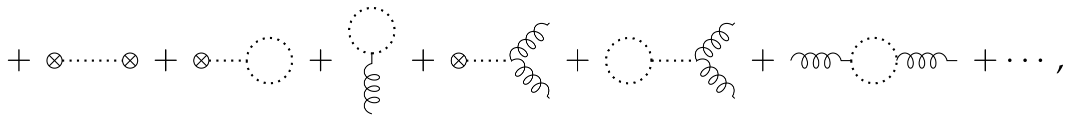

(2.22)

where we sum over only connected contributions.

One sees that the effective action for $\bar{\varphi}$ has two parts: there is the original action, but with $\phi$ replaced by $\bar{\varphi}$, i.e., the first term on the rhs of (2.22); plus several terms which act as corrections to $S\left[\bar{\varphi}\right]$ and which can be organized in a diagrammatic expansion. This expansion consists only of connected contributions where hard momenta modes appear fully contracted. The Feynman rules determining the form of these graphs can be obtained from (2.6). This is the part which gives meaning to the word "effective." These diagrams come in two types: there are those without any external $\bar{\varphi}$, e.g., the first two in (2.22); and those with external $\bar{\varphi}$. Simple as that. On the one hand, diagrams with no external $\bar{\varphi}$ contribute to an effective Lagrangian for the sources alone. On the other hand, diagrams with external $\bar{\varphi}$ correspond to operators whose coefficients contain information about the high-energy physics we ignored. Amongst both these types of diagrams, only sources for $\Phi$ appear, by the mere way we have defined the effective action (cf. (2.9)). Since the only two ways in which hard momenta modes can appear are by either sources or vacuum bubbles, tree diagrams (diagrams with no loops)

[4] This statement is not trivial and will *not* be proven in this work.

necessarily contain sources (e.g., the first and fourth of (2.22)). This information will be useful in the next chapter.

In Chapter 3, we will see how to apply the EFT formalism to the inspiral problem. There, the process of integrating out hard modes—as described in this chapter—will be identified with a *near* region dictating the orbital dynamics. We will be able to separate the terms resulting from this process in a way similar to what has been done here, in which graphs without any external soft modes contribute to an effective dynamics for the sources alone. Once the hard modes have been integrated out, the system is treated as a single composite object, as is most appropriate in the *far* region. Then, we will also be interested in integrating out the soft modes. This is done in a way similar to what was explained for hard modes. But the diagrams then will come only in one type: those without any external modes, since all modes have been integrated out. Although this is not trivial to prove, we claim that the terms we find at the end of our calculations—considering both near and far regions—can then be properly understood as an effective action describing the complete dynamics for the sources and its emission observables.

This concludes the present chapter. Now, with the EFT apparatus in our hands, it is time to understand how to apply it to the inspiral problem.

# Chapter 3

# Setup

In this chapter, we understand how to apply the EFT approach explained in Chapter 2 to the inspiral problem of compact binaries. In Section 3.1, we start from the hierarchy of scales explained in Chapter 1 and argue in favor of an initial theory, talking a little about its characteristics. In Section 3.2, we implement the weak-field limit, in which we assume that both standard gravity and the scalar field are only slightly perturbed by the presence of sources, enabling us to identify some DOFs. In Section 3.3, we decompose these DOFs into orbital and radiative parts, depending on the scaling of their momenta. In Section 3.4, we discuss how to integrate out the orbital modes, yielding a theory of interacting point-particles and radiative fields. Finally, in Section 3.5, we integrate out the radiative fields, yielding both a conservative and a dissipative dynamics for the point-particles.

## 3.1 The starting point

We start by going back to the hierarchy of scales (1.8). A theory which completely describes the system has to somehow manage to account for all the DOFs involved in each one of the scales present in (1.8). However, such a complete theory would be too complicated. If our purpose is to study the dynamics between the two bodies and the emission observables of the compact binary, the intricate short-distance physics happening inside the objects may not be so relevant to us. For this reason, we might want to start from a simpler theory, an EFT in which these internal DOFs have already been integrated out, meaning we can treat the constituents as point-particles coupled to both gravity and the extra scalar field. Similarly to the example of Chapter 2, our theory now has a UV cutoff, $r_s^{-1}$. In this scenario, UV divergences signaling the incompleteness of the theory at small scales are bound to appear. It should be possible to treat these divergences in the usual way, namely by adding operators to the Lagrangian whose coefficients are chosen such that they end up cancelling out the UV poles [23]. We will not, however, look into this in the present work.

With these first considerations in mind, the way in which we model our compact binary is as follows,

$$S = S_R + S_\phi + S_{\rm pp}. \tag{3.1}$$

Here, $S_R$ denotes the Einstein-Hilbert action, dictating the gravitational dynamics of standard GR, and may also include a gauge-fixing constraint for the gravitational field. We also have the scalar piece, $S_\phi$, describing the dynamics of the scalar field, universally coupled to gravity and with an interesting potential which is motivated in Appendix C,

$$S_\phi = \int dt d^d \boldsymbol{x} \sqrt{-g} \left( -\frac{1}{2} g^{\mu\nu} \phi_\mu \phi_\nu - \sum_{p=3}^{\infty} \sum_{\substack{q \le p \\ \text{even}}} \frac{\lambda_{p,q}}{p!} m_{\rm Pl}^{2-q} \Lambda^{2-p} \phi^{p-q} \left( g^{\mu\nu} \phi_\mu \phi_\nu \right)^{q/2} \right), \tag{3.2}$$

where $\lambda_{p,q}$ are dimensionless self-couplings.[1] These first two parts, $S_{\rm EH}$ and $S_\phi$, which involve integrating over an arbitrary spacetime point $\boldsymbol{x}$, can also be collectively referred to as the *bulk* action. Finally, the point-particle action, $S_{\rm pp}$, is the part of the action concerning the effective description of the two bodies as point-particles coupled to standard gravity and the scalar field, and consists of a sum over the *worldline* actions of the two particles. Taking inspiration from [12], we write it as

$$S_{\rm pp} = -\sum_a m_a \int d\tau_a \left( 1 - \alpha_a \frac{\phi(x_a)}{2\Lambda} + \cdots \right), \tag{3.3}$$

where $a \in \{1, 2\}$ indexes the particles, $m_a$ are their masses, $\tau_a$ their proper times, $\alpha_a$ are dimensionless $\phi$-charges and $x_a$ denotes the worldlines of the particles. In the ellipsis, we include any higher-order couplings and operators necessary for the effective point-particle description. These operators, of course, are required to satisfy all the appropriate symmetries, such as diffeomorphism invariance [23]. Notice how $S_R$ and $S_\phi$ are exact, i.e., they have nothing to do with the effective description. The effective description pertains only to the point-particle action. Another important aspect to take note of is that the only new thing about (3.1) in comparison to [12] is the presence of scalar self-interactions (cf. (3.2)).

We have emphasized how this starting point is to be understood as an EFT of point-particles, in which the DOFs of the small scale $r_s$ are assumed to have been integrated out. And how, for this reason, the focus of this initial theory lies in

[1] The use of both the reduced Planck mass $m_{\rm Pl}$ and its dimensionally transmutated version $\Lambda$ in (3.2) is intended to simplify computations.

describing what happens up until energy scales $\sim r_s^{-1}$. But, similarly to Chapter 2, we want to lower the cutoff. How much? Once again, the hierarchy of scales (1.8) provides the answer. Above $r_s$, the next length scale in the hierarchy is $r$. Therefore, we want to lower the cutoff to $r^{-1}$. The reason is that, besides the orbital dynamics happening at lengths $\sim r$, we are also interested in the emission observables of the compact binary, taking place at the only length scale left after that, $\lambda$. Following the path paved in Chapter 2, we need to decompose the modes in our theory based on these two length scales available, and then integrate out the modes relevant at distances $\sim r$. But before we do that, let us make an important approximation that will help us identify the modes we want to decompose.

## 3.2 The weak-field limit

Our EFT of point-particles is composed of three main dynamical quantities for which we want to solve: there are the worldlines of the point-particles, $x_a$; there is the spacetime metric, $g_{\mu\nu}$; and there is the extra scalar field, $\phi$. Finding exact solutions turns out to be a really messy job, even in the absence of the scalar field. And a simplifying assumption is more than welcome. The one we will use here is called the *weak-field limit*.

First, consider what happens in the absence of the point-particles. In this case, it is possible to show that the metric reduces to that of flat Minkowski spacetime, while the scalar field vanishes,

$$g^{(0)}_{\mu\nu} = \eta_{\mu\nu}, \qquad \phi_0 = 0. \tag{3.4}$$

Once we add in the interacting point-particles, spacetime gets perturbed, and so does the scalar field. In the *weak-field limit*, we assume that the deviations from symmetry (3.4) are small, such that we can decompose the metric as that of flat Minkowski spacetime plus a small perturbation,

$$g_{\mu\nu} = \eta_{\mu\nu} + \frac{h_{\mu\nu}}{\Lambda}, \tag{3.5}$$

while the scalar field, having zero background value, is itself its own small perturbation.

Substitution of (3.5) into (3.1) yields several action terms. And the assumption that the fields are small allows us to treat these terms perturbatively. First, there are the kinetic actions for $h_{\mu\nu}$ and $\phi$,

$$\begin{aligned} S_0[h] &= \int \mathrm{d}t d^d x \left( \frac{1}{4} (\partial_\mu h)^2 - \frac{1}{2} (\partial_\sigma h_{\mu\nu})^2 \right), \\ S_0[\phi] &= \int dt d^d \boldsymbol{x} \left( -\frac{1}{2} \eta^{\mu\nu} \partial_\mu \phi \partial_\nu \phi \right), \end{aligned} \tag{3.6}$$

where the harmonic gauge is used. We can now understand why the Planck mass $\Lambda$ is there in (3.5): to ensure that the gravitational field $h_{\mu\nu}$ be canonically normalized. We do not need to worry about this in the case of the scalar field, since it is canonically normalized by definition (cf. (3.2)). There are also interaction terms coming from the bulk action. For instance, there is a $\phi^3$ self-interaction term,

$$S_{\phi^3} = -\frac{\lambda_3}{3!} \frac{m_{\mathrm{Pl}}^2}{\Lambda} \int dt d^d \boldsymbol{x} \phi^3,$$

as well as an $h(\partial\phi)^2$ interaction,

$$S_{h(\partial\phi)^2} = \frac{1}{2\Lambda} \int dt d^d \boldsymbol{x} \left( h^{\mu\nu} - \frac{1}{2} \eta^{\mu\nu} h \right) \partial_\mu \phi \partial_\nu \phi, \tag{3.7}$$

among infinitely many others. Then there are worldline couplings coming from the point-particle action (3.3), such as linear couplings,

$$S_{\mathrm{pp}}^h = \sum_a m_a \int \frac{dt_a}{\sqrt{1 - \boldsymbol{v}_a^2}} \frac{h_{\mu\nu}(x_a)}{2\Lambda} v_a^\mu v_a^\nu, \tag{3.8}$$

$$S_{\mathrm{pp}}^\phi = \sum_a \alpha_a m_a \int \mathrm{d}t_a \sqrt{1 - \boldsymbol{v}_a^2} \frac{\phi(x_a)}{2\Lambda}, \tag{3.9}$$

where $v_a^\mu \equiv dx_a^\mu / dt_a = (1, \boldsymbol{v}_a)$.

The weak-field limit used here is a legitimate one in the case of the gravitational field, i.e., spacetime gets only slightly perturbed by the presence of the point-particles. This is the nature of gravity. All terms coming from the Einstein-Hilbert action will necessarily have two derivatives, making the gravitational field fall with distance, especially since the sources are so small. But as we will see, a $\phi^3$ self-interaction drives the scalar field to a non-perturbative regime, in which it takes on increasingly larger values. So such an assumption is not valid in this case, and this will lead to inconsistencies.

## 3.3 Decomposition into orbital and radiative modes

Now that we have identified the field variables as $h_{\mu\nu}$ and $\phi$, we can proceed to do something similar to what was done in (2.2), i.e., we must perform a decomposition into hard and soft modes. We do this using the two length scales that are left in the problem, namely $r$ and $\lambda$. Since the frequency dependence of the Fourier modes is inherited from the source, $\omega \sim v/r$ is always satisfied, so we can only decompose the modes according to how the spatial momentum scales [25]. In a way similar to what was done in Chapter 2, we write

$$g_{\mu\nu} = \eta_{\mu\nu} + \frac{H_{\mu\nu}}{\Lambda} + \frac{\bar{h}_{\mu\nu}}{\Lambda}, \qquad \phi = \Phi + \bar{\varphi}, \tag{3.10}$$

where $H_{\mu\nu}$ and $\Phi$ are the hard components, while $\bar{h}_{\mu\nu}$ and $\bar{\varphi}$ are the soft components, defined according to how the spatial momentum scales,

$$\begin{array}{ccc} \partial_0 H_{\mu\nu} \sim \frac{v}{r} H_{\mu\nu}, & \partial_i H_{\mu\nu} \sim \frac{1}{r} H_{\mu\nu}, & \partial_\alpha \bar{h}_{\mu\nu} \sim \frac{v}{r} \bar{h}_{\mu\nu}, \\ \partial_0 \Phi \sim \frac{v}{r} \Phi, & \partial_i \Phi \sim \frac{1}{r} \Phi, & \partial_\alpha \bar{\varphi} \sim \frac{v}{r} \bar{\varphi}. \end{array} \tag{3.11}$$

This is nothing more than (2.2) applied to the inspiral problem. The only difference being that, since we will work in dimensional regularization, here we integrate over all momenta, i.e., from $-\infty$ to $\infty$. It is not immediately clear how this could lead to anything consistent. However, as we will see, for hard modes we make an approximation which compensates another approximation made for the soft component, leading to the final answer.

Since $\boldsymbol{k} \sim 1/r$ for $H_{\mu\nu}$ and $\Phi$, where $r$ is the typical orbital size, these are called *orbital* or *potential* modes. On the other hand, $\bar{h}_{\mu\nu}$ and $\bar{\varphi}$, with $\boldsymbol{k} \sim v/r$, which is the typical frequency of the emitted radiation, are called *radiative* modes. Notice how no information has been used about the transformation properties of the gravitational field nor the scalar field, i.e., the fact that $h_{\mu\nu}$ is a tensor and $\phi$ a scalar has been and will be irrelevant in this discussion. In fact, the reasoning being followed here can be applied to fields of any kind.

## 3.4 Integrating out orbital modes: the near zone

Once we perform the decomposition of modes into the action, what we obtain is a theory of orbital and radiative fields coupled to point-particles. Our job now

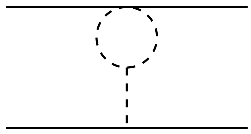

Figure 3.1

is to take this theory and get rid of the orbital modes, just as we did for the hard modes in Chapter 2. Again, we do this via a generating functional, which for (3.1) looks like

$$Z\left[x_a\right] = \int \mathcal{D}h\mathcal{D}\phi e^{iS_R[h]+iS_\phi[h,\phi]+iS_{\rm pp}[x_a,h,\phi]}. \tag{3.12}$$

In (3.12), the point-particle action contains terms which function as sources for the fields. After these fields have been decomposed into orbital and radiative parts, (3.12) becomes

$$Z\left[x_a\right] = \int \mathcal{D}\bar{h}\mathcal{D}\bar{\varphi}\mathcal{D}H\mathcal{D}\Phi e^{iS_R\left[H,\bar{h}\right]+iS_\phi\left[H,\bar{h},\Phi,\bar{\varphi}\right]+iS_{\rm pp}\left[x_a,H,\bar{h},\Phi,\bar{\varphi}\right]}. \tag{3.13}$$

Recasting (3.13) into the form

$$Z\left[x_a\right] \equiv \int \mathcal{D}\bar{h}\mathcal{D}\bar{\varphi} e^{iS_{\rm eff}\left[x_a,\bar{h},\bar{\varphi}\right]}, \tag{3.14}$$

and then comparing (3.13) with (3.14), we are able to see that

$$e^{iS_{\rm eff}\left[x_a,\bar{h},\bar{\varphi}\right]} = \int \mathcal{D}H\mathcal{D}\Phi e^{iS_R\left[H,\bar{h}\right]+iS_\phi\left[H,\bar{h},\Phi,\bar{\varphi}\right]+iS_{\rm pp}\left[x_a,H,\bar{h},\Phi,\bar{\varphi}\right]}. \tag{3.15}$$

Taking the logarithm of both sides of (3.15), what we find is

$$iS_{\rm eff}\left[x_a,\bar{h},\bar{\varphi}\right] = \log \int \mathcal{D}H\mathcal{D}\Phi e^{iS_R\left[H,\bar{h}\right]+iS_\phi\left[H,\bar{h},\Phi,\bar{\varphi}\right]+iS_{\rm pp}\left[x_a,H,\bar{h},\Phi,\bar{\varphi}\right]}.$$

Analogously to Chapter 2, the computation of $S_{\rm eff}\left[x_a,\bar{h},\bar{\varphi}\right]$ involves a diagrammatic expansion. And the diagrams involved in this expansion describe processes which are said to take place in the so-called *near zone*.

As we have learned in Chapter 2, some of the diagrams involved in the computation of the effective action contain *loops* (cf. the second, third, fifth and sixth diagrams of (2.22)). In the present context, this is no different, one example being the diagram of Fig. 3.1. We will soon see what each component of this graph represents. For now, it is enough for us to know that such loop diagrams are suppressed by powers of $1/L$ with respect to tree diagrams, where $L \sim mvr$ is the total angular momentum of the system [22]. However, for an astrophysical system such as a compact binary, $1/L$ is extremely small,[2]

$$1/L \sim 9 \times 10^{-77} \left(\frac{m_\odot}{m}\right)^2 v.$$

Therefore, we will choose to neglect loop effects and focus on tree-level diagrams.[3] Let us understand a little better what these diagrams look like.

### 3.4.1 Orbital propagators and radiative modes

Remaining faithful to the close analogy with Chapter 2, the definitions in (3.11) show that orbital modes always appear off-shell. Thus, one needs *orbital propagators* for the computation of near zone diagrams. These can be obtained by using (3.6) to get kinetic actions for the orbital fields, which in fact are found to look exactly like (3.6), but with $h_{\mu\nu}$ and $\phi$ respectively replaced by $H_{\mu\nu}$ and $\Phi$,

$$\begin{aligned} S_0[H] &= \int dt d^d\boldsymbol{x} \left(\frac{1}{4}\left(\partial_\mu H\right)^2 - \frac{1}{2}\left(\partial_\sigma H_{\mu\nu}\right)^2\right), \\ S_0[\Phi] &= \int dt d^d\boldsymbol{x} \left(-\frac{1}{2}\eta^{\mu\nu}\partial_\mu\Phi\partial_\nu\Phi\right). \end{aligned} \tag{3.16}$$

Following the usual QFT procedure, one can invert the differential operators in (3.16) to yield propagators for these fields,

$$\begin{aligned} \left\langle TH_{\mu\nu}\left(x^0,\boldsymbol{x}\right)H_{\alpha\beta}\left(y^0,\boldsymbol{y}\right)\right\rangle &= P_{\mu\nu;\alpha\beta}\int_{\boldsymbol{k}}\frac{d\omega}{2\pi}\frac{i}{\omega^2-\boldsymbol{k}^2+ia}e^{-i\omega\left(x^0-y^0\right)+i\boldsymbol{k}\cdot(\boldsymbol{x}-\boldsymbol{y})}, \\ \left\langle T\Phi\left(x^0,\boldsymbol{x}\right)\Phi\left(y^0,\boldsymbol{y}\right)\right\rangle &= \int_{\boldsymbol{k}}\frac{d\omega}{2\pi}\frac{i}{\omega^2-\boldsymbol{k}^2+ia}e^{-i\omega\left(x^0-y^0\right)+i\boldsymbol{k}\cdot(\boldsymbol{x}-\boldsymbol{y})}, \end{aligned} \tag{3.17}$$

where

$$P_{\mu\nu;\alpha\beta} \equiv \frac{1}{2}\left(\eta_{\mu\alpha}\eta_{\nu\beta} + \eta_{\mu\beta}\eta_{\nu\alpha} - \frac{2}{d-1}\eta_{\mu\nu}\eta_{\alpha\beta}\right). \tag{3.18}$$

By noting that the typical time scale of the problem is $\sim r/v$, and using the fact that for orbital modes $\boldsymbol{k} \sim 1/r$, (3.17) can be used to find out that orbital fields scale as

$$H_{\mu\nu} \sim \Phi \sim \frac{v^{1/2}}{r}.$$

[2] Remember that $\hbar = 1$.

[3] Even though we neglect loop effects in this work, the interested reader can refer to [29] for the leading quantum corrections to the two-body potential.

Notice that in (3.17) we have explicitly used the Feynman prescription, which is forced upon us by the path integral formulation. However, the prescription should not matter here, because orbital modes should never go on-shell. Nevertheless, in dimensional regularization we still integrate from $-\infty$ to $\infty$, so we need another way of accounting for this fact. We do this by using $\omega \ll \boldsymbol{k}$ to write a geometric series for the propagator,

$$\frac{1}{\omega^2 - \boldsymbol{k}^2 + ia} = \frac{1}{-\boldsymbol{k}^2} \sum_{n=0}^{\infty} \frac{\omega^{2n}}{\boldsymbol{k}^{2n}}. \tag{3.19}$$

Because $\omega/\boldsymbol{k} \sim v$, (3.19) is in fact an expansion in the small parameter $v^2$. Substituting (3.19) into (3.17), one finds

$$\begin{aligned} \left\langle TH_{\mu\nu}\left(x^0, \mathbf{x}\right) H_{\alpha\beta}\left(y^0, \mathbf{y}\right)\right\rangle &= \sum_{n=0}^{\infty} P_{\mu\nu;\alpha\beta} \int_{\boldsymbol{k}} \frac{d\omega}{2\pi} \frac{i}{-\boldsymbol{k}^2} \frac{\omega^{2n}}{\boldsymbol{k}^{2n}} e^{-i\omega\left(x^0-y^0\right)+i\boldsymbol{k}\cdot(\boldsymbol{x}-\boldsymbol{y})}, \\ \left\langle T\Phi\left(x^0, \boldsymbol{x}\right) \Phi\left(y^0, \boldsymbol{y}\right)\right\rangle &= \sum_{n=0}^{\infty} \int_{\boldsymbol{k}} \frac{d\omega}{2\pi} \frac{i}{-\boldsymbol{k}^2} \frac{\omega^{2n}}{\boldsymbol{k}^{2n}} e^{-i\omega\left(x^0-y^0\right)+i\boldsymbol{k}\cdot(\boldsymbol{x}-\boldsymbol{y})}. \end{aligned} \tag{3.20}$$

Of course, we are still integrating over all possible momenta, even those not satisfying $\omega \ll \boldsymbol{k}$. Due to this, problems may arise in this region, i.e., where $\omega \sim \boldsymbol{k}$. Because $\omega \sim v/r$, this is the region where $\boldsymbol{k}$ is soft. Thus, this approximation is bound to result in IR divergences at some point. We will see how to deal with those in the next section. In any case, (3.20) allows one not to consider the complete propagators (3.17) in diagrams, but instead treat each term in (3.20) perturbatively. For example, we have the leading-order (LO) terms

$$\begin{aligned} \left\langle TH_{\mu\nu}\left(x^0, \mathbf{x}\right) H_{\alpha\beta}\left(y^0, \mathbf{y}\right)\right\rangle_{v^0} &= \delta\left(x^0 - y^0\right) P_{\mu\nu;\alpha\beta} \int_{\boldsymbol{k}} \frac{i}{-\boldsymbol{k}^2} e^{i\boldsymbol{k}\cdot(\boldsymbol{x}-\boldsymbol{y})}, \\ \left\langle T\Phi\left(x^0, \boldsymbol{x}\right) \Phi\left(y^0, \boldsymbol{y}\right)\right\rangle_{v^0} &= \delta\left(x^0 - y^0\right) \int_{\boldsymbol{k}} \frac{i}{-\boldsymbol{k}^2} e^{i\boldsymbol{k}\cdot(\boldsymbol{x}-\boldsymbol{y})}, \end{aligned} \tag{3.21}$$

which are *instantaneous*[4] propagators represented in Feynman diagrams as shown in Fig. 3.2. Meanwhile, higher-order terms in (3.20) are treated as *propagator insertions* which can be added at various orders in $v$. Each new correction is displayed as a cross in the previous propagators. For instance, the next-to-leading

[4]Instantaneous in the sense that the Dirac deltas in (3.21) impose equal times.

(a) $H_{\mu\nu}$ (b) $\Phi$

Figure 3.2

(NLO) terms of (3.20) are given by

$$\left\langle TH_{\mu\nu}\left(x^0,\mathbf{x}\right)H_{\alpha\beta}\left(y^0,\mathbf{y}\right)\right\rangle_{v^2} = P_{\mu\nu;\alpha\beta}\int_{\boldsymbol{k}}\frac{i}{-\boldsymbol{k}^4}e^{i\boldsymbol{k}\cdot(\boldsymbol{x}-\boldsymbol{y})}\frac{d^2}{dx^0dy^0}\delta\left(x^0-y^0\right),$$
$$\left\langle T\Phi\left(x^0,\boldsymbol{x}\right)\Phi\left(y^0,\boldsymbol{y}\right)\right\rangle_{v^2} = \int_{\boldsymbol{k}}\frac{i}{-\boldsymbol{k}^4}e^{i\boldsymbol{k}\cdot(\boldsymbol{x}-\boldsymbol{y})}\frac{d^2}{dx^0dy^0}\delta\left(x^0-y^0\right),$$

and are represented in Feynman diagrams as shown in Fig. 3.3. Then $v^4$ corrections have two crosses, $v^6$ corrections have three crosses, and so on. *Radiative modes*, on the other hand, are always external in near zone diagrams, and are represented as shown in Fig. 3.4.

### 3.4.2 Worldline vertices

The effective action resulting from near zone computations is defined differently from what we find in Chapter 2. This is because, in (3.15), one encounters sources for both orbital *and* radiative modes, while in Chapter 2 we defined the effective action such that the sources for soft modes would only appear after integrating out the hard component (cf. (2.9)).

In the absence of loops, sources are the only way in which any type of mode can appear. And, in the present context, the sources are the point-particles. Thus, we must know how to represent them in Feynman diagrams.

In order to see how sources appear, let us carry on with the splitting between orbital and radiative fields into the point-particle action. In doing so, one is able to find several *worldline vertices*. For example, from (3.8), one can obtain a linear

(a) $H_{\mu\nu}$ (b) $\Phi$

Figure 3.3

(a) $\bar{h}_{\mu\nu}$ (b) $\bar{\varphi}$

Figure 3.4

coupling between orbital gravitons and the point-particles,[5]

$$S_{\text{pp}}^{H} \equiv \sum_a m_a \int \frac{dt_a}{\sqrt{1-v_a^2}} \frac{H_{\mu\nu}\left(x_a\right)}{2\Lambda} v_a^{\mu} v_a^{\nu}. \tag{3.22}$$

In a similar fashion to what was done for orbital propagators, we can exploit the low-velocity regime to expand (3.22) in powers of $v$, the LO term being

$$S_{\text{pp}}^{Hv^0} = \sum_a m_a \int dt_a \frac{H_{00}\left(x_a\right)}{2\Lambda}. \tag{3.23}$$

Selecting one of the particles in the sum of (3.23), say particle 1, we find

$$S_1^{Hv^0} = m_1 \int dt_1 \frac{H_{00}\left(x_1\right)}{2\Lambda}. \tag{3.24}$$

The vertex corresponding to (3.24) is portrayed in Fig. 3.5a. The solid, horizontal line depicts the worldline of particle 1. The worldline of particle 2 is exhibited just below it, as in the example of Fig. 3.7. Higher-order terms in this expansion are treated as *worldline insertions*, and are represented according to their scaling. One instance is the NLO coupling to particle 1 coming from (3.22),

$$S_1^{Hv^1} = m_1 \int dt_1 \frac{H_{0i}\left(x_a\right)}{\Lambda} v_1^i,$$

which leads to the vertex presented in Fig. 3.5b. All the above reasoning equally applies to $\Phi$ and radiative modes.

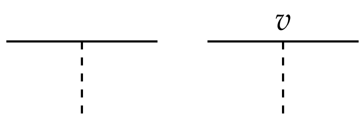


(a) (b)

Figure 3.5

[5]Following [22], we use the term *gravitons* to refer to the various polarizations of the gravitational field $h_{\mu\nu}$, even though we are not quantizing anything.

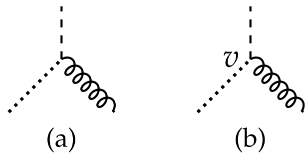


Figure 3.6

### 3.4.3 Bulk vertices

Finally, we have *bulk vertices*. These are vertices coming from the bulk action. To give an example, let us consider (3.7). One of the action terms which come from (3.7), after decomposing the modes, is

$$S_{H\partial\Phi\partial\bar{\varphi}} = \frac{1}{\Lambda}\int dt d^d\boldsymbol{x}\left(H^{\mu\nu} - \frac{1}{2}\eta^{\mu\nu}H\right)\partial_\mu\Phi\partial_\nu\bar{\varphi}. \tag{3.25}$$

However, we must be careful here, because a time derivative acting on $\Phi$ scales differently from a spatial derivative (cf. (3.11)). The spatial derivative constitutes the LO term of (3.25),

$$S_{H\partial_i\Phi\partial\bar{\varphi}} = \frac{1}{\Lambda}\int dt d^d\boldsymbol{x}\left(H^{i\nu}\partial_i\Phi\partial_\nu\bar{\varphi} - \frac{1}{2}\delta^{ij}H\partial_i\Phi\partial_j\bar{\varphi}\right),$$

which leads to the vertex shown in Fig. 3.6a. The time derivative, on the other hand, scales with an extra power of $v$, and therefore constitutes the NLO term of (3.25),

$$S_{H\partial_0\Phi\partial\bar{\varphi}} = \frac{1}{\Lambda}\int dt d^d\boldsymbol{x}\left(H^{0\nu}\partial_0\Phi\partial_\nu\bar{\varphi} + \frac{1}{2}H\partial_0\Phi\partial_0\bar{\varphi}\right),$$

leading to the vertex shown in Fig. 3.6b.

The action terms resulting from decomposing the fields into orbital and radiative parts are numerous, and they can all be represented in a specific, systematic way in Feynman diagrams. An example of a diagram with many of the elements we have seen so far is reproduced in Fig. 3.7. Also, a full list with all the action

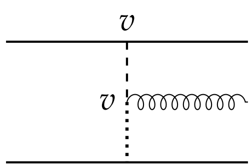


Figure 3.7

terms used in the computations present in this work can be found in Appendix B.

### 3.4.4 Conservative and radiative sectors

In Chapter 2, we saw how diagrams involved in the computation of the effective action could be grouped into two main categories, according to whether external soft modes were present or not. Likewise, near zone diagrams can be divided into two *sectors*. The difference between them is equally straightforward: one of them has external radiative modes; the other does not. However, this distinction has profound consequences.

Graphs with no emitted radiation make up the *conservative sector*. It is an action which does not involve any field, only degrees of freedom concerning the two-body distribution. Thus, it can only be interpreted as contributing to an effective two-body dynamics, i.e., an effective Lagrangian for a discrete system of two interacting point-particles. This will become more transparent as we go along and advance into the next chapter, where, among other things, we reproduce the Newtonian potential using the EFT approach, as a consistency check of the formalism.

Diagrams with external radiative modes are said to compose the *radiative sector*. One example of the latter is the one in Fig. 3.7. This is a very rich sector, and involves a more detailed discussion, due to the presence of external radiative fields. We will refer to it as $S_{\text{rad}}\left[x_a, \bar{h}, \bar{\varphi}\right]$. This part consists of radiative modes coupled to the two-body distribution. Now, the source is treated as a single *composite system*, i.e., the compact binary. We will not bother looking into possible nonlinear couplings that the radiative fields may have with the composite system. Instead, let us focus on terms linear in these fields. These come from near zone diagrams with a single external radiative mode, such as the one in Fig. 3.7. One can group all of these terms into one-graviton and -scalar emission amplitudes,

$$\Gamma\left[\bar{h}\right] = \frac{1}{2\Lambda}\int dt d^d\boldsymbol{x} T^{\mu\nu}\left(t,\boldsymbol{x}\right)\bar{h}_{\mu\nu}\left(t,\boldsymbol{x}\right), \tag{3.26}$$

$$\Gamma\left[\bar{\varphi}\right] = \frac{1}{2\Lambda}\int dt d^d\boldsymbol{x} J\left(t,\boldsymbol{x}\right)\bar{\varphi}\left(t,\boldsymbol{x}\right). \tag{3.27}$$

The above equations define linear sources for the two different radiative fields we have. The first equation, (3.26), defines the *stress-energy pseudotensor* $T^{\mu\nu}$ of the system, while (3.27) defines what we will refer to as the *scalar source* $J$. In this work, we will care only about the latter.

Both (3.26) and (3.27) can be organized as multipole expansions around the center of mass (CM), which we assume to be at the origin. This is thoroughly done in [30] for both cases. But for the scalar case we find

$$\Gamma\left[\bar{\varphi}\right] = \frac{1}{2\Lambda}\int dt \sum_{\ell=0}^{\infty}\frac{1}{\ell!}\mathcal{I}^{L}\left(t\right)\left(\partial_{L}\bar{\varphi}\right)\left(t,\mathbf{0}\right), \tag{3.28}$$

where the *scalar multipole moments* $\mathcal{I}^L$ are given in $d=3$ by

$$\mathcal{I}^{L} = \sum_{p=0}^{\infty}\frac{(2\ell+1)!!}{(2p)!!\,(2\ell+2p+1)!!}\int d^{3}\boldsymbol{x}\left(\partial_{0}^{2p}J\right)\left(t,\boldsymbol{x}\right)\left|\boldsymbol{x}\right|^{2p}\boldsymbol{x}_{\mathrm{STF}}^{L}. \tag{3.29}$$

Remembering that the typical frequencies characterizing the source satisfy $\omega\sim v/r$, and that the typical size of the composite system is $r$, one is able to discover that (3.29) is really an expansion in the small parameter $v$, the LO term being

$$\int d^{3}\boldsymbol{x}J\left(t,\boldsymbol{x}\right)\boldsymbol{x}_{\mathrm{STF}}^{L}. \tag{3.30}$$

In this work, we will focus only on the monopole and dipole cases of (3.30). These can be respectively obtained by setting $\ell=0$ and $\ell=1$ in (3.30), i.e., $\int d^{3}\boldsymbol{x}J\left(t,\boldsymbol{x}\right)$ and $\int d^{3}\boldsymbol{x}J\left(t,\boldsymbol{x}\right)\boldsymbol{x}^{i}$.

We can also write (3.27) in partial Fourier space, i.e., we perform an inverse Fourier transform on the spatial dependence only,

$$\Gamma\left[\bar{\varphi}\right] = \frac{1}{2\Lambda}\int_{\boldsymbol{k}} dt J\left(t,\boldsymbol{k}\right)\bar{\varphi}\left(t,-\boldsymbol{k}\right), \tag{3.31}$$

where

$$J\left(t,\boldsymbol{k}\right) = \int d^{3}\boldsymbol{x}J\left(t,\boldsymbol{x}\right)e^{-i\boldsymbol{k}\cdot\boldsymbol{x}}. \tag{3.32}$$

Expanding the exponential in (3.32), we arrive at

$$J\left(t,\boldsymbol{k}\right) = \sum_{\ell=0}^{\infty}\frac{\left(-i\right)^{\ell}}{\ell!}\left(\int d^{3}\boldsymbol{x}J\left(t,\boldsymbol{x}\right)\boldsymbol{x}^{L}\right)\boldsymbol{k}_{L}. \tag{3.33}$$

Using this expression, we will see in the next chapter how straightforward it is to read off contributions to the scalar multipole moments from radiative diagrams with a single radiated mode, a procedure known in the literature as *matching*.

## 3.5 Integrating out radiative modes: the far zone

Up until now, we have been very insistent in drawing a relationship between what we were doing and what had been established in Chapter 2. Once we finish using that framework to help us integrate out the orbital modes, we are done as far as Chapter 2 is concerned. Anything that we might decide to do afterwards is necessarily beyond the scope of that chapter. But we can still use some of the tools we have learned. Let us see how.

We saw how integrating out the orbital modes led to two kinds of terms in $S_{\text{eff}}\left[x_a, \bar{h}, \bar{\varphi}\right]$, one of them involving fields and sources, and the other involving sources only. This showed how this process not only served the purpose of yielding an effective theory at large distances. In particular, it also led to an effective two-body dynamics which could be interpreted as the result of the exchange of orbital modes between the two particles. If we also integrate out the radiative modes, only a theory for dynamical sources should be left. This is interesting on its own, but there are also more profound reasons for doing so.

Remember that we used $\omega \ll \boldsymbol{k}$ to expand near zone propagators in powers of $\omega^2/\boldsymbol{k}^2$. But we were still integrating over all possible momenta. This resulted in a loss of information about the region in which that approximation was not valid, i.e., the region $\omega \sim \boldsymbol{k}$. This is precisely where radiative modes play their part (cf. (3.11)). And our ignorance about it manifests itself in the form of IR poles. At the same time, integrating out orbital modes means we are losing information about the orbital scale. If we decide to integrate out radiative fields, this loss will be manifested in the form of UV poles appearing in calculations. Thus, we have an interplay between orbital and radiation scales. One lacks information about the other, and each deficiency leads to a different type of divergence. As it turns out, the UV divergences that shall appear in integrating out radiative modes end up cancelling out the IR divergences that we had before. This is how it should be. After all, before integrating either orbital or radiative modes, we had a theory concerning both scales. This cancellation between near zone IR poles and far zone UV poles is the so-called *zero-bin subtraction* in the literature, and it also gives us a motivation for integrating out radiative fields, i.e., to remedy near zone IR poles.

After integrating out the orbital modes, the theory we obtain is one of interacting point-particles and radiative fields coupled to moments of the two-body distribution. This is given by $S_{\text{eff}}\left[x_a, \bar{h}, \bar{\varphi}\right]$. What we want to do now is get rid of the radiative modes too, just as we did for the orbital modes. Taking inspiration

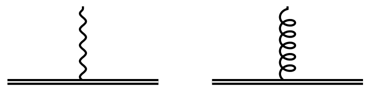


Figure 3.8

from (2.10) and (3.15), we might define the effective action resulting from this procedure as

$$e^{iS_{\text{eff}}[x_a]} \equiv \int \mathcal{D}\bar{h}_{\mu\nu}\mathcal{D}\bar{\varphi}e^{iS_{\text{eff}}[x_a,\bar{h},\bar{\varphi}]}. \tag{3.34}$$

Taking the logarithm on both sides of (3.34), what we get is

$$iS_{\text{eff}}[x_a] = \log \int \mathcal{D}\bar{h}_{\mu\nu}\mathcal{D}\bar{\varphi}e^{iS_{\text{eff}}[x_a,\bar{h},\bar{\varphi}]}.$$

Similarly to what happened in the near zone, finding $S_{\text{eff}}[x_a]$ involves the computation of connected Feynman diagrams, here describing processes which are said to belong in the *far zone*. Once again, we neglect loop diagrams.

As explained before, we are now left only with a single type of term in the effective action, that in which no external fields appear. Indeed, finding an effective two-particle dynamics for the sources alone was actually one of our main motivations for integrating out radiative modes. And because this type of term is also present after integrating out orbital modes (namely in the conservative sector), it is common to both $S_{\text{eff}}\left[x_a,\bar{h},\bar{\varphi}\right]$ and $S_{\text{eff}}[x_a]$. For this reason, from now on we are going to refer only to $S_{\text{eff}}$ and $S_{\text{rad}}$, the former being the effective two-particle dynamics, the latter containing couplings to the radiative fields.

We emphasize that we will work only with linear couplings between radiative fields and the composite system. These are given by (3.26) and (3.27), corresponding to the vertices shown in Fig. 3.8. The double line denotes the binary as a single object, as is most appropriate in the far zone. Sometimes, we will want to specify a particular multipole moment under consideration, or a term of a multipole moment. For instance, say we want to consider the coupling of a scalar quadrupole moment $\mathcal{I}^{ij}(t)$ to the composite system, i.e.,[6]

$$\frac{1}{4\Lambda}\int dt\mathcal{I}^{ij}(t)\left(\partial_{ij}\bar{\varphi}\right)(t,\mathbf{0}).$$

In this case, we indicate this fact explicitly, as appears in Fig. 3.9. Naturally, then,

[6]This is given by the $\ell = 2$ term of (3.28).

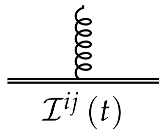


Figure 3.9

worldline vertices in the far zone are simply given by these linear couplings of radiative fields to the composite system. As for bulk vertices, these are obtained in exactly the same manner as carried out in the near zone, but now only radiative fields are involved. Some examples of far zone diagrams, which generally involve the emission and reabsorption of radiative modes by the composite system, are found in Chapter 5.

### 3.5.1 Radiative propagators

Now that we are integrating out radiative modes, they are finally going to appear contracted. For this reason, we need *radiative* propagators, in a fashion similar to the orbital case of Section 3.4.1. These can be obtained from the kinetic actions for the radiative fields, which are found to look like

$$\begin{aligned} S_0\left[\bar{h}\right] &= \int dt d^d \boldsymbol{x} \left(\frac{1}{4}\left(\partial_\mu \bar{h}\right)^2 - \frac{1}{2}\left(\partial_\sigma \bar{h}_{\mu\nu}\right)^2\right), \\ S_0\left[\bar{\varphi}\right] &= \int dt d^d \boldsymbol{x} \left(-\frac{1}{2}\eta^{\mu\nu}\partial_\mu \bar{\varphi}\partial_\nu \bar{\varphi}\right). \end{aligned} \tag{3.35}$$

Again, one can invert the differential operators of (3.35) in order to find propagators,

$$\begin{aligned} \left\langle T\bar{h}_{\mu\nu}\left(x^0, \mathbf{x}\right)\bar{h}_{\alpha\beta}\left(y^0, \mathbf{y}\right)\right\rangle &= P_{\mu\nu;\alpha\beta}\int_{\boldsymbol{k}} \frac{d\omega}{2\pi}\frac{i}{\omega^2 - \boldsymbol{k}^2 + ia} e^{-i\omega\left(x^0 - y^0\right) + i\boldsymbol{k}\cdot(\boldsymbol{x}-\boldsymbol{y})}, \\ \left\langle T\bar{\varphi}\left(x^0, \boldsymbol{x}\right)\bar{\varphi}\left(y^0, \boldsymbol{y}\right)\right\rangle &= \int_{\boldsymbol{k}} \frac{d\omega}{2\pi}\frac{i}{\omega^2 - \boldsymbol{k}^2 + ia} e^{-i\omega\left(x^0 - y^0\right) + i\boldsymbol{k}\cdot(\boldsymbol{x}-\boldsymbol{y})}. \end{aligned} \tag{3.36}$$

By noting that the typical time scale of the problem is $\sim r/v$, and that for radiative modes $\boldsymbol{k} \sim v/r$, one can use (3.36) to find out that radiative fields scale as

$$\bar{h}_{\mu\nu} \sim \bar{\varphi} \sim v/r.$$

Once again, the $ia$-prescription is forced upon us by the path integral formulation, as is explicitly shown in (3.36). And now, the prescription is relevant, because $\omega \sim \boldsymbol{k}$. In other words, radiative modes can go on-shell.[7] We have no right, then, to expand (3.36) in powers of $\omega^2/\boldsymbol{k}^2$. Instead, the multipole expansion involved in (3.28) implicitly uses the fact that $kr \sim v \ll 1$ for radiative modes (i.e., $\boldsymbol{k} \sim \omega \sim v/r$), compensating for the expansion in $\omega^2/\boldsymbol{k}^2$ used for orbital propagators. This is at the core of the reason why far zone UV poles should cancel out near zone IR poles. For a thorough discussion, see [31]. Here, we only sketch the proof of this claim, taking great inspiration from [27].

First, we call

$$I \equiv \frac{e^{i\boldsymbol{k}\cdot\boldsymbol{r}}}{\omega^2 - \boldsymbol{k}^2}, \qquad N \equiv \frac{e^{i\boldsymbol{k}\cdot\boldsymbol{r}}}{-\boldsymbol{k}^2} \sum_{m=0}^{\infty} \frac{\omega^{2m}}{\boldsymbol{k}^{2m}}, \qquad F \equiv \frac{1}{\omega^2 - \boldsymbol{k}^2} \sum_{n=0}^{\infty} \frac{(i\boldsymbol{k}\cdot\boldsymbol{r})^n}{n!}, \tag{3.37}$$

where $\boldsymbol{x} \sim r$. The first of the integrands defined in (3.37) is that of the complete theory, i.e., that which we would find in computations had we not decomposed the modes into orbital and radiative parts. In the second integrand, we perform an expansion in powers of $\omega^2/\boldsymbol{k}^2$, as we do for orbital propagators in the near zone. Finally, the last definition involves the multipole expansion in powers of $\boldsymbol{k}r$ involved in the far zone. Notice that the propagator expansion introduces powers of $\boldsymbol{k}^2$ into the denominators of momentum integrals, leading to IR poles. Meanwhile, the multipole expansion introduces powers of $\boldsymbol{k}$ into numerators, leading to UV poles. Now, we write the following trivial equality,

$$I = N + F + I - N - F. \tag{3.38}$$

Integrating both sides of (3.38) over $\boldsymbol{k}$, we find

$$\int_{\boldsymbol{k}} I = \int_{\boldsymbol{k}} N + \int_{\boldsymbol{k}} F + \int_{\boldsymbol{k}} (I - N - F)\,. \tag{3.39}$$

We then split the last integral over $|\boldsymbol{k}|$ on the rhs of (3.39) into two parts, one for $|\boldsymbol{k}| > \bar{k}$, and the other for $|\boldsymbol{k}| < \bar{k}$, where $\bar{k}$ is some energy scale such that $\omega < \bar{k} < 1/r$. In other words, we write

$$\int_{\boldsymbol{k}} I = \int_{\boldsymbol{k}} N + \int_{\boldsymbol{k}} F + \int_{\boldsymbol{k}} \theta\left(|\boldsymbol{k}| - \bar{k}\right)(I - N - F) + \int_{\boldsymbol{k}} \theta\left(\bar{k} - |\boldsymbol{k}|\right)(I - N - F)\,. \tag{3.40}$$

[7] Indeed, these are the modes which are ultimately lost as radiation by the system and whose phase is measured by our detectors.

The near zone corresponds to the region $|\boldsymbol{k}| > \bar{k}$, for which one can show that $\omega < |\boldsymbol{k}|$. In this case, the propagator expansion can be performed, so that we have

$$\int_{\boldsymbol{k}} \theta\left(|\boldsymbol{k}| - \bar{k}\right) I = \int_{\boldsymbol{k}} \theta\left(|\boldsymbol{k}| - \bar{k}\right) N. \tag{3.41}$$

Meanwhile, the far zone corresponds to the region $|\boldsymbol{k}| < \bar{k}$, for which we find $|\boldsymbol{k}|\, r < 1$. In this case, we perform the multipole expansion, i.e.,

$$\int_{\boldsymbol{k}} \theta\left(\bar{k} - |\boldsymbol{k}|\right) I = \int_{\boldsymbol{k}} \theta\left(\bar{k} - |\boldsymbol{k}|\right) F. \tag{3.42}$$

Plugging (3.41) and (3.42) into (3.40), we find

$$\int_{\boldsymbol{k}} I = \int_{\boldsymbol{k}} N + \int_{\boldsymbol{k}} F - \int_{\boldsymbol{k}} \theta\left(|\boldsymbol{k}| - \bar{k}\right) F - \int_{\boldsymbol{k}} \theta\left(\bar{k} - |\boldsymbol{k}|\right) N. \tag{3.43}$$

Again, we use the propagator expansion for $|\boldsymbol{k}| > \bar{k}$, and the multipole expansion for $|\boldsymbol{k}| < \bar{k}$, but now to show that

$$\begin{aligned} \int_{\boldsymbol{k}} \theta\left(|\boldsymbol{k}| - \bar{k}\right) F &= \int_{\boldsymbol{k}} \theta\left(|\boldsymbol{k}| - \bar{k}\right) \frac{1}{-\boldsymbol{k}^2} \sum_{m,n=0}^{\infty} \frac{\omega^{2m}}{\boldsymbol{k}^{2m}} \frac{\left(i\boldsymbol{k}\cdot\boldsymbol{r}\right)^n}{n!}, \\ \int_{\boldsymbol{k}} \theta\left(\bar{k} - |\boldsymbol{k}|\right) N &= \int_{\boldsymbol{k}} \theta\left(\bar{k} - |\boldsymbol{k}|\right) \frac{1}{-\boldsymbol{k}^2} \sum_{m,n=0}^{\infty} \frac{\omega^{2m}}{\boldsymbol{k}^{2m}} \frac{\left(i\boldsymbol{k}\cdot\boldsymbol{r}\right)^n}{n!}, \end{aligned} \tag{3.44}$$

so that, upon substitution into (3.43), (3.44) yields

$$\int_{\boldsymbol{k}} I = \int_{\boldsymbol{k}} N + \int_{\boldsymbol{k}} F + \int_{\boldsymbol{k}} \frac{1}{\boldsymbol{k}^2} \sum_{m,n=0}^{\infty} \frac{\omega^{2m}}{\boldsymbol{k}^{2m}} \frac{\left(i\boldsymbol{k}\cdot\boldsymbol{r}\right)^n}{n!}. \tag{3.45}$$

The last integral on the rhs of (3.45), however, vanishes in dimensional regularization, so that, in the end, the complete theory can be properly regarded as a split between near and far zone contributions,

$$\int_{\boldsymbol{k}} I = \int_{\boldsymbol{k}} N + \int_{\boldsymbol{k}} F.$$

**The optical theorem**

The *ia*-prescription, when used in far zone computations, has profound consequences. This becomes clearer in light of the so-called *Sokhotski-Plemelj formula*, which roughly states that, in the sense of distributions, the following equality holds,

$$\frac{1}{x \pm ia} = \mathrm{PV}\frac{1}{x} \mp i\pi\delta\left(x\right),$$

where PV stands for principal value [12, 28, 32]. When applied to the Feynman prescription, this theorem tells us that [12]

$$\frac{i}{\omega^2 - \boldsymbol{k}^2 + ia} = \mathrm{PV}\frac{i}{\omega^2 - \boldsymbol{k}^2} + \pi\delta\left(\omega^2 - \boldsymbol{k}^2\right). \tag{3.46}$$

Upon substitution into (3.36), (3.46) shows that the Feynman propagator presents both a real and an imaginary part, the former being related to when radiative modes go on-shell ($\omega = \pm\left|\boldsymbol{k}\right|$). This reasoning is reminiscent of the optical theorem of QFT [33]. Indeed, when used in a diagram such as that of Fig. 5.1, the *imaginary* part of the Feynman propagator leads to a *real* part of the effective action, and thus further contributes to the effective two-particle potential. Meanwhile, the *real* part of the Feynman propagator leads to an *imaginary* part of the effective action. And the latter can be related to a decay width via the *optical theorem* applied to the context of gravitational dynamics,

$$\frac{1}{T}\,\mathrm{Im}\,S_{\mathrm{eff}}\left[x_a\right] = \frac{1}{2}\int dE d\Omega \frac{d^2\Gamma}{dE d\Omega}, \tag{3.47}$$

where $T \to \infty$ is an arbitrarily long period of time and $d\Gamma$ is the differential rate for graviton (or scalar) emission, which can be related to the emitted power via $dP = Ed\Gamma$ [22, 27, 28]. Thus, the imaginary part of the effective action can be used to compute an observable of extreme importance to us: the emitted power.

An interesting, although informal explanation for this sudden appearance of an imaginary part of the effective action, having a neat physical interpretation which can be used to compute an important observable, is as follows. At the beginning, we had both fields and particles as DOFs. By integrating out the fields, we chose to look only at a subset of these DOFs, i.e., the discrete system of two particles. But this system is not isolated, because there can be transfer of energy between the particles and the external, radiative fields. Indeed, this is the case if the system loses energy in the form of radiation. This information cannot be lost. It has to be accounted for in some way by our formalism. The way in which it is accounted for is by giving rise to this imaginary part of the effective action, containing information about an energy transfer between the two-particle system and its surroundings.

# Chapter 4

# Near zone dynamics

In this chapter, we calculate contributions coming from many near zone diagrams. In Section 4.1, we focus on the conservative sector, i.e., terms contributing to the effective potential between the two particles. In Section 4.2, on the other hand, we focus on the radiative sector, computing several contributions to the scalar source and performing a matching procedure in order to read off monopole and dipole moments.

## 4.1 Conservative sector

In this section, we compute several contributions to the conservative sector. In Section 4.1.1, we compute a familiar result—the Newtonian potential—using the EFT formalism. In Section 4.1.2, we compute an $O\left(\alpha^2\right)$ correction to the Newtonian potential which has also been computed in [12], leading to an effective gravitational constant. Finally, from Section 4.1.3 to 4.1.5, we focus on the computation of the leading contributions from a $\phi^3$, a $\phi\left(\partial\phi\right)^2$ and $\phi^4$ self-interaction, respectively.

### 4.1.1 The Newtonian potential

As a warm-up for what is about to come, let us compute the diagram of Fig. 4.1. In order to do so, we need the following ingredients: the leading propagator (B.1) for orbital gravitons; and the leading linear coupling (B.4) of gravitons to the

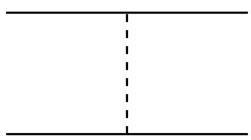

Figure 4.1

worldlines. What we find is

$$iS_{\text{eff}}\big|_{\text{Fig. 4.1}} = \int_{\boldsymbol{k}} dt_1 dt_2 \frac{m_1 m_2}{4\Lambda^2} \delta\left(t_1 - t_2\right) P_{00;00} \frac{e^{i\boldsymbol{k}\cdot[\boldsymbol{x}_1(t_1) - \boldsymbol{x}_2(t_2)]}}{\boldsymbol{k}^2}. \tag{4.1}$$

Notice that there are two integrations over time and a single delta function. This is because there are two vertices in the diagram connected by a single propagator, which happens to be instantaneous. We will always use instantaneous near zone propagators in this work. Thus, something similar will always happen, i.e., we will always be able to perform all but one of the integrals over time with the aid of delta functions. Because of that, we will not mention this fact again in the future. Doing so in (4.1) yields

$$iS_{\text{eff}}\big|_{\text{Fig. 4.1}} = \int_{\boldsymbol{k}} dt \frac{m_1 m_2}{4\Lambda^2} P_{00;00} \frac{e^{i\boldsymbol{k}\cdot(\boldsymbol{x}_1 - \boldsymbol{x}_2)}}{\boldsymbol{k}^2}, \tag{4.2}$$

where—even though this has been and will always be omitted—$\boldsymbol{x}_1$ and $\boldsymbol{x}_2$ are both computed at time $t$. Now we use (3.18) into (4.2) to write

$$iS_{\text{eff}}\big|_{\text{Fig. 4.1}} = i \int_{\boldsymbol{k}} dt \frac{m_1 m_2}{4\Lambda^2} \frac{d-2}{d-1} \frac{e^{i\boldsymbol{k}\cdot(\boldsymbol{x}_1 - \boldsymbol{x}_2)}}{\boldsymbol{k}^2}. \tag{4.3}$$

Now we define

$$\boldsymbol{r} \equiv \boldsymbol{x}_1 - \boldsymbol{x}_2. \tag{4.4}$$

We will use this definition throughout the whole work. Substituting (4.4) into (4.3), we arrive at

$$iS_{\text{eff}}\big|_{\text{Fig. 4.1}} = i \int dt \frac{m_1 m_2}{4\Lambda^2} \frac{d-2}{d-1} \int_{\boldsymbol{k}} \frac{e^{i\boldsymbol{k}\cdot\boldsymbol{r}}}{\boldsymbol{k}^2}. \tag{4.5}$$

The integral over $\boldsymbol{k}$ in (4.5) can be performed with the aid of (A.32), so that (4.5) becomes

$$iS_{\text{eff}}\big|_{\text{Fig. 4.1}} = i \int dt \frac{m_1 m_2}{4\Lambda^2} \frac{d-2}{d-1} \frac{\Gamma\left(d/2 - 1\right)}{(4\pi)^{d/2}} \left(\frac{r^2}{4}\right)^{1-d/2}, \tag{4.6}$$

where $r \equiv |\boldsymbol{r}|$. Substituting the definition of $\Lambda$ and $\epsilon$, (4.6) becomes

$$iS_{\text{eff}}\big|_{\text{Fig. 4.1}} = i \int dt \frac{m_1 m_2}{2m_{\text{Pl}}^2 r} \frac{\epsilon + 1}{\epsilon + 2} \frac{\Gamma\left(\frac{\epsilon+1}{2}\right)}{(4\pi)^{3/2}} \left(\frac{2}{\mu\sqrt{4\pi} r}\right)^{\epsilon}. \tag{4.7}$$

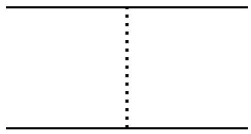

Figure 4.2

Substituting the definition of $m_{\text{Pl}}$ into (4.7), one gets

$$iS_{\text{eff}}\big|_{\text{Fig. 4.1}} = i\int dt \frac{4G_{\text{N}}m_1m_2}{r}\frac{\epsilon+1}{\epsilon+2}\frac{\Gamma\left(\frac{\epsilon+1}{2}\right)}{\sqrt{4\pi}}\left(\frac{2}{\mu\sqrt{4\pi}r}\right)^{\epsilon}. \tag{4.8}$$

Expanding in $\epsilon$ to order zero, (4.8) becomes

$$iS_{\text{eff}}\big|_{\text{Fig. 4.1}} = i\int dt \frac{G_{\text{N}}m_1m_2}{r}. \tag{4.9}$$

We can then derive a Lagrangian from (4.9),

$$\mathcal{L}_{\text{N}} = \frac{G_{\text{N}}m_1m_2}{r} \sim mv^2. \tag{4.10}$$

These last steps—using the definitions of $\Lambda$, $\epsilon$ and $m_{\text{Pl}}$, as well as the expansion to order zero in $\epsilon$ and the extraction of a Lagrangian—will often take place at the end of calculations. So we shall skip these steps from now on. In (4.10), we can clearly see a result of great familiarity to us, the *Newtonian potential*. This is at least one sign of consistency of the formalism being employed. We have indicated the scaling of this contribution. This is because we will denote future contributions according to how they scale with respect to this Newtonian result. This should become clearer in the next section, where we consider an $O\left(\alpha^2\right)$ correction to this potential, coming from a diagram very similar to that of Fig. 4.1, but with the exchange of an orbital scalar instead of an orbital graviton.

### 4.1.2 A correction to the Newtonian potential

Now that we have computed the diagram of Fig. 4.1, it is only natural to try and consider a very similar diagram, but with the exchange of an orbital scalar instead of an orbital graviton. This is given in Fig. 4.2. In order to compute this diagram, we need analogous ingredients to the ones we have just used, but replacing the graviton for a scalar everywhere: the leading propagator (B.2) for orbital scalars; and the leading linear coupling (B.5) of orbital scalars to the worldlines. What we

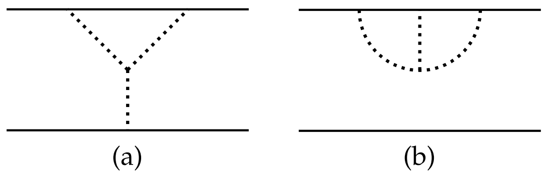


Figure 4.3

find is

$$iS_{\text{eff}}\big|_{\text{Fig. 4.2}} = i\int dt \frac{\alpha_1\alpha_2 m_1 m_2}{4\Lambda^2}\int_{\boldsymbol{k}}\frac{e^{i\boldsymbol{k}\cdot\boldsymbol{r}}}{\boldsymbol{k}^2}. \tag{4.11}$$

The same integral as that of (4.5) appears now in (4.11). Again, we compute it with the aid of (A.32), yielding the following Lagrangian,

$$\mathcal{L}_{\alpha^2} = \frac{2G_{\text{N}}\alpha_1\alpha_2 m_1 m_2}{r} \sim mv^2\cdot\alpha^2. \tag{4.12}$$

We have denoted Lagrangian (4.12) according to how it scales with respect to (4.10). From this we can infer that (4.12) enters at 0PN if we are only interested in the scaling with $v$. Some quantities will always be denoted according to how they scale with respect to Newtonian results. This will help with power counting in the expansion parameter $v$.

Taking into account both (4.10) and (4.12), one can define an *effective gravitational constant* between objects 1 and 2,

$$\tilde{G}_{12} \equiv G_{\text{N}}\left(1+2\alpha_1\alpha_2\right),$$

as has also been pointed out in [12]. The first and most obvious consequence of this is that the gravitational constant—as measured from the potential between two bodies—depends on the bodies under consideration. And because we assume that the scalar charges of different objects are not necessarily the same, we need scalar charges to be small in order for the WEP not to be violated. From limits found in [34] on some PPN parameters, we can expect $|\alpha| \lesssim 10^{-3}$.

### 4.1.3 Cubic non-derivative self-interaction

Now we are interested in computing the leading contribution of the $\phi^3$ self-interaction to the conservative part of the near zone. The only potential diagram is that of Fig. 4.3a. However, as will soon be explained, the diagram of Fig. 4.3b will also be relevant, due to the appearance of an IR divergence in Fig. 4.3a. Besides previously used ingredients, we also need the $\Phi^3$ self-coupling (B.8). Let us start with Fig. 4.3a. As mentioned, this is a potential diagram, meaning the orbital distance $r$ should appear in its result. What we find is

$$iS_{\text{eff}}\big|_{\text{Fig. 4.3a}, \phi^3} = i\int_k dt \left(-\lambda_3 \frac{m_{\text{Pl}}^2 \alpha_1^2 \alpha_2 m_1^2 m_2}{16\Lambda^4}\frac{e^{i\boldsymbol{k}\cdot\boldsymbol{r}}}{\boldsymbol{k}^2}\int_{\boldsymbol{q}} \frac{1}{\boldsymbol{q}^2\left(\boldsymbol{q}+\boldsymbol{k}\right)^2}\right), \tag{4.13}$$

where we have performed an integral over $\boldsymbol{x}$ to yield a $d$-dimensional delta function which imposes momentum conservation at the bulk vertex, and then used this delta function to perform one of the momentum integrals. This will always take place whenever we have a bulk vertex, and therefore steps like these will always be omitted. Moving on with our computations, we use (A.41) to perform the integral over $\boldsymbol{q}$ in (4.13). Once this is done, the following integral appears,

$$\int_{\boldsymbol{k}} \frac{e^{i\boldsymbol{k}\cdot\boldsymbol{r}}}{\left(\boldsymbol{k}^2\right)^{3-d/2}}. \tag{4.14}$$

If it wasn't for the exponential in (4.14), this integral would present both UV and IR divergences. However, the oscillating phase takes care of the UV divergence, leaving an IR pole only. As will soon be explained, this already signals the necessity of self-energy graphs. To compute (4.14), we use (A.32) again, so that (4.13) yields the following Lagrangian,

$$\mathcal{L}^{\text{near}}_{\alpha^3\lambda_3 L v^{-1}} = \sum_a \frac{\lambda_3}{16\pi} G_{\text{N}}\alpha_a m_a \alpha_1\alpha_2 m_1 m_2 \left(2\log\bar{\mu}r - \frac{1}{\epsilon_{\text{IR}}} - 1\right) \sim mv^2\cdot\alpha^3\lambda_3 L v^{-1}. \tag{4.15}$$

There are several things that we must say about (4.15). First, we have borrowed the Lagrangian notation of [23]. Secondly, we have considered the mirror image of Fig. 4.3a in writing (4.15). This is something we will always do for diagrams that have a mirror image. Also, we have used the definition

$$\bar{\mu} \equiv \mu\sqrt{4\pi}e^{\gamma/2}, \tag{4.16}$$

also present in [23]. We will use this definition again in the future. Finally, we have indicated the origin of the divergence in (4.15). Since one of our purposes is to track divergences, we will always indicate the origin of every divergence appearing from now on.

As discussed in Chapter 3, the appearance of IR divergences in the near zone indicates the need to consider its IR completion, i.e., the far zone. But the coefficient of the IR divergence in (4.15) does not have the form of a multipole-radiation coupling. This is because, in order to properly identify coefficients of near zone IR poles, one must also take into account self-energy contributions [23]. In the case at hand, this is given by Fig. 4.3b. What we find for this graph is

$$iS_{\text{eff}}\big|_{\text{Fig. 4.3b}, \, \phi^3} = i \int_{\boldsymbol{k}} dt \left( -\lambda_3 \frac{m_{\text{Pl}}^2 \alpha_1^3 m_1^3}{48\Lambda^4} \frac{1}{\boldsymbol{k}^2} \int_{\boldsymbol{q}} \frac{1}{\boldsymbol{q}^2 \left(\boldsymbol{q}+\boldsymbol{k}\right)^2} \right). \tag{4.17}$$

An integral similar to that of (4.13) appears now in (4.17). This is once again performed with the aid of (A.41), yielding

$$iS_{\text{eff}}\big|_{\text{Fig. 4.3b}, \, \phi^3} = i \int dt \left( -\lambda_3 \frac{m_{\text{Pl}}^2 \alpha_1^3 m_1^3}{48\Lambda^4} \frac{\Gamma\left(2-d/2\right)}{\left(4\pi\right)^{d/2}} \frac{\Gamma^2\left(d/2-1\right)}{\Gamma\left(d-2\right)} \int_{\boldsymbol{k}} \frac{1}{\left(\boldsymbol{k}^2\right)^{3-d/2}} \right). \tag{4.18}$$

The integral over $\boldsymbol{k}$ in (4.18) is similar to (4.14), with the exception of the exponential, which is now absent. The integral is now *scaleless*, meaning there are no dimensionful quantities besides that being integrated over. Thus, if the integral itself is dimensionful, then it must vanish, since no dimensionful quantities are available to equate the result of the integral with. In the above instance, the integral has energy units of $2\epsilon$. So it is *not* dimensionful in $d = 3$. In fact, it is then logarithmically divergent. However, we are working with dimensional regularization, in which we analytically continue from $d \neq 3$, and divergences end up as poles in $\epsilon$. In this scenario, the integral still vanishes as $d \to 3$, but it vanishes in a very special way. Because it is logarithmically divergent in $d = 3$, both UV and IR poles are present. And as it turns out, these cancel each other out, as demonstrated in Appendix A.7. Since we want to track divergences and identify the coefficient of the IR pole, we carry this cancellation explicitly throughout calculations, as shown in (A.47). Substituting (A.47) into (4.18), we are able to arrive at the following Lagrangian,

$$\mathcal{L}^{\text{self}}_{\alpha^3\lambda_3 L v^{-1}} = \sum_a \frac{\lambda_3}{16\pi} \frac{G_{\text{N}} \alpha_a^3 m_a^3}{3} \left( \frac{1}{\epsilon_{\text{UV}}} - \frac{1}{\epsilon_{\text{IR}}} \right). \tag{4.19}$$

Putting (4.15) and (4.19) together, we find

$$\begin{aligned}\mathcal{L}^{\text{near+self}}_{\alpha^3\lambda_3 Lv^{-1}} &= \frac{\lambda_3}{16\pi}\frac{G_{\rm N}\mathcal{I}_0^3}{3}\left(2\log\bar{\mu}r - 1 - \frac{1}{\epsilon_{\rm IR}}\right) \\ &+ \left(\frac{1}{\epsilon_{\rm UV}} + 1 - 2\log\bar{\mu}r\right)\sum_a \frac{\lambda_3}{16\pi}\frac{G_{\rm N}\alpha_a^3 m_a^3}{3} \sim mv^2\cdot\alpha^3\lambda_3 Lv^{-1}.\end{aligned} \tag{4.20}$$

From the scaling with $v$, we can see that this contribution enters the effective potential at $-0.5$PN. The coefficient of the IR pole in (4.20) now finally has the form of a monopole-radiation coupling, and we have anticipated a notation which will only be introduced later on, $\mathcal{I}_0 \equiv \sum_a \alpha_a m_a$ (cf. (4.40)). This notation also gives us insight as to what should be done to get rid of the IR pole in (4.20): consider a far zone diagram with the interaction between three conserved monopoles via a $\bar{\varphi}^3$ vertex. Such a diagram should contain a UV pole which exactly cancels out the IR pole in (4.20). This is the zero-bin subtraction in action, as explained in [23] and in Chapter 3 of this work. We will compute the relevant far zone contribution in Chapter 5.

Besides the IR pole in (4.20), we also find a UV pole. As explained in Chapter 3, the UV completion to the near zone must have something to do with the fact that we are neglecting the finite sizes of the objects. In other words, the UV singularity in (4.20) is due to the point-particle treatment of the EFT we started with. Since it comes from a self-energy graph, this UV pole can be easily absorbed by a counterterm renormalizing the masses of the particles, and therefore does not affect the two-particle potential. In any case, we see that renormalization is required already at first order in the $\phi^3$ self-interaction.

### 4.1.4 Cubic self-interaction with derivatives

Next, let us compute the leading contribution from the $\phi\,(\partial\phi)^2$ self-interaction to the conservative part of the near zone. The potential diagram should look just like Fig. 4.3a, but we must replace one vertex for the other, i.e., the only different ingredient needed is the self-coupling $\Phi\,(\partial_i\Phi)^2$, given by the action term (B.11). What we find is

$$iS_{\rm eff}\big|_{\text{Fig. 4.3a},\,\phi(\partial\phi)^2} = i\int dt\left[-\lambda_{3,2}\frac{\alpha_1^2\alpha_2 m_1^2 m_2}{96\Lambda^4}\left(\int_k \frac{e^{i\boldsymbol{k}\cdot\boldsymbol{r}}}{\boldsymbol{k}^2}\int_q\frac{2}{\boldsymbol{q}^2} + \left(\int_k\frac{e^{i\boldsymbol{k}\cdot\boldsymbol{r}}}{\boldsymbol{k}^2}\right)^2\right)\right], \tag{4.21}$$

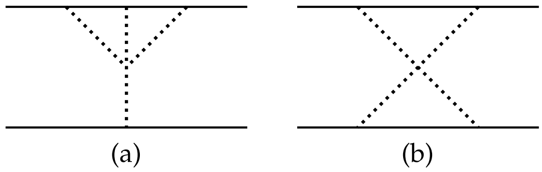

Figure 4.4

where we had to complete squares in the numerator, a step which always takes place for self-interactions with derivatives. The integral over $\boldsymbol{q}$ in (4.21) is another type of scaleless integral. But, in this case, it is dimensionful even in $d = 3$. So there is nothing to worry about, it certainly vanishes. We are then left with the same integral which appeared in both (4.5) and (4.11). Again, we use (A.32) to compute it, so that (4.21) gives

$$\mathcal{L}_{\alpha^3 \lambda_{3,2} v^2} = -\sum_a \lambda_{3,2} \frac{2G_\mathrm{N}^2 \alpha_a m_a \alpha_1 \alpha_2 m_1 m_2}{3r^2} \sim mv^2 \cdot \alpha^3 \lambda_{3,2} v^2. \tag{4.22}$$

From the scaling with $v$, we can see that this contribution enters the effective potential at 1PN. As has been indicated by the absence of the words "near" or "self", this contribution is the final one for the $\phi\,(\partial\phi)^2$ self-interaction. This is because no IR divergences are encountered, so there is no need to invoke the far zone, and consequently self-energy contributions. An analogous diagram in GR (as well as its mirror image) gives $-\sum_a G_\mathrm{N}^2 m_a m_1 m_2 / r^2$ [22]. This is very similar to (4.22), and the reason for this is very simple. Being inherited from the Ricci scalar, all bulk vertices in GR present exactly two derivatives, much like the $\phi\,(\partial\phi)^2$ self-interaction. This is an indication that all results coming from the $\phi\,(\partial\phi)^2$ should resemble standard GR results.

### 4.1.5 Quartic non-derivative self-interaction

Next, we want to compute the leading contribution coming from the $\phi^4$ self-interaction to the conservative part of the near zone. The relevant potential diagrams are those of Fig. 4.4. The only different ingredient needed is the $\Phi^4$ self-coupling, given by the action term (B.14). For the graph of Fig. 4.4a, one is able to find

$$iS_\mathrm{eff}\big|_{\text{Fig. 4.4a}} = i \int_{\boldsymbol{k},\boldsymbol{q}} dt \left( -\lambda_4 \frac{m_\mathrm{Pl}^2 \alpha_1^3 \alpha_2 m_1^3 m_2}{96\Lambda^6} \frac{e^{i\boldsymbol{k}\cdot\boldsymbol{r}}}{\boldsymbol{k}^2 (\boldsymbol{q}+\boldsymbol{k})^2} \int_{\boldsymbol{p}} \frac{1}{\boldsymbol{p}^2 (\boldsymbol{p}+\boldsymbol{q})^2} \right). \tag{4.23}$$

The integral over $\boldsymbol{p}$ is once again the same integral which appeared in (4.13) and (4.17). We perform it with the aid of (A.41). After doing so, the following integral appears,

$$\int_q \frac{1}{(\boldsymbol{q}^2)^{2-d/2}(\boldsymbol{q}+\boldsymbol{k})^2}. \tag{4.24}$$

This integral is very similar to the one we have just computed, i.e., the one appearing in (4.13), (4.17) and (4.23). But it has a different power in the denominator. The integral over $|\boldsymbol{q}|$ present in (4.24) looks something like this,

$$\int_0^\infty \frac{|\boldsymbol{q}|^{d-1}\, d\,|\boldsymbol{q}|}{(\boldsymbol{q}^2)^{2-d/2}(\boldsymbol{q}+\boldsymbol{k})^2}. \tag{4.25}$$

In $d=3$, (4.25) becomes

$$\int_0^\infty \frac{|\boldsymbol{q}|\, d\,|\boldsymbol{q}|}{(\boldsymbol{q}+\boldsymbol{k})^2}. \tag{4.26}$$

For $\boldsymbol{q}$ soft, i.e., $\boldsymbol{q} \ll \boldsymbol{k}$, (4.26) yields

$$\int |\boldsymbol{q}|\, d\,|\boldsymbol{q}| \sim \boldsymbol{q}^2 \to 0.$$

On the other hand, for $\boldsymbol{q}$ hard, meaning $\boldsymbol{q} \gg \boldsymbol{k}$, (4.26) yields

$$\int \frac{d\,|\boldsymbol{q}|}{|\boldsymbol{q}|} \sim \log|\boldsymbol{q}| \to \infty.$$

Thus, we have a UV divergence in (4.24). Using (A.41) to compute this integral, we find

$$iS_{\text{eff}}\big|_{\text{Fig. 4.4a}} = i\int dt\left(-\lambda_4 \frac{m_{\text{Pl}}^2\alpha_1^3\alpha_2 m_1^3 m_2}{96\Lambda^6}\frac{\Gamma^3(d/2-1)}{(4\pi)^d}\frac{\Gamma(3-d)}{\Gamma(3d/2-3)}\int_k \frac{e^{i\boldsymbol{k}\cdot\boldsymbol{r}}}{(\boldsymbol{k}^2)^{4-d}}\right), \tag{4.27}$$

where we can now see that the UV divergence is translated into a pole in the gamma function $\Gamma(3-d)$. The integral over $\boldsymbol{k}$ can be performed with the aid of (A.32), so that (4.27) yields

$$iS_{\text{eff}}\big|_{\text{Fig. 4.4a}+1\leftrightarrow 2} = i\int dt \sum_a \frac{\lambda_4}{12\pi}\frac{G_{\text{N}}^2\alpha_a^2 m_a^2 \alpha_1\alpha_2 m_1 m_2}{r}\left(\frac{1}{\epsilon_{\text{UV}}} - 3 - 3\log\bar{\mu}r\right). \tag{4.28}$$

Meanwhile, for the graph of Fig. 4.4b, one can arrive at

$$iS_{\text{eff}}|_{\text{Fig. 4.4b}} = i\int_{\boldsymbol{k}} dt \left( -\lambda_4 \frac{m_{\text{Pl}}^2 \alpha_1^2 \alpha_2^2 m_1^2 m_2^2}{64\Lambda^6} e^{i\boldsymbol{k}\cdot\boldsymbol{r}} \left( \int_{\boldsymbol{q}} \frac{1}{\boldsymbol{q}^2 (\boldsymbol{q}+\boldsymbol{k})^2} \right)^2 \right). \tag{4.29}$$

Once again, the integral over $\boldsymbol{q}$ is one we have been finding in several other places, namely in (4.13), (4.17) and (4.23). We can compute it with the aid of (A.41), so that (4.29) becomes

$$iS_{\text{eff}}|_{\text{Fig. 4.4b}} = i\int dt \left( -\lambda_4 \frac{m_{\text{Pl}}^2 \alpha_1^2 \alpha_2^2 m_1^2 m_2^2}{64\Lambda^6} \frac{\Gamma^2(2-d/2)}{(4\pi)^d} \frac{\Gamma^4(d/2-1)}{\Gamma^2(d-2)} \int_{\boldsymbol{k}} \frac{e^{i\boldsymbol{k}\cdot\boldsymbol{r}}}{(\boldsymbol{k}^2)^{4-d}} \right). \tag{4.30}$$

The integral over $\boldsymbol{k}$ is exactly the same as that of (4.27), and we can compute it with (A.32), so that (4.30) becomes

$$iS_{\text{eff}}|_{\text{Fig. 4.4b}} = i\int dt \left( -\frac{\lambda_4 \pi}{16} \frac{G_N^2 \alpha_1^2 \alpha_2^2 m_1^2 m_2^2}{r} \right). \tag{4.31}$$

Putting (4.28) and (4.31) together, we are able to find the following Lagrangian,

$$\begin{aligned} \mathcal{L}_{\alpha^4\lambda_4 Lv} = &\sum_a \frac{\lambda_4}{12\pi} \frac{G_N^2 \alpha_a^2 m_a^2 \alpha_1 \alpha_2 m_1 m_2}{r} \left( \frac{1}{\epsilon_{\text{UV}}} - 3 - 3\log \bar{\mu} r \right) \\ &- \frac{\lambda_4 \pi}{16} \frac{G_N^2 \alpha_1^2 \alpha_2^2 m_1^2 m_2^2}{r} \sim mv^2 \cdot \alpha^4 \lambda_4 Lv. \end{aligned} \tag{4.32}$$

From the scaling with $v$, we can see that this contribution enters the effective potential at 0.5PN. Again, there is no need to consider self-energy nor far zone contributions, since no IR divergences are encountered.

Similarly to the $\phi^3$ case, the UV pole in (4.32) is related to the point-like nature of the sources. But here, it cannot be absorbed by a simple renormalization of the masses, because it is accompanied by a $1/r$ behavior of the potential. Since this behavior is the same as that coming from a linear exchange between the two particles (cf. (4.12)), one expects this UV pole to lead to the renormalization of the linear coupling of $\phi$ to the point-particles. With this, we see that renormalization is also required already at first order in the $\phi^4$ self-interaction.

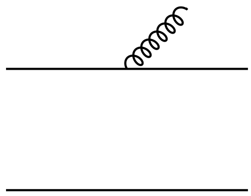

Figure 4.5

## 4.2 Radiative sector

In this section, we compute several contributions to the scalar source, reading off monopole and dipole moments through a matching procedure. In Section 4.2.1, we focus on the leading contribution, that coming from a simple emission of a radiative scalar from each particle. From Section 4.2.2 to 4.2.4, we turn to the computation of the leading contributions from a $\phi^3$, a $\phi\,(\partial\phi)^2$ and $\phi^4$ self-interaction, respectively.

### 4.2.1 Leading order

The leading contribution from the scalar field to the radiative part of the near zone comes from the diagram of Fig. 4.5 and its mirrored counterpart. Such diagrams represent a direct linear coupling between radiative scalars and the point-like sources. Therefore, the only ingredient required is the leading linear coupling (B.6). What we find is

$$iS_{\text{rad}}\big|_{\text{Fig. 4.5}} = \frac{i}{2\Lambda}\int dt \alpha_1 m_1 \bar{\varphi}\,(t,\boldsymbol{x}_1)\,. \tag{4.33}$$

We now write $\bar{\varphi}\,(t,\boldsymbol{x}_1)$ in partial Fourier space, i.e.,

$$\bar{\varphi}\,(t,\boldsymbol{x}_1) = \int_{\boldsymbol{k}} \bar{\varphi}\,(t,-\boldsymbol{k})\, e^{-i\boldsymbol{k}\cdot\boldsymbol{x}_1}. \tag{4.34}$$

Substituting (4.34) into (4.33), we find

$$iS_{\text{rad}}\big|_{\text{Fig. 4.5}} = \frac{i}{2\Lambda}\int_{\boldsymbol{k}} dt\left(\alpha_1 m_1 e^{-i\boldsymbol{k}\cdot\boldsymbol{x}_1}\right)\bar{\varphi}\,(t,-\boldsymbol{k})\,. \tag{4.35}$$

Comparing (4.35) with (3.31), we are able to infer that

$$J_{\text{Fig. 4.5}}\,(t,\boldsymbol{k}) = \alpha_1 m_1 e^{-i\boldsymbol{k}\cdot\boldsymbol{x}_1}. \tag{4.36}$$

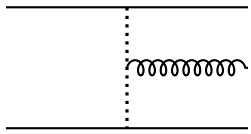

Figure 4.6

These last two steps—writing the external radiative scalar in partial Fourier space and then identifying the contribution to $J\,(t, \boldsymbol{k})$—will always take place in radiative diagrams, and therefore will be omitted in future computations. Expanding the exponential in (4.36), we are able to find

$$J_{\text{Fig. 4.5}+1\leftrightarrow 2}\,(t, \boldsymbol{k}) = \sum_{\ell=0}^{\infty} \frac{(-i)^{\ell}}{\ell!} \left( \sum_a \alpha_a m_a \boldsymbol{x}_a^L \right) \boldsymbol{k}_L. \tag{4.37}$$

By comparing (4.37) with (3.33), one can infer that

$$\int d^3\boldsymbol{x} J_{\text{Fig. 4.5}+1\leftrightarrow 2}\,(t, \boldsymbol{x})\, \boldsymbol{x}^L = \sum_a \alpha_a m_a \boldsymbol{x}_a^L. \tag{4.38}$$

Taking the symmetric trace-free part of both sides of (4.38), one is able to find that

$$\int d^3\boldsymbol{x} J_{\text{Fig. 4.5}+1\leftrightarrow 2}\,(t, \boldsymbol{x})\, \boldsymbol{x}^L_{\text{STF}} = \sum_a \alpha_a m_a \left[ \boldsymbol{x}_a^L \right]_{\text{STF}}. \tag{4.39}$$

But the lhs of (4.39) can be identified with the leading term of expression (3.29), i.e., (3.30). We will call this $\mathcal{I}_0^L$,

$$\mathcal{I}_0^L \equiv \sum_a \alpha_a m_a \left[ \boldsymbol{x}_a^L \right]_{\text{STF}}. \tag{4.40}$$

This process of comparison with (3.33) in order to read off contributions to multipole moments will take place again in the future. In this case, minor steps will be omitted, and we shall simply present a general multipole, or at least both the monopole and dipole moments, which are the ones we want to focus on.

### 4.2.2 Cubic non-derivative self-interaction

Now, we want to consider the leading contribution from the $\phi^3$ self-interaction to the scalar source. This comes from the diagram of Fig. 4.6. This diagram represents the coupling of a radiative scalar to a potential exchange between the two particles. However, in the $\phi^3$ case, this potential exchange cannot be understood as that happening in Fig. 4.2, since the $\phi^3$ vertex introduces two extra momentum powers in the denominator. In order to compute Fig. 4.6, we need the $\Phi^2\bar{\varphi}$ self-coupling (B.9). The corresponding scalar source can be written in the following form,

$$J_{\text{Fig. 4.6}, \phi^3}(t, \boldsymbol{k}) = -\lambda_3 \frac{m_{\text{Pl}}^2 \alpha_1 \alpha_2 m_1 m_2}{4\Lambda^2} e^{-i\boldsymbol{k}\cdot\boldsymbol{x}_1} \int_{\boldsymbol{q}} \frac{e^{i\boldsymbol{q}\cdot\boldsymbol{r}}}{\boldsymbol{q}^2 (\boldsymbol{q}-\boldsymbol{k})^2} + 1 \leftrightarrow 2. \tag{4.41}$$

The two extra momentum powers are now evident by the $(\boldsymbol{q}-\boldsymbol{k})^2$ in the denominator of (4.41). In order to obtain up to dipolar contributions from this expression, we must multipole expand in the external momentum $\boldsymbol{k}$ to first order.[1] For the denominator, we use

$$\frac{1}{(\boldsymbol{q}-\boldsymbol{k})^2} = \frac{1}{\boldsymbol{q}^2} + \frac{2(\boldsymbol{q}\cdot\boldsymbol{k})}{\boldsymbol{q}^4} + O\left(\boldsymbol{k}^2\right). \tag{4.42}$$

Similar denominator expansions will take place again in the future, in which case they shall be skipped. Once we use (4.42) into (4.41), we arrive at an expression involving the following integrals,

$$\int_{\boldsymbol{q}} \frac{e^{i\boldsymbol{q}\cdot\boldsymbol{r}}}{\boldsymbol{q}^4}, \qquad \int_{\boldsymbol{q}} \frac{\boldsymbol{q}}{\boldsymbol{q}^6} e^{i\boldsymbol{q}\cdot\boldsymbol{r}}. \tag{4.43}$$

The integrals in (4.43) can be easily performed with the aid of (A.32) and (A.33), respectively, and end up turning (4.41) into the following expression,

$$J_{\text{Fig. 4.6}, \phi^3}(t, \boldsymbol{k}) = \frac{\lambda_3}{16\pi} \frac{\alpha_1 \alpha_2 m_1 m_2 r}{2} e^{-i\boldsymbol{k}\cdot\boldsymbol{x}_1} \left(1 + \frac{i}{2}\boldsymbol{k}\cdot\boldsymbol{r} + O\left(\boldsymbol{k}^2\right)\right) + 1 \leftrightarrow 2. \tag{4.44}$$

But we also need to expand the exponential to first order in $\boldsymbol{k}$. Once this is done, (4.44) becomes

$$J_{\text{Fig. 4.6}, \phi^3}(t, \boldsymbol{k}) = \sum_a \frac{\lambda_3}{16\pi} \frac{\alpha_1 \alpha_2 m_1 m_2 r}{2} \left[1 - i\boldsymbol{k}\cdot\boldsymbol{x}_a + O\left(\boldsymbol{k}^2\right)\right]. \tag{4.45}$$

This last step of expanding the exponential to first order in $\boldsymbol{k}$ will be omitted in future computations. No IR divergences are encountered in (4.45). Hence, there is no need to consider couplings to self-energy graphs. Comparison of (4.45) with

[1] We will commit the abuse of notation of referring to an expansion in $\boldsymbol{k}/\boldsymbol{q} \sim \boldsymbol{k}\cdot\boldsymbol{x}_a \sim v$ as an expansion in $\boldsymbol{k}$.

(3.33) enables us to read off contributions to the monopole and dipole moments,

$$\mathcal{I}_{\lambda_3} = \frac{\lambda_3}{16\pi}\alpha_1\alpha_2 m_1 m_2 r, \qquad \mathcal{I}^i_{\lambda_3} = \sum_a \frac{\lambda_3}{16\pi}\frac{\alpha_1\alpha_2 m_1 m_2 r}{2}\boldsymbol{x}^i_a.$$

### 4.2.3 Cubic self-interaction with derivatives

Next, let us turn to the leading contribution from the $\phi\,(\partial\phi)^2$ self-interaction to the scalar source. This also comes from Fig. 4.6, but exchanging the $\Phi^2\bar{\varphi}$ vertex for the $(\partial_i\Phi)^2\,\bar{\varphi}$ self-coupling of (B.12). In this case, Fig. 4.6 does indeed represent a coupling to the potential exchange of Fig. 4.2, because the two derivatives of the $\phi\,(\partial\phi)^2$ self-interaction introduce two momentum powers in the numerator, compensating for the ones explained in the previous section. After completing squares, Fig. 4.6 yields

$$J_{\text{Fig. 4.6},\,\phi(\partial\phi)^2}(t,\boldsymbol{k}) = -\sum_a \lambda_{3,2}\frac{\alpha_1\alpha_2 m_1 m_2}{12\Lambda^2}e^{-i\boldsymbol{k}\cdot\boldsymbol{x}_a}\int_{\boldsymbol{q}}\frac{e^{i\boldsymbol{q}\cdot\boldsymbol{r}}}{\boldsymbol{q}^2} + O\left(\boldsymbol{k}^2\right). \tag{4.46}$$

The integral over $\boldsymbol{q}$ is one we have seen in (4.5), (4.11) and (4.21). We can perform it with the aid of (A.32). Once this is done, (4.46) can be shown to give

$$J_{\text{Fig. 4.6},\,\phi(\partial\phi)^2}(t,\boldsymbol{k}) = -\sum_a \lambda_{3,2}\frac{2G_{\text{N}}\alpha_1\alpha_2 m_1 m_2}{3r}\left(1 - i\boldsymbol{k}\cdot\boldsymbol{x}_a\right) + O\left(\boldsymbol{k}^2\right). \tag{4.47}$$

The scalar source (4.47) resembles an analogous result computed in [35] for the stress-energy pseudotensor $T^{\mu\nu}$ at 1PN. This corroborates the similarities between the $\phi\,(\partial\phi)^2$ self-interaction and GR. Once again, no IR divergences are found. Therefore, we do not need to invoke couplings to self-energy graphs. Comparing (4.47) with (3.33), we are able to read off monopolar and dipolar contributions,

$$\mathcal{I}_{\lambda_{3,2}} = -\lambda_{3,2}\frac{4G_{\text{N}}\alpha_1\alpha_2 m_1 m_2}{3r}, \qquad \mathcal{I}^i_{\lambda_{3,2}} = -\sum_a \lambda_{3,2}\frac{2G_{\text{N}}\alpha_1\alpha_2 m_1 m_2}{3r}\boldsymbol{x}^i_a. \tag{4.48}$$

As can be seen, (4.48) is indeed reminiscent of (4.12).

### 4.2.4 Quartic non-derivative self-interaction

Next, let us compute the leading radiative contribution coming from the $\phi^4$ self-interaction. The main diagram is that of Fig. 4.7a. This diagram represents a coupling of radiative scalars to the potential process depicted in Fig. 4.3a. Since

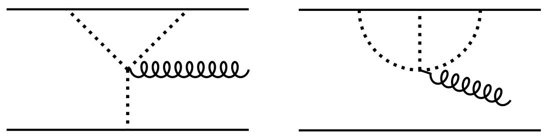

(a) (b)

Figure 4.7

we have encountered an IR divergence in that graph, we expect to be required to consider also the diagram of Fig. 4.7b, which portrays a radiative coupling to the self-energy contribution of Fig. 4.3b. In order to compute these graphs, we need the $\Phi^3\bar{\varphi}$ self-coupling (B.15). The diagram of Fig. 4.7a can be shown to give

$$J_{\text{Fig. 4.7a}}\left(t,\boldsymbol{k}\right) = -\lambda_4 \frac{m_{\text{Pl}}^2 \alpha_1^2 \alpha_2 m_1^2 m_2}{8\Lambda^4} e^{-i\boldsymbol{k}\cdot\boldsymbol{x}_2} \int_{\boldsymbol{q}} \frac{e^{i\boldsymbol{q}\cdot\boldsymbol{r}}}{\left(\boldsymbol{q}+\boldsymbol{k}\right)^2} \int_{\boldsymbol{p}} \frac{1}{\boldsymbol{p}^2\left(\boldsymbol{p}+\boldsymbol{q}\right)^2}. \tag{4.49}$$

The integral over $\boldsymbol{p}$ in (4.49) is once again the same one appearing in (4.13), (4.17), (4.23) and (4.29). After performing it with the aid of (A.41), we can expand the denominator in (4.49) to first order in $\boldsymbol{k}$, yielding two integrals, one at each order. At zeroth order, we have an integral over $\boldsymbol{q}$ which looks exactly the same as that over $\boldsymbol{k}$ in (4.14). This one has an IR divergence, as already discussed. Besides, we have the following integral in the first-order term,

$$\int_{\boldsymbol{q}} \frac{\boldsymbol{q} e^{i\boldsymbol{q}\cdot\boldsymbol{r}}}{\left(\boldsymbol{q}^2\right)^{4-d/2}}.$$

This integral also contains an IR divergence. After performing these two and going through some algebra, we are able to find

$$\begin{aligned} J_{\text{Fig. 4.7a}+1\leftrightarrow 2}\left(t,\boldsymbol{k}\right) =& \frac{\lambda_4}{8\pi} G_{\text{N}} \alpha_1 \alpha_2 m_1 m_2 \times \\ & \times \left[ \sum_a \alpha_a m_a \left( 2\log\bar{\mu}r - \frac{1}{\epsilon_{\text{IR}}} - 1 \right) \right. \\ & - i\boldsymbol{k}\cdot \sum_a \frac{2\alpha_a m_a}{3} \left( 2\log\bar{\mu}r - \frac{1}{\epsilon_{\text{IR}}} - \frac{4}{3} \right) \boldsymbol{x}_a \\ & \left. - i\boldsymbol{k}\cdot \sum_{a\neq b} \frac{\alpha_a m_a}{3} \left( 2\log\bar{\mu}r - \frac{1}{\epsilon_{\text{IR}}} - \frac{1}{3} \right) \boldsymbol{x}_b + O\left(k^2\right) \right], \end{aligned} \tag{4.50}$$

where we have used (4.16). As expected, we encounter IR divergences, with the monopolar contribution of (4.50) closely resembling result (4.15). We need, then, to incorporate self-energy contributions. This is given by the diagram of Fig. 4.7b. This graph might help us identify the coefficients of the IR poles of (4.50). What we find is

$$J_{\text{Fig. 4.7b}}(t, \boldsymbol{k}) = -\lambda_4 \frac{m_{\text{Pl}}^2 \alpha_1^3 m_1^3}{24\Lambda^4} e^{-i\boldsymbol{k}\cdot\boldsymbol{x}_1} \int_{\boldsymbol{q},\boldsymbol{p}} \frac{1}{\boldsymbol{q}^2 (\boldsymbol{p}+\boldsymbol{q})^2 (\boldsymbol{p}+\boldsymbol{k})^2}. \tag{4.51}$$

We must then expand the denominator in (4.51) to first order in $\boldsymbol{k}$. However, the first-order term of this expansion will involve the following integral,

$$\int_{\boldsymbol{q},\boldsymbol{p}} \frac{\boldsymbol{p}}{\boldsymbol{q}^2 \boldsymbol{p}^4 (\boldsymbol{p}+\boldsymbol{q})^2},$$

which vanishes due to the changes of variables $\boldsymbol{q} \to -\boldsymbol{q}$ and $\boldsymbol{p} \to -\boldsymbol{p}$. We are then left with only the zeroth-order term,

$$J_{\text{Fig. 4.7b}}(t, \boldsymbol{k}) = -\lambda_4 \frac{m_{\text{Pl}}^2 \alpha_1^3 m_1^3}{24\Lambda^4} e^{-i\boldsymbol{k}\cdot\boldsymbol{x}_1} \int_{\boldsymbol{q},\boldsymbol{p}} \frac{1}{\boldsymbol{q}^2 \boldsymbol{p}^2 (\boldsymbol{p}+\boldsymbol{q})^2} + O\left(\boldsymbol{k}^2\right). \tag{4.52}$$

The integrals over $\boldsymbol{q}$ and $\boldsymbol{p}$ in (4.52) are exactly the same as those over $\boldsymbol{k}$ and $\boldsymbol{q}$ in (4.17). Those led to the scaleless cancellation of divergences shown in (4.19). In a similar fashion, we are able to find

$$J_{\text{Fig. 4.7b}+1\leftrightarrow 2}(t, \boldsymbol{k}) = \sum_a \frac{\lambda_4}{24\pi} G_{\text{N}} \alpha_a^3 m_a^3 \left(\frac{1}{\epsilon_{\text{UV}}} - \frac{1}{\epsilon_{\text{IR}}}\right)(1 - i\boldsymbol{k}\cdot\boldsymbol{x}_a) + O\left(\boldsymbol{k}^2\right). \tag{4.53}$$

Putting (4.50) and (4.53) together, we are able to write

$$\begin{aligned}
&J_{\text{Fig. 4.7a}+1\leftrightarrow 2}(t, \boldsymbol{k}) + J_{\text{Fig. 4.7b}+1\leftrightarrow 2}(t, \boldsymbol{k}) = \\
&= \frac{\lambda_4}{8\pi} \frac{G_{\text{N}}}{3} \Bigg[ \mathcal{I}_0^3 \left(2\log\bar{\mu}r - 1 - \frac{1}{\epsilon_{\text{IR}}}\right) + \left(\frac{1}{\epsilon_{\text{UV}}} + 1 - 2\log\bar{\mu}r\right) \sum_a \alpha_a^3 m_a^3 \\
&- i\boldsymbol{k}\cdot\Bigg( \mathcal{I}_0^2 \boldsymbol{\mathcal{I}}_0 \left(2\log\bar{\mu}r - \frac{1}{3} - \frac{1}{\epsilon_{\text{IR}}}\right) + \left(\frac{1}{\epsilon_{\text{UV}}} + \frac{1}{3} - 2\log\bar{\mu}r\right) \sum_a \alpha_a^3 m_a^3 \boldsymbol{x}_a \\
&- 2\alpha_1\alpha_2 m_1 m_2 \boldsymbol{\mathcal{I}}_0 \Bigg) \Bigg] + O\left(\boldsymbol{k}^2\right)
\end{aligned} \tag{4.54}$$

Now the coefficients of both IR poles in (4.54) are reminiscent of multipole-radiation couplings, and we have used $\boldsymbol{\mathcal{I}}_0$, the dipole moment coming from (4.40). These coefficients give us a hint as to the far zone diagrams which should be considered: first, three conserved monopole moments interacting via a $\bar{\varphi}^4$ vertex, with the emission of a radiative mode from the vertex; then two conserved monopoles and a dipole moment interacting similarly. The first of these diagrams should cancel out the IR pole in the monopolar contribution of (4.54). The second one should cancel out the IR pole in the dipolar contribution. Because of the similarities between the monopolar contribution of (4.54) and (4.20), whatever happens to the latter in the far zone should also happen to the former. For this reason, we will only compute one of these, namely the far zone contribution from the $\phi^3$ self-interaction to the conservative sector. As we will see, this contribution has problems, and thus so does the $\phi^4$ self-interaction in its radiative sector, leading to the conclusion that both models should be discarded. Hence, there is also no point in computing the second of the diagrams we have just described, i.e., that which should lead to the cancellation of the IR pole in the dipolar contribution of (4.54). Therefore, we will not compute any of these two far zone diagrams in this work. Analogously to all other UV divergences encountered in the near zone, the ones in (4.54) must originate from the fact that we are treating otherwise extended bodies as point-particles.

# Chapter 5

# Far zone dynamics

In this chapter, we will see two main far zone contributions which should be considered. First, in Section 5.1, we will compute the contribution from the interaction between two general multipole couplings to the composite system, and verify how the use of the Feynman prescription naturally leads to an expression for the emitted power. Then, in Section 5.2, we complete the leading contribution from the $\phi^3$ self-interaction to the conservative sector, by computing a far zone diagram which should yield a UV pole that cancels out the IR pole found in the near zone.

## 5.1 Dissipative sector

The first far zone diagram we shall consider is the one shown in Fig. 5.1. This diagram describes the process of emission and reabsorption of a radiative mode corresponding to a general multipole moment by the composite system. That is, each one of the two linear radiative couplings in Fig. 5.1 corresponds to the one-scalar emission amplitude given by (3.28). Besides this one-scalar emission amplitude, we also need the propagator (B.3) for radiative scalars in order to compute this diagram. One interesting remark is that the Feynman prescription seems to take into account both physical possibilities in which the mode is emitted at a point and reabsorbed at the other, as well as the other way around. We are able to find

$$iS_{\text{eff}}\big|_{\text{Fig. 5.1}} = i \sum_{\ell=0}^{\infty} \sum_{\tilde{\ell}=0}^{\infty} \frac{(-i)^{\ell}\, i^{\tilde{\ell}}}{8\Lambda^2 \ell! \tilde{\ell}!} \int_{-\infty}^{\infty} \frac{d\omega}{2\pi} \mathcal{I}^{L}(-\omega)\, \mathcal{I}^{\tilde{L}}(\omega) \int_{\boldsymbol{k}} \frac{\boldsymbol{k}_L \boldsymbol{k}_{\tilde{L}}}{\boldsymbol{k}^2 - \omega^2 - ia}, \tag{5.1}$$

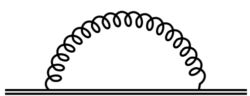

Figure 5.1

where

$$\mathcal{I}^{L}(\omega) = \int dt \mathcal{I}^{L}(t) e^{i\omega t}. \tag{5.2}$$

Note that by taking the complex conjugate of (5.2) and using the fact that $t$, $\omega$ and $\mathcal{I}^{L}$ are all real quantities, one can arrive at

$$\mathcal{I}^{L*}(\omega) = \int dt \mathcal{I}^{L}(t) e^{-i\omega t}. \tag{5.3}$$

But the rhs is just $\mathcal{I}^{L}(-\omega)$. Thus, (5.3) tells us that

$$\mathcal{I}^{L*}(\omega) = \mathcal{I}^{L}(-\omega). \tag{5.4}$$

Substituting (5.4) into (5.1), we can arrive at

$$iS_{\text{eff}}\big|_{\text{Fig. 5.1}} = i\sum_{\ell=0}^{\infty}\sum_{\tilde{\ell}=0}^{\infty}\frac{(-i)^{\ell} i^{\tilde{\ell}}}{8\Lambda^{2}\ell!\tilde{\ell}!}\int_{-\infty}^{\infty}\frac{d\omega}{2\pi}\mathcal{I}^{L*}(\omega)\mathcal{I}^{\tilde{L}}(\omega)\int_{\boldsymbol{k}}\frac{\boldsymbol{k}_{L}\boldsymbol{k}_{\tilde{L}}}{\boldsymbol{k}^{2}-\omega^{2}-ia}. \tag{5.5}$$

In order to proceed, we must perform the integral over $\boldsymbol{k}$. This integral contains no divergences in $d=3$, so we can set this straight away in (5.5), leading to

$$iS_{\text{eff}}\big|_{\text{Fig. 5.1}} = i\sum_{\ell=0}^{\infty}\sum_{\tilde{\ell}=0}^{\infty}\frac{4\pi G_{\text{N}}(-i)^{\ell} i^{\tilde{\ell}}}{\ell!\tilde{\ell}!}\int_{-\infty}^{\infty}\frac{d\omega}{2\pi}\mathcal{I}^{L*}(\omega)\mathcal{I}^{\tilde{L}}(\omega)\int_{\boldsymbol{k}}\frac{\boldsymbol{k}_{L}\boldsymbol{k}_{\tilde{L}}}{\boldsymbol{k}^{2}-\omega^{2}-ia}. \tag{5.6}$$

Now, in order to perform the integral over $\boldsymbol{k}$, we separate the angular integral from the integral over $|\boldsymbol{k}|$. The angular integral can be performed with the aid of the following result [30],

$$\int d\Omega \boldsymbol{n}_{P} = \begin{cases} 0, & p \text{ odd}, \\ \frac{4\pi}{(p+1)}\delta_{(k_1 k_2}\cdots\delta_{k_{p-1}k_p)}, & p \text{ even}. \end{cases} \tag{5.7}$$

This result will not be proven in the present work. As discussed in [30], result (5.7) imposes $\ell=\tilde{\ell}$ in (5.6). This is because the multipole moments are trace-free, and for $\ell\neq\tilde{\ell}$ at least two indices of the same moment appear contracted, yielding zero due to the trace-free condition. Even when $\ell=\tilde{\ell}$, some of the terms in the double series of (5.6) will present indices of the same moment contracted. We need to keep track only of the terms in which all indices of a moment are contracted with all indices of the other. These are the only terms which do not vanish. As explained in [30], this is accounted for by a factor of $\ell!/(2\ell-1)!!$. These considerations turn

(5.6) into

$$iS_{\text{eff}}\big|_{\text{Fig. 5.1}} = i\sum_{\ell=0}^{\infty}\frac{2G_{\text{N}}}{\pi\ell!\,(2\ell+1)!!}\int_{-\infty}^{\infty}\frac{d\omega}{2\pi}\left|\mathcal{I}^{L}(\omega)\right|^{2}\int_{0}^{\infty}\frac{\boldsymbol{k}^{2(\ell+1)}d\left|\boldsymbol{k}\right|}{\boldsymbol{k}^{2}-\omega^{2}-ia}, \tag{5.8}$$

where we have called $\left|\mathcal{I}^{L}(\omega)\right|^{2}\equiv\mathcal{I}^{L*}(\omega)\,\mathcal{I}^{L}(\omega)$. Now we must perform the integral over $|\boldsymbol{k}|$. Notice that this integral can also be written as

$$\int_{0}^{\infty}\frac{d\left|\boldsymbol{k}\right|}{\left(\boldsymbol{k}^{2}\right)^{-\ell-1}\left(\boldsymbol{k}^{2}-\omega^{2}-ia\right)}. \tag{5.9}$$

We now use (A.3) to write

$$\begin{aligned}\frac{1}{\left(\boldsymbol{k}^{2}\right)^{-\ell-1}} &= \frac{1}{\Gamma(-\ell-1)}\int_{0}^{\infty}x^{-\ell-2}e^{-x\boldsymbol{k}^{2}}dx,\\ \frac{1}{\boldsymbol{k}^{2}-\omega^{2}-ia} &= \int_{0}^{\infty}e^{y\left(\omega^{2}+ia\right)}e^{-y\boldsymbol{k}^{2}}dy.\end{aligned} \tag{5.10}$$

Substituting (5.10) into (5.9), we are able to write

$$\int_{0}^{\infty}\frac{\boldsymbol{k}^{2(\ell+1)}d\left|\boldsymbol{k}\right|}{\boldsymbol{k}^{2}-\omega^{2}-ia}=\frac{1}{\Gamma(-\ell-1)}\int_{0}^{\infty}dx\,x^{-\ell-2}\int_{0}^{\infty}dy\,e^{y\left(\omega^{2}+ia\right)}\int_{0}^{\infty}d\left|\boldsymbol{k}\right|e^{-(x+y)\boldsymbol{k}^{2}}. \tag{5.11}$$

The integrand of the integral over $|\boldsymbol{k}|$ is even, so we can also write (5.11) as

$$\int_{0}^{\infty}\frac{\boldsymbol{k}^{2(\ell+1)}d\left|\boldsymbol{k}\right|}{\boldsymbol{k}^{2}-\omega^{2}-ia}=\frac{1}{2\Gamma(-\ell-1)}\int_{0}^{\infty}dx\,x^{-\ell-2}\int_{0}^{\infty}dy\,e^{y\left(\omega^{2}+ia\right)}\int_{-\infty}^{\infty}d\left|\boldsymbol{k}\right|e^{-(x+y)\boldsymbol{k}^{2}}. \tag{5.12}$$

We can now perform the integral over $|\boldsymbol{k}|$ as a Gaussian integral, with the aid of (A.16), so that (5.12) yields

$$\int_{0}^{\infty}\frac{\boldsymbol{k}^{2(\ell+1)}d\left|\boldsymbol{k}\right|}{\boldsymbol{k}^{2}-\omega^{2}-ia}=\frac{\sqrt{\pi}}{2\Gamma(-\ell-1)}\int_{0}^{\infty}\int_{0}^{\infty}dx\,dy\,x^{-\ell-2}e^{y\left(\omega^{2}+ia\right)}\left(x+y\right)^{-1/2}. \tag{5.13}$$

We now perform the change of variables $x=t\alpha$ and $y=t\,(1-\alpha)$. This change of variables has Jacobian equal to $t$, and imposes $t>0$, as well as $0<\alpha<1$, so that (5.13) turns out to be

$$\int_{0}^{\infty}\frac{\boldsymbol{k}^{2(\ell+1)}d\left|\boldsymbol{k}\right|}{\boldsymbol{k}^{2}-\omega^{2}-ia}=\frac{\sqrt{\pi}}{2\Gamma(-\ell-1)}\int_{0}^{1}d\alpha\,\alpha^{-\ell-2}\int_{0}^{\infty}dt\,t^{-\ell-3/2}e^{t(1-\alpha)\left(\omega^{2}+ia\right)}. \tag{5.14}$$

To perform the integral over $t$, we use (A.3) again, so that (5.14) becomes

$$\int_0^\infty \frac{\boldsymbol{k}^{2(\ell+1)} d\,|\boldsymbol{k}|}{\boldsymbol{k}^2-\omega^2-ia} = \frac{\sqrt{\pi}\Gamma\left(-\ell-1/2\right)\left(-\omega^2-ia\right)^{\ell+1/2}}{2\Gamma\left(-\ell-1\right)} \int_0^1 d\alpha \alpha^{-\ell-2}\left(1-\alpha\right)^{\ell+1/2}. \tag{5.15}$$

Now the integral over $\alpha$ is simply the definition of the beta function, i.e., (A.4). Substitution of this definition into (5.15) yields the following expression,

$$\int_0^\infty \frac{\boldsymbol{k}^{2(\ell+1)} d\,|\boldsymbol{k}|}{\boldsymbol{k}^2-\omega^2-ia} = \frac{\sqrt{\pi}\Gamma\left(-\ell-1/2\right)\left(-\omega^2-ia\right)^{\ell+1/2}}{2\Gamma\left(-\ell-1\right)} B\left(-\ell-1,\ell+3/2\right). \tag{5.16}$$

Now we use relation (A.9) to write this beta function in terms of gamma functions, turning (5.16) into

$$\int_0^\infty \frac{\boldsymbol{k}^{2(\ell+1)} d\,|\boldsymbol{k}|}{\boldsymbol{k}^2-\omega^2-ia} = \frac{1}{2}\left(-\omega^2-ia\right)^{\ell+1/2}\Gamma\left(3/2+\ell\right)\Gamma\left(-1/2-\ell\right). \tag{5.17}$$

We can use the fact that $\ell$ is a non-negative integer to write the gamma functions in (5.17) in the following way,

$$\begin{aligned}\Gamma\left(3/2+\ell\right) &= \frac{(1+2\ell)!!}{2^{1+\ell}}\sqrt{\pi},\\ \Gamma\left(-1/2-\ell\right) &= \frac{\left(-2\right)^{1+\ell}}{(1+2\ell)!!}\sqrt{\pi}.\end{aligned} \tag{5.18}$$

Substituting (5.18) into (5.17), we arrive at

$$\int_0^\infty \frac{\boldsymbol{k}^{2(\ell+1)} d\,|\boldsymbol{k}|}{\boldsymbol{k}^2-\omega^2-ia} = \frac{\pi}{2}\left(-\omega^2-ia\right)^{\ell+1/2}\left(-1\right)^{1+\ell}. \tag{5.19}$$

We can then substitute (5.19) into (5.8), yielding

$$iS_{\text{eff}}\big|_{\text{Fig. 5.1}} = i\sum_{\ell=0}^{\infty}\frac{G_{\text{N}}}{\ell!\,(2\ell+1)!!}\int_{-\infty}^{\infty}\frac{d\omega}{2\pi}\left(-\omega^2-ia\right)^{\ell+1/2}\left(-1\right)^{1+\ell}\left|\mathcal{I}^L\left(\omega\right)\right|^2. \tag{5.20}$$

In the limit $a\to 0^+$, $-\omega^2-ia\to\omega^2 e^{-i\pi}$. Taking this limit in (5.20), we are finally able to find out that the effective action associated with the diagram of Fig. 5.1 is actually purely imaginary, and given by the following expression,

$$S_{\text{eff}}\big|_{\text{Fig. 5.1}} = i\sum_{\ell=0}^{\infty}\frac{G_{\text{N}}}{\ell!\,(2\ell+1)!!}\int_{-\infty}^{\infty}\frac{d\omega}{2\pi}\left|\omega\right|^{2\ell+1}\left|\mathcal{I}^L\left(\omega\right)\right|^2,$$

so that

$$\text{Im } S_{\text{eff}}\big|_{\text{Fig. 5.1}} = \sum_{\ell=0}^{\infty} \frac{G_{\text{N}}}{\ell!\,(2\ell+1)!!} \int_{-\infty}^{\infty} \frac{d\omega}{2\pi} |\omega|^{2\ell+1} \left|\mathcal{I}^L(\omega)\right|^2. \tag{5.21}$$

Comparing (5.21) with (3.47) and relating the emission rate to the emitted power, one finds that Fig. 5.1 yields

$$P = \sum_{\ell=0}^{\infty} \frac{2G_{\text{N}}}{\ell!\,(2\ell+1)!!} \left\langle \left( \frac{d^{\ell+1}}{dt^{\ell+1}} \mathcal{I}^L \right)^2 \right\rangle. \tag{5.22}$$

This is the leading expression for the emitted power. In principle, any far zone diagram can lead to a nonzero imaginary part of the effective action, and therefore can contribute to the emitted power. Note that each term in (5.22) corresponds to a pair of multipoles of the same order. That is, we always have monopole with monopole, dipole with dipole, and so on. In general, a given multipole moment has the following scaling,

$$\mathcal{I}^L \sim \beta m r^\ell, \tag{5.23}$$

where $\beta$ is a dimensionless constant resulting from some combination of $v$, $L$, $\alpha_a$, $\lambda_3$, $\lambda_{3,2}$, $\lambda_4$, or any other dimensionless coupling in the theory. Using (5.23) into (5.22) and noting that time derivatives scale as $v/r$, we find out that the series in (5.22) is truly an expansion in the small parameter $v$,

$$P \sim m^2 L^{-1} \beta^2 \sum_{\ell=0}^{\infty} v^{2\ell+5}, \tag{5.24}$$

the $\ell$-th term being

$$P_{\beta^2 v^{2\ell-4}} \sim m^2 L^{-1} v^9 \cdot \beta^2 v^{2\ell-4}. \tag{5.25}$$

The reason why we have written (5.25) in this way is in order to emphasize the scaling with respect to the standard GR result for the leading gravitational flux, which is actually quadrupolar and can be written for a circular orbit of frequency $\omega$ and radius $R$ as

$$P_g \equiv \frac{32}{5} \frac{G_{\text{N}}^4 M^3 \mu^2}{R^5} \sim m^2 L^{-1} v^9, \tag{5.26}$$

where $\mu \equiv m_1 m_2 / M$ is now being used to denote the reduced mass of the system, with $M \equiv \sum_a m_a$ [12]. Thus, given a certain scalar multipole moment, we know $\beta$ and $\ell$, and therefore we are able to infer at what order this multipole moment enters the emitted power.

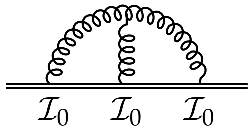


Figure 5.2

## 5.2 Cubic non-derivative self-interaction

Next, we want to consider the leading contribution from the $\phi^3$ self-interaction to the far zone. This comes from the diagram of Fig. 5.2. If we think about it, its computation should look just like that of Fig. 4.3b. This is because we are considering conserved sources, i.e., $\mathcal{I}_0$. For this reason, we can essentially recycle previous results (cf. (4.19)), replacing $\sum_a \alpha_a^3 m_a^3$ by $\mathcal{I}_0^3$. But for instructive purposes let us try to go through the computation just a bit. We need to select the monopole term in the one-scalar emission amplitude (3.28), and then substitute the monopole moment given in (4.40). We also need the $\bar{\varphi}^3$ self-coupling (B.10). Putting all of this together, we are able to find an expression involving a product such as follows,

$$\int dt_a \mathcal{I}_0 e^{ik_0 t_a} \int dt_b \mathcal{I}_0 e^{iq_0 t_b} \int dt_c \mathcal{I}_0 e^{ip_0 t_c}. \tag{5.27}$$

If the sources were time-dependent, this would yield a product of Fourier transforms. But since $\dot{\mathcal{I}}_0 = 0$, (5.27) yields

$$\mathcal{I}_0^3 \int dt_a e^{ik_0 t_a} \int dt_b e^{iq_0 t_b} \int dt_c e^{ip_0 t_c}. \tag{5.28}$$

But each one of the integrals in (5.28), of course, yields a delta function selecting frequency equal to zero,

$$\mathcal{I}_0^3 \left(2\pi\right)^3 \delta\left(k_0\right) \delta\left(q_0\right) \delta\left(p_0\right),$$

so that the integration involved in Fig. 5.2 turns out to look just like that of Fig. 4.3b, yielding the result

$$\mathcal{L}^{\text{far}}_{\alpha^3 \lambda_3 L v^{-1}} = \frac{\lambda_3}{16\pi} \frac{G_N \mathcal{I}_0^3}{3} \left( \frac{1}{\epsilon_{\text{UV}}} - \frac{1}{\epsilon_{\text{IR}}} \right). \tag{5.29}$$

# Chapter 6

# Results and conclusions

In this chapter, we discuss the results obtained in Chapters 4 and 5. In Section 6.1, we use a result from [12] in order to compare leading monopolar power with leading dipolar power emitted in scalars, in the absence of self-interactions. In Section 6.2, we discuss the troublesome behavior of the $\phi^3$ model in its conservative sector, and argue as to its origins. In Section 6.3, we analyze the leading contributions from the $\phi\,(\partial\phi)^2$ self-interaction, verifying its similarities with GR and determining a phenomenological bound on a combination of parameters. In Section 6.4, we analyze the troublesome behavior of the $\phi^4$ self-interaction in its radiative sector, drawing a connection with the $\phi^3$ self-interaction. Finally, in Section 6.5, we summarize the conclusions coming from our results.

## 6.1 Monopole vs dipole without self-interactions

A massless scalar field without self-interactions, in the context of the inspiral problem, has already been studied in [12]. In the discussion that follows, we are going to use several results from that paper which have not been worked out here.

We have seen, as has also been done in [12], that the leading monopole moment coming from the scalar field is obtained by setting $\ell = 0$ into (4.40), i.e.,

$$\mathcal{I}_0 = \sum_a \alpha_a m_a. \tag{6.1}$$

In principle, the contribution from (6.1) to the emitted power would have the following scaling,

$$P_{\alpha^2 v^{-4}} \sim m^2 L^{-1} v^9 \cdot \alpha^2 v^{-4}, \tag{6.2}$$

and would therefore enter at $-2$PN. However, as has also been pointed out in [12], $\alpha_a$ and $m_a$ are constants, i.e., (6.1) is conserved, so that it cannot contribute to the emitted power, since monopolar power comes with a time derivative of the monopole moment (cf. (5.22)). We are then required to go to the next order, which consists of two main contributions. First, we can compute $v^2$ corrections to the monopole moment (6.1). This has already been done in [12], and yields the answer

$$\mathcal{I}_{v^2} = -\frac{1}{6}\sum_a \alpha_a m_a v_a^2 + g_{12}\frac{G_N m_1 m_2}{r}, \tag{6.3}$$

where[1]

$$\begin{aligned} g_{12} &\equiv \frac{\kappa_{12}}{6}\left(\alpha_1 - \alpha_2\right) - \frac{7}{6}\left(\alpha_1 + \alpha_2\right), \\ \kappa_{12} &= \frac{m_1 - m_2}{m_1 + m_2}. \end{aligned} \tag{6.4}$$

We could then consider how mixed terms involving (6.1) and (6.3) would enter the emitted power. However, once again, (6.1) is conserved, so this contribution also vanishes. Another contribution to the next order comes from the leading dipole moment, obtained by setting $\ell = 1$ into (4.40),

$$\mathcal{I}_0^i = \sum_a \alpha_a m_a \boldsymbol{x}_a^i. \tag{6.5}$$

The dipole moment enters the expression for the emitted power with two time derivatives acting on it (cf. (5.22)). By taking two time derivatives of (6.5), we arrive at something proportional to the accelerations of the particles. Since the particles do accelerate due to the binding forces which hold the system together, this does lead to a nonzero loss of energy in the form of radiation [28]. For consistency with what is going to be examined shortly, let us consider the case of an elliptical orbit. Using the CM frame condition $\sum_a m_a \boldsymbol{x}_a = \boldsymbol{0}$, one can write the positions of the particles in terms of $\boldsymbol{r}$ only (cf. (4.4)),

$$\boldsymbol{x}_1 = \frac{m_2}{M}\boldsymbol{r}, \qquad \boldsymbol{x}_2 = -\frac{m_1}{M}\boldsymbol{r}. \tag{6.6}$$

The elliptical orbit can then be parametrized in terms of the azimuth angle $\theta$ by

$$r = \frac{a\left(1 - e^2\right)}{1 + e\cos\theta}, \tag{6.7}$$

where $a$ is the semi-major axis and $e$ is the eccentricity [36]. Using (6.6) and (6.7) into (6.5), and then plugging (6.5) into the dipole term of expression (5.22) for the

[1]Note that, in writing (6.4), we have neglected $O\left(\alpha^2\right)$ terms, as well as a quadratic matter coupling which is considered in [12].

emitted power, one is able to find, after some algebra,

$$P_{\text{dip}} = \frac{G_{\text{N}}^3 M^2 \mu^2}{3a^4} \frac{(\alpha_1 - \alpha_2)^2 \left(e^2 + 2\right)}{\left(1 - e^2\right)^{5/2}} \sim m^2 L^{-1} v^9 \cdot \alpha^2 v^{-2}. \tag{6.8}$$

One can now see explicitly that (6.8) enters at $-1$PN. As has also been pointed out in [12], the closer the scalar charges of the objects, the smaller the value of the dipole power, which is the case for a BH-BH system or two comparable neutron stars. Thus, the optimal scenario is that of a BH-NS system [12].[2] In the limit $e \to 0$, we find for (6.8) an expression valid for a circular orbit of radius $a \to R$,

$$P_{\text{dip}} \to \frac{2G_{\text{N}}^3 M^2 \mu^2}{3R^4} (\alpha_1 - \alpha_2)^2 \,.$$

But we must remind ourselves that our goal is to compare leading monopolar power with leading dipolar power, in the absence of self-interactions. And since no monopolar power enters at this order, we must go to higher order still. Once more, going to the next order involves the consideration of two main types of contribution. First, we can consider how quadratic terms in the $v^2$ corrections (6.3) enter the emitted power. And secondly, we can compute $v^2$ corrections to the dipole moment (6.5), and then see how mixed terms involving these corrections and the leading dipole moment (6.5) enter the emitted power. However, for purposes of comparison between monopolar and dipolar power, only the leading contribution (6.8) is relevant. We can then proceed to the consideration of the first of these types of contribution, i.e., quadratic terms in the $v^2$ monopolar corrections (6.3). For a circular orbit, $v_a$ and $r$ are both constant, in which case (6.3) does not contribute to the emitted power. This is the reason why we have considered the case of an elliptical orbit when computing (6.8). Doing the same here, we are able to find, after some algebra,

$$P_{\text{mono}} = \frac{G_{\text{N}}^4 M^3 \mu^2}{4a^5} \frac{e^2 \left(e^2 + 4\right)}{\left(1 - e^2\right)^{7/2}} \left( \sum_a \frac{\alpha_a \mu}{3m_a} - g_{12} \right)^2 \sim m^2 L^{-1} v^9 \cdot \alpha^2 v^0, \tag{6.9}$$

where one can now see explicitly that this contribution enters at 0PN. If we divide

[2] Note that the scalar charge of a BH must be zero due to the no-hair theorem [12, 37].

(6.9) by (6.8), we arrive at

$$\frac{P_{\text{mono}}}{P_{\text{dip}}} = \frac{3G_{\text{N}}M}{4a} \frac{e^2\left(e^2+4\right)}{\left(e^2+2\right)\left(1-e^2\right)} \left(\frac{\frac{\mu}{3}\sum_a \frac{\alpha_a}{m_a} - g_{12}}{\alpha_1-\alpha_2}\right)^2. \tag{6.10}$$

Considering the case, for instance, of a BH-NS system, in which we have $\alpha_{\text{BH}} = 0$ due to the no-hair theorem [12, 37], (6.10) can be worked out to give

$$\frac{P_{\text{mono}}}{P_{\text{dip}}} = \frac{25}{12}u^2\left(1-\frac{2}{5}\rho_{\text{NS}}\right)^2 \frac{e^2\left(e^2+4\right)}{\left(1-e^2\right)\left(e^2+2\right)}, \tag{6.11}$$

where we have cleverly called

$$u \equiv \sqrt{\frac{G_{\text{N}}M}{a}},$$

and $\rho_{\text{NS}}$ is the fractional mass of the NS,

$$\rho_{\text{NS}} \equiv \frac{m_{\text{NS}}}{M}.$$

Strikingly, (6.11) does not depend on the $\phi$-charge of the NS, which we of course assume to be non-zero, otherwise there would be no monopolar nor dipolar power emitted. Since a typical NS is of relatively low mass ($\sim m_\odot$) in comparison with a stellar BH ($\sim (3-10)\, m_\odot$), we will go on and assume $\rho_{\text{NS}} = 0.2$ [22]. At the same time, $u$ is of order of the typical relative velocity of the system, which spans roughly $0.1 < u < 0.4$ during the inspiral phase [22]. So we plot (6.11) as a function of the eccentricity for the values $u = 0.1, 0.2, 0.3, 0.4$. This is shown in Fig. 6.1. The Mathematica notebook used to arrive at this plot is available at `https://www.dropbox.com/s/mcu3d8cni78ox4r/mono-dip.nb?dl=0`.

*We conclude that, in the absence of self-interactions, leading monopolar power becomes important only for highly eccentric orbits ($e \gtrsim 0.8$). Also, the slower the bodies move, the higher the eccentricity required.*

## 6.2 Cubic non-derivative self-interaction

The leading contribution from the $\phi^3$ self-interaction to the radiative dynamics comes only from Fig. 4.6, and yields the scalar source given in (4.45). We find no divergences in (4.45). So this contribution seems promising, resulting in the

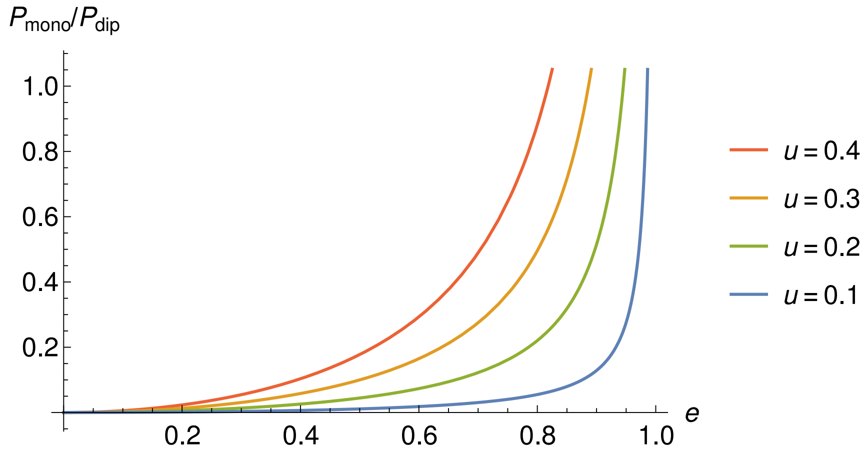


Figure 6.1

following monopole and dipole moments,

$$\mathcal{I}_{\lambda_3} = \frac{\lambda_3}{16\pi}\alpha_1\alpha_2 m_1 m_2 r, \qquad \mathcal{I}^i_{\lambda_3} = \sum_a \frac{\lambda_3}{16\pi}\frac{\alpha_1\alpha_2 m_1 m_2 r}{2}\boldsymbol{x}^i_a.$$

In the conservative sector, on the other hand, we encounter some problems. The coefficient of the IR pole in (4.20) is indeed minus the coefficient of the UV pole in (5.29), so that these two cancel out. However, there is an IR pole coming from the far zone. And it looks exactly like that of (4.20). This means that, overall, nothing changes, and the final, leading effective Lagrangian coming from the $\phi^3$ self-interaction will look just like (4.20), entering at $-0.5$PN,

$$\begin{aligned}\mathcal{L}_{\alpha^3\lambda_3 L v^{-1}} &= \frac{\lambda_3}{16\pi}\frac{G_N \mathcal{I}_0^3}{3}\left(2\log\bar{\mu}r - 1 - \frac{1}{\epsilon_{\text{IR}}}\right) \\ &\quad + \left(\frac{1}{\epsilon_{\text{UV}}} + 1 - 2\log\bar{\mu}r\right)\sum_a \frac{\lambda_3}{16\pi}\frac{G_N\alpha_a^3 m_a^3}{3}.\end{aligned} \tag{6.12}$$

This was expected, since the contribution from the far zone, albeit due to the cancellation of two divergences, is zero nevertheless. But it is important to emphasize the origin of each divergence, since this leads to the ultimate cause of inconsistencies. The IR divergence in (4.20) is due to a lack of information at *large* distances, and is compensated by the UV divergence in (5.29), which signals a lack of information at *short* distances. In other words, the near (far) zone is the UV (IR) completion of the far (near) zone. And the near zone might yet have its own UV completion, since we are treating astrophysical bodies as if they had no internal structure, when we know for a fact they do. However, there is no IR completion to the far zone.

And this is why the IR pole in (5.29) is so problematic. Generally speaking, an IR divergence means that something is going wrong at large distances. Our goal here is to argue that, in the presence of a $\phi^3$ self-interaction, the scalar field is driven into a non-perturbative regime as the distance from the source increases.

In order to see this, let us try to reproduce the physical situation leading to the IR divergence. The IR singularity comes from the far zone diagram of Fig. 5.2, in which a static source interacts three times with a $\bar{\varphi}^3$ vertex via emission and reabsorption of radiative scalars. The first thing we note is that the source is static. Secondly, only scalars are present, i.e., the response of the metric is being neglected, meaning spacetime can be taken as that of Minkowski. Finally, the $\phi^3$ self-interaction is present. Thus, if we can solve for the scalar field generated by a static source in Minkowski spacetime and in the presence of a $\phi^3$ potential, this might give us some insight as to the cause of the issue. The answer should be the solution to the following equation of motion (EOM),

$$\Box\phi = \frac{\lambda_3}{2}\phi^2 - \frac{1}{2}J, \tag{6.13}$$

where we have set $m_{\text{Pl}} = 1$ for simplicity. We will take the source to be spherical and static, with radius and mass set equal to unity,

$$J = \begin{cases} \frac{3\alpha}{4\pi}, & 0 < d < 1, \\ 0, & d > 1, \end{cases}$$

where $d$ is the distance from the source.[3] And we shall analyze the cases $\alpha = 1$ and $\alpha = -1$, so that we can see the differences between positive and negative $\phi$-charge. Because the source is static and spherically symmetric, $\phi$ should only depend on $d$. Plugging this into (6.13) yields

$$\phi'' + \frac{2}{d}\phi' - \frac{\lambda_3}{2}\phi^2 + \frac{1}{2}J = 0, \tag{6.14}$$

where $'$ denotes derivative with respect to $d$. In order to solve (6.14), we need boundary conditions. In particular, we require that the field is well-behaved at the origin, meaning both $\phi$ and $\phi'$ go to zero as $d \to 0$. Also, we impose continuity of $\phi$ and $\phi'$ at the surface of the solid sphere. We cannot solve this problem analytically. Instead, we need to resort to numerical methods.

[3] Unfortunately, $r$ is already being used to denote the size of the orbit.

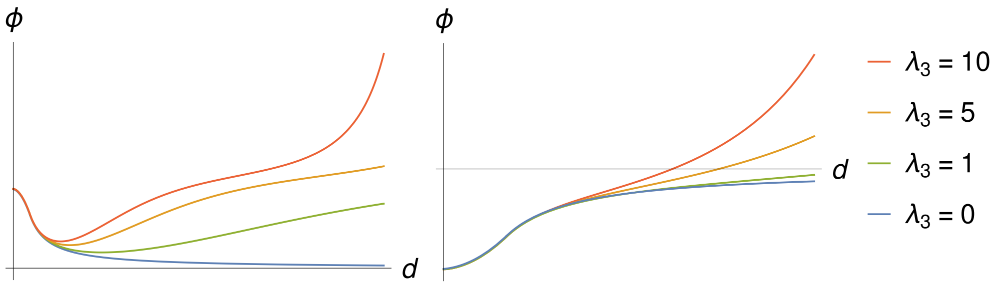


(a) $\alpha > 0$ (b) $\alpha < 0$

Figure 6.2

Plugging (6.14) and its boundary conditions into Mathematica, we arrive at the plots shown in Fig. 6.2. In Fig. 6.2a, we have set $\alpha = 1$, to see the behavior of the solution for positive $\alpha$. In Fig. 6.2b, we have set $\alpha = -1$, to see the behavior for negative $\alpha$. In blue, we have the analytical solution in the absence of the $\phi^3$ self-interaction. From green to red, we have numerical solutions for the increasing values of $\lambda_3 = 1, 5, 10$. The choice of colors is purposeful, meaning to draw a merely illustrative association between the troublesome behavior of the field at large distances with the infrared divergence we have encountered. We have also shifted the field so that the analytical solution would go to zero at infinity. After all, in Chapter 3 we have assumed an expansion around the background value $\phi = 0$ during the weak-field limit. The Mathematica notebook used to arrive at these plots is available at `https://www.dropbox.com/s/xzkgxyk0b4xaqvg/num.nb?dl=0`.

As can be seen in Fig. 6.2, the numerical solutions found in the presence of a $\phi^3$ self-interaction tend to diverge for a finite value of $d$. In particular, Mathematica finds a singularity at about $d \approx 23.6$ and $d \approx 5.4$ for the red solutions of Fig. 6.2a and 6.2b, respectively. This is a problem in itself, since the $\phi^3$ potential seems to render the scalar field unphysical given a perfectly static source. But moreover, we have assumed in Chapter 3 that the scalar fluctuations around the background value $\phi = 0$ were small. But the numerical solutions of Fig. 6.2 clearly tell us otherwise. The approximation gets worse the larger the value of $d$.

*We claim that this singular behavior of the $\phi^3$ model at large distances might be the ultimate cause of the IR divergence found in the far zone. Thus, this inconsistency is not necessarily a flaw of the formalism, but of the model employed and the assumptions made. In any case, the $\phi^3$ self-interaction drives the scalar field to arbitrarily large values, so that this model should be discarded.*

## 6.3 Cubic self-interaction with derivatives

The $\phi\,(\partial\phi)^2$ self-interaction is the most promising of all three, since its two derivatives make it the closest to GR. For the effective Lagrangian, we have simply the 1PN contribution (4.22), since all other diagrams vanish,

$$\mathcal{L}_{\alpha^3\lambda_{3,2}v^2} = -\sum_a \lambda_{3,2}\frac{2G_N^2\alpha_a m_a \alpha_1\alpha_2 m_1 m_2}{3r^2},$$

and no divergences are encountered.

For the radiative dynamics, the situation is similar, i.e., the only non-vanishing contribution is that of Fig. 4.6. The scalar source is then simply (4.47). The latter is reminiscent of the Newtonian correction (4.12). Indeed, the graph of Fig. 4.6, in the $\phi\,(\partial\phi)^2$ case, can be understood as arising from the insertion of an external radiative mode into the propagator of Fig. 4.2 via a $\phi\,(\partial\phi)^2$ vertex. This insertion splits the propagator in two, adding an extra power of $\boldsymbol{q}^2$ in the denominator. However, the split comes with no extra integration, since momentum is conserved at the vertex and the external momentum is not integrated over. At the same time, the two derivatives of the self-interaction contribute with a power of $\boldsymbol{q}^2$ in the numerator, compensating for the extra propagator. Overall, the scaling of the diagram does not change, and its contribution looks the same. Comparing (4.47) with (3.33), we are able to read off leading monopole and dipole moments coming from the $\phi\,(\partial\phi)^2$ self-interaction,

$$\mathcal{I}_{\lambda_{3,2}} = -\lambda_{3,2}\frac{4G_N\alpha_1\alpha_2 m_1 m_2}{3r}, \qquad \mathcal{I}^i_{\lambda_{3,2}} = -\sum_a \lambda_{3,2}\frac{2G_N\alpha_1\alpha_2 m_1 m_2}{3r}\boldsymbol{x}^i_a. \tag{6.15}$$

Because the $\phi\,(\partial\phi)^2$ self-interaction is so well-behaved, it is justifiable to compute its leading contribution to the emitted power. In principle, this comes from substituting the leading monopole moment of (4.40) and the one in (6.15) into the monopole term of (5.22). But since the monopole moment in (4.40) is conserved, this contribution vanishes, and we have to go to higher order. One option is the dipole order. However, for consistency with the expansion in $v$, we would also need to compute corrections to the monopole moments, and also higher-order far zone diagrams, such that these would enter the emitted power at the same order as the dipole. But, for the sake of simplicity, let us not worry about this here, and compute simply the dipole power resulting from substituting the dipole moment of (4.40) and the dipole moment of (6.15) into (5.22). Assuming the case of a circular orbit, this results in

$$P_{\lambda_{3,2}} = \lambda_{3,2}\alpha_1\alpha_2 \frac{8G_N^4 M^2 \mu^2}{9R^5} \left(\alpha_1 - \alpha_2\right)\left(m_1 - m_2\right) \sim m^2 L^{-1} v^9 \cdot \alpha^3 \lambda_{3,2} v^0. \tag{6.16}$$

From the scaling with $v$, we can see that (6.16) enters the emitted power at 0PN. One interesting aspect of (6.16) is that, due to the differences $\alpha_1 - \alpha_2$, $m_1 - m_2$, and also due to our ignorance about the signs of the coupling constants, (6.16) could, in principle, be negative, implying an amount of energy being absorbed by the system.[4] This is no reason for concern, as long as (6.16) is only a small correction to the leading quadrupolar power predicted by GR (cf. (5.26)). Another feature of (6.16) is that, the smaller the differences $\alpha_1 - \alpha_2$ and $m_1 - m_2$, the smaller the amount of power involved, in a way similar to what was discussed in Section 6.3 for the specific case of the scalar charge in the leading dipole power. From the 90% upper bound on the 0PN test coefficient discussed in [38], one can expect the following constraint,

$$\left|\lambda_{3,2}\alpha_1\alpha_2\left(\alpha_1 - \alpha_2\right)\right| \lesssim \frac{0.72}{\sqrt{1-4\eta}}, \tag{6.17}$$

where $\eta \equiv \mu/M$ is the symmetric mass ratio. The latter is a measure of how close the masses of the constituents are to each other. In this regard, we have two main possible scenarios. First, the masses of the constituents can be roughly the same, in which case $\eta$ reaches its maximum value of $1/4$ and the rhs of (6.17) goes to infinity, and we find no constraint. The second possibility is that the masses are too far apart from each other, in which case $\eta$ approaches zero and the constraint (6.16) reaches its peak. In other words, the constraint is strongest in the extreme mass ratio limit [22]. For this limiting case, we plug $\eta \to 0$ into (6.17), and of course what we find is

$$\left|\lambda_{3,2}\alpha_1\alpha_2\left(\alpha_1 - \alpha_2\right)\right| \lesssim 0.72.$$

At first, this constraint does not seem very satisfying. This might be because we have neglected many other contributions entering at the same order.

The aforementioned 90% upper bound discussed in [38] comes from direct GW detections. There are, however, indirect evidences of GWs. One of them is

[4] Note that we are assuming a sign convention in which positive power means energy being *lost* by the system, i.e., $dE/dt = -P$, just as in [22].

the orbital decay of B1913+16, the first binary pulsar ever discovered. The rate of change of its orbital period is known to agree with that predicted by the emission of standard quadrupolar radiation to within an outstanding precision of 0.2% [34, 39]. This quantity is computed in terms of the 0PN flux. So if (6.9) and (6.16)—both entering at 0PN—are also to account for this decay, these contributions should be constrained to be about $10^{-3}$ times the quadrupole formula of GR, providing good limits for several parameters in our theory. This would require, however, computing (6.16) for the case of an elliptical orbit, since B1913+16 has an eccentricity of about 0.6. We leave the actual computation of these limits for a future work, as well as the incorporation of several more GR tests into the picture.

*We conclude that the $\phi\left(\partial\phi\right)^2$ self-interaction behaves in a way similar to GR, being promising in both conservative and dissipative sectors. This is due to the fact that it has two derivatives, much like any self-interaction in GR. From one of its leading contributions to the emitted power, we can constrain $\left|\lambda_{3,2}\alpha_1\alpha_2\left(\alpha_1-\alpha_2\right)\right| \lesssim 0.72$, where we assume the extreme mass ratio limit.*

## 6.4 Quartic non-derivative self-interaction

The leading contribution from the $\phi^4$ self-interaction to the conservative sector is given by (4.32) alone,

$$\mathcal{L}_{\alpha^4\lambda_4 Lv} = \sum_a \frac{\lambda_4}{12\pi}\frac{G_\mathrm{N}^2\alpha_a^2 m_a^2\alpha_1\alpha_2 m_1 m_2}{r}\left(\frac{1}{\epsilon_\mathrm{UV}} - 3 - 3\log\bar{\mu}r\right) - \frac{\lambda_4\pi}{16}\frac{G_\mathrm{N}^2\alpha_1^2\alpha_2^2 m_1^2 m_2^2}{r}. \tag{6.18}$$

From the scaling with $v$ (cf. (4.32)), one can see that this contribution enters at 0.5PN. Since no IR divergences arise in this final Lagrangian, this contribution looks promising. As explained in Chapter 4, the UV pole in (6.18) is related to the point-like nature of the initial EFT assumed for the description of the two bodies (cf. (3.3)). Therefore, this pole offers a window into probing internal DOFs. Because this UV pole is accompanied by a $1/r$ behavior of the potential—the same behavior coming from the linear exchange depicted in Fig. 4.2—, we expect it to lead to the renormalization of the scalar charges. In order to see this, consider the addition of the following counterterms to the point-particle action,

$$S^\phi_\mathrm{c.t.} \equiv \sum_a c_\phi^{(a)} m_a \int d\tau_a \frac{\phi\left(x_a\right)}{2\Lambda}, \tag{6.19}$$

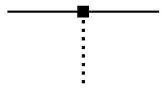

Figure 6.3

where $c_\phi^{(a)}$ are the coefficients for the counterterms and we again borrow the notation of [23]. If we perturb (6.19) around Minkowski spacetime and decompose the fields into orbital and radiative parts, we can arrive at the following counterterm for the leading linear coupling of point-particles to orbital scalars,

$$S_{\text{c.t.}}^{\Phi v^0} \equiv \sum_a c_\phi^{(a)} m_a \int dt_a \frac{\Phi\left(x_a\right)}{2\Lambda}, \tag{6.20}$$

represented in Feynman diagrams for each particle as shown in Fig. 6.3. From (6.20), as well as (B.5), we can compute the diagram shown in Fig. 6.4, which, together with its mirror image, yields the following effective Lagrangian,

$$\mathcal{L}_{c_\phi \alpha} \equiv \sum_{a \neq b} \frac{2G_{\text{N}} c_\phi^{(a)} \alpha_b m_1 m_2}{r}. \tag{6.21}$$

In order for (6.21) to cancel out the UV pole in (6.18), we must select

$$c_\phi^{(a)} = -\frac{1}{\epsilon_{\text{UV}}} \frac{\lambda_4}{24\pi} G_{\text{N}} \alpha_a^3 m_a^2,$$

leading to an RG flow equation for the scalar charge,

$$\mu \frac{d}{d\mu} \alpha_{a,\text{ren}}\left(\mu\right) = \frac{\lambda_4}{8\pi} G_{\text{N}} \alpha_a^3 m_a^2.$$

In the radiative sector, on the other hand, the $\phi^4$ self-interaction is problematic. This can be seen by looking at (4.54), where the monopolar contribution looks just like the near zone contribution from the $\phi^3$ vertex. Even though we have not computed the relevant far zone diagram in this work, we can expect that it will contribute to this monopole moment in the same way that Fig. 5.2 does to

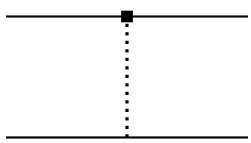

Figure 6.4

the final Lagrangian (6.12). Then at least one IR divergence should remain in the final answer, similarly to what happened in the conservative sector of the $\phi^3$ self-interaction. Indeed, the graphs of Fig. 4.7 can be obtained by plugging an external radiative mode into the bulk vertices of Fig. 4.3 via a $\phi^4$ vertex. Differently from the case explained in Section 6.3, this does not yield an extra propagator, since this mode is inserted into a vertex and not into the middle of a propagator. For the same reason, no extra integration appears. Also, because the self-interaction is non-derivative, no powers of $\boldsymbol{q}$ are brought into the numerator. Overall, nothing changes, and the contributions look the same.

*Therefore, it seems inevitable to conclude that the issues arising in the leading contribution from the $\phi^4$ self-interaction to the radiative sector are due once more to the non-perturbative nature of the $\phi^3$ self-interaction, and that, for this reason, the $\phi^4$ model should also be discarded.*

## 6.5 Conclusions

To summarize, we discover that, in the absence of self-interactions, leading monopolar power exists only for elliptical orbits, and it overcomes leading dipolar power at high eccentricities ($e \gtrsim 0.8$). Moreover, the slower the bodies move, the higher the eccentricities required for leading monopolar power to start dominating.

At the same time, we find that both $\phi^3$ and $\phi^4$ models should be discarded. The former presents an inconsistency in the conservative sector, and the latter presents an inconsistency in the radiative sector of the same nature. In spite of that, we still discuss the UV behavior of the $\phi^4$ self-interaction, leading to the renormalization of the scalar charges. This is because the UV-divergent $\phi^4$ diagram may still appear as a subdiagram of some higher-order self-interaction $\phi^n$. One such example is given in Fig. 6.5, which presents a momentum integration of the following form,

$$\int_{\boldsymbol{k},\boldsymbol{q}_1,\cdots,\boldsymbol{q}_{n-2}} \frac{e^{i\boldsymbol{k}\cdot\boldsymbol{r}}}{\boldsymbol{k}^2\left(\boldsymbol{k}-\boldsymbol{q}_1\right)^2\left(\boldsymbol{q}_1-\boldsymbol{q}_2\right)^2\cdots\left(\boldsymbol{q}_{n-3}-\boldsymbol{q}_{n-2}\right)^2\boldsymbol{q}_{n-2}^2}. \tag{6.22}$$

The last two integrals in (6.22)—those over $\boldsymbol{q}_{n-3}$ and $\boldsymbol{q}_{n-2}$—are present whenever $n \geq 4$, and are precisely the ones we have found in (4.23), thus being UV-divergent.

As for the $\phi\,(\partial\phi)^2$ self-interaction, we find that it behaves in a way similar to any cubic self-coupling coming from standard GR. This is due to the fact that it presents two derivatives, much like any self-interaction coming from the Ricci scalar. From its contribution to the dissipative sector, we are able to constrain

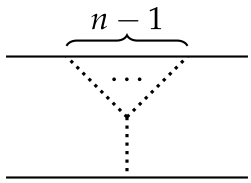


Figure 6.5

$|\lambda_{3,2}\alpha_1\alpha_2\,(\alpha_1-\alpha_2)| \lesssim 0.72$, where the extreme mass ratio limit is understood.

For the future, we plan to investigate both IR and UV behaviors of a general non-derivative self-interaction $\phi^n$ and a general self-interaction with many derivatives $\partial^m\phi^n$.

# Appendix A

# Identities and integrals

In this appendix, we present and prove several identities and integrals used in our calculations.

## A.1 The gamma function

The gamma function is defined as

$$\Gamma(z) \equiv \int_0^\infty x^{z-1} e^{-x} dx. \tag{A.1}$$

On the rhs of (A.1), we perform the change of variables $x \to x\Delta$, with $\Delta > 0$, so that

$$\Gamma(z) = \Delta^z \int_0^\infty x^{z-1} e^{-x\Delta} dx. \tag{A.2}$$

Dividing both sides of (A.2) by $\Gamma(z)\,\Delta^z$, we finally arrive at the following equality,

$$\frac{1}{\Delta^z} = \frac{1}{\Gamma(z)} \int_0^\infty x^{z-1} e^{-x\Delta} dx. \tag{A.3}$$

We will use identity (A.3) to prove several results in this appendix.

## A.2 The beta function

The beta function is defined as

$$B(x,y) \equiv \int_0^1 t^{x-1} (1-t)^{y-1} dt. \tag{A.4}$$

Let us try and use (A.4) to find a relation between the gamma function and the beta function. First, we use the definition (A.1) of the gamma function to write

$$\Gamma(x)\Gamma(y) = \int_0^\infty \int_0^\infty e^{-u-v} u^{x-1} v^{y-1} du dv. \tag{A.5}$$

We then change variables according to $u = zt$ and $v = z(1-t)$. In order to cover the same domain of integration, we need $z > 0$ and $0 < t < 1$. Also, the Jacobian of the transformation is $z$, so that (A.5) becomes

$$\Gamma(x)\Gamma(y) = \int_0^\infty z^{x+y-1} e^{-z} dz \int_0^1 t^{x-1} (1-t)^{y-1} dt. \tag{A.6}$$

Notice the appearance of a gamma function in (A.6), namely

$$\Gamma(x+y) = \int_0^\infty z^{x+y-1} e^{-z} dz. \tag{A.7}$$

Substituting (A.7) back into (A.6), we find

$$\Gamma(x)\Gamma(y) = \Gamma(x+y) \int_0^1 t^{x-1} (1-t)^{y-1} dt, \tag{A.8}$$

where we can identify the definition (A.4) of the beta function. Substituting (A.4) into (A.8), one is able to find the following relation,

$$B(x,y) = \frac{\Gamma(x)\Gamma(y)}{\Gamma(x+y)}. \tag{A.9}$$

## A.3 The Gaussian integral

In this section, we compute the *gaussian integral*,

$$\int_{-\infty}^{\infty} e^{-ax^2} dx, \tag{A.10}$$

where $a > 0$. In order to compute (A.10), first we consider its square,

$$\left(\int_{-\infty}^{\infty} e^{-ax^2} dx\right)^2 = \int_{-\infty}^{\infty} \int_{-\infty}^{\infty} e^{-a\left(x^2+y^2\right)} dxdy. \tag{A.11}$$

We now move into polar coordinates, i.e., we define $r$ and $\varphi$ such that $x \equiv r\cos\varphi$ and $y \equiv r\sin\varphi$. In order to cover the same domain of integration, we need $r \geq 0$ and $0 \leq \varphi < 2\pi$. Also, the Jacobian of the transformation is $r$. Plugging these considerations into (A.11), one finds

$$\left(\int_{-\infty}^{\infty} e^{-ax^2} dx\right)^2 = \int_0^{2\pi} d\varphi \int_0^\infty e^{-ar^2} rdr. \tag{A.12}$$

The integral over $\varphi$ yields simply $2\pi$, so that (A.12) becomes

$$\left(\int_{-\infty}^{\infty} e^{-ax^2} dx\right)^2 = 2\pi \int_0^{\infty} e^{-ar^2} r dr. \tag{A.13}$$

Now let us call $w \equiv r^2$, so that (A.13) becomes

$$\left(\int_{-\infty}^{\infty} e^{-ax^2} dx\right)^2 = \pi \int_0^{\infty} e^{-aw} dw. \tag{A.14}$$

The integral over $w$ is now easy to perform, and yields $1/a$. Thus, (A.14) writes simply

$$\left(\int_{-\infty}^{\infty} e^{-ax^2} dx\right)^2 = \frac{\pi}{a}. \tag{A.15}$$

Consideration of the square root of (A.15) tell us that the integral we wanted to compute yields either $\sqrt{\pi/a}$ or $-\sqrt{\pi/a}$. But the area below the integrand of (A.10) must be a positive number. Therefore, we must pick

$$\int_{-\infty}^{\infty} e^{-ax^2} dx = \sqrt{\frac{\pi}{a}}. \tag{A.16}$$

Raising (A.16) to the power of $d$ and referring to the variables as the components of a spatial vector $\boldsymbol{k} \equiv (\boldsymbol{k}_1, \cdots, \boldsymbol{k}_d)$, it is easy to see that

$$\int d^d \boldsymbol{k} e^{-a\boldsymbol{k}^2} = \left(\frac{\pi}{a}\right)^{d/2}. \tag{A.17}$$

Dividing both sides of (A.17) by $(2\pi)^d$, one finds

$$\int_{\boldsymbol{k}} e^{-a\boldsymbol{k}^2} = (4\pi a)^{-d/2}. \tag{A.18}$$

Result (A.18) will be useful in several computations in this appendix.

## A.4 The tadpole integral

In this section, we compute that which we will call the *tadpole integral*,

$$\int_{\boldsymbol{k}} \frac{1}{(\boldsymbol{k}^2 - \omega^2)^n}. \tag{A.19}$$

First, we use (A.3) to write

$$\frac{1}{\left(\boldsymbol{k}^2-\omega^2\right)^n}=\frac{1}{\Gamma\left(n\right)}\int_0^\infty x^{n-1}e^{-x\left(\boldsymbol{k}^2-\omega^2\right)}dx. \tag{A.20}$$

Substituting (A.20) into (A.19), we arrive at

$$\int_{\boldsymbol{k}}\frac{1}{\left(\boldsymbol{k}^2-\omega^2\right)^n}=\frac{1}{\Gamma\left(n\right)}\int_0^\infty x^{n-1}e^{x\omega^2}dx\int_{\boldsymbol{k}}e^{-x\boldsymbol{k}^2}. \tag{A.21}$$

Now, we use (A.18) to perform the Gaussian integral over $\boldsymbol{k}$ in (A.21), yielding

$$\int_{\boldsymbol{k}}\frac{1}{\left(\boldsymbol{k}^2-\omega^2\right)^n}=\frac{1}{\left(4\pi\right)^{d/2}\Gamma\left(n\right)}\int_0^\infty x^{n-d/2-1}e^{x\omega^2}dx. \tag{A.22}$$

The integral over $x$ can now be performed with the aid of (A.3), so that (A.22) finally becomes

$$\int_{\boldsymbol{k}}\frac{1}{\left(\boldsymbol{k}^2-\omega^2\right)^n}=\frac{\Gamma\left(n-d/2\right)}{\left(4\pi\right)^{d/2}\Gamma\left(n\right)}\left(-\omega^2\right)^{d/2-n}. \tag{A.23}$$

## A.5 The Fourier integral

We want to compute that which we will call the *Fourier integral*,

$$\int_{\boldsymbol{k}}\frac{e^{i\boldsymbol{k}\cdot\boldsymbol{r}}}{\boldsymbol{k}^{2\alpha}}. \tag{A.24}$$

In order to compute this integral, first we use (A.3) to write the following equality,

$$\frac{1}{\boldsymbol{k}^{2\alpha}}=\frac{1}{\Gamma\left(\alpha\right)}\int_0^\infty x^{\alpha-1}e^{-x\boldsymbol{k}^2}dx. \tag{A.25}$$

Substituting (A.25) into (A.24), one finds

$$\int_{\boldsymbol{k}}\frac{e^{i\boldsymbol{k}\cdot\boldsymbol{r}}}{\boldsymbol{k}^{2\alpha}}=\frac{1}{\Gamma\left(\alpha\right)}\int_0^\infty x^{\alpha-1}dx\int_{\boldsymbol{k}}e^{-x\left(\boldsymbol{k}^2-\frac{i\boldsymbol{k}\cdot\boldsymbol{r}}{x}\right)}. \tag{A.26}$$

In order to proceed, one must complete squares in the argument of the exponential on the rhs of (A.26), i.e., we write

$$\boldsymbol{k}^2-\frac{i\boldsymbol{k}\cdot\boldsymbol{r}}{x}=\left(\boldsymbol{k}-i\frac{\boldsymbol{r}}{2x}\right)^2+\frac{r^2}{4x^2}, \tag{A.27}$$

where $r \equiv |\boldsymbol{r}|$. Substituting (A.27) back into (A.26), one is able to find

$$\int_{\boldsymbol{k}} \frac{e^{i\boldsymbol{k}\cdot\boldsymbol{r}}}{\boldsymbol{k}^{2\alpha}} = \frac{1}{\Gamma(\alpha)} \int_0^\infty x^{\alpha-1} e^{-\frac{r^2}{4x}} dx \int_{\boldsymbol{k}} e^{-x\left(\boldsymbol{k}-i\frac{\boldsymbol{r}}{2x}\right)^2}. \tag{A.28}$$

Now we perform the change of variables $\boldsymbol{k} \to \boldsymbol{k} + i\boldsymbol{r}/2x$ on the rhs of (A.28), yielding

$$\int_{\boldsymbol{k}} \frac{e^{i\boldsymbol{k}\cdot\boldsymbol{r}}}{\boldsymbol{k}^{2\alpha}} = \frac{1}{\Gamma(\alpha)} \int_0^\infty x^{\alpha-1} e^{-\frac{r^2}{4x}} dx \int_{\boldsymbol{k}} e^{-x\boldsymbol{k}^2}. \tag{A.29}$$

Using result (A.18) into (A.29), one finds

$$\int_{\boldsymbol{k}} \frac{e^{i\boldsymbol{k}\cdot\boldsymbol{r}}}{\boldsymbol{k}^{2\alpha}} = \frac{1}{(4\pi)^{d/2}} \frac{1}{\Gamma(\alpha)} \int_0^\infty x^{\alpha-d/2-1} e^{-\frac{r^2}{4x}} dx. \tag{A.30}$$

Now we perform the change of variables $x \to 1/x$ in (A.30), yielding

$$\int_{\boldsymbol{k}} \frac{e^{i\boldsymbol{k}\cdot\boldsymbol{r}}}{\boldsymbol{k}^{2\alpha}} = \frac{1}{(4\pi)^{d/2}} \frac{1}{\Gamma(\alpha)} \int_0^\infty x^{d/2-\alpha-1} e^{-x\frac{r^2}{4}} dx. \tag{A.31}$$

Finally, we can use (A.3) to write (A.31) as

$$\int_{\boldsymbol{k}} \frac{e^{i\boldsymbol{k}\cdot\boldsymbol{r}}}{\boldsymbol{k}^{2\alpha}} = \frac{1}{(4\pi)^{d/2}} \frac{\Gamma(d/2-\alpha)}{\Gamma(\alpha)} \left(\frac{r^2}{4}\right)^{\alpha-d/2}. \tag{A.32}$$

If we differentiate with respect to $\boldsymbol{r}$ on both sides of (A.32), we are also able to arrive at

$$\int_{\boldsymbol{k}} \frac{\boldsymbol{k}}{\boldsymbol{k}^{2\alpha}} e^{i\boldsymbol{k}\cdot\boldsymbol{r}} = -\frac{i}{(4\pi)^{d/2}} \frac{\Gamma(d/2-\alpha)}{\Gamma(\alpha)} (\alpha - d/2) \left(\frac{r^2}{4}\right)^{\alpha-d/2-1} \frac{\boldsymbol{r}}{2}. \tag{A.33}$$

## A.6 One-loop integral

In this section, we want to compute the following integral,

$$\int_{\boldsymbol{k}} \frac{1}{\boldsymbol{k}^{2\alpha} (\boldsymbol{k}+\boldsymbol{q})^{2\beta}}. \tag{A.34}$$

First, we use (A.3) to write

$$\begin{aligned}\frac{1}{\boldsymbol{k}^{2\alpha}} &= \frac{1}{\Gamma(\alpha)}\int_0^\infty x^{\alpha-1}e^{-x\boldsymbol{k}^2}dx,\\ \frac{1}{(\boldsymbol{k}+\boldsymbol{q})^{2\beta}} &= \frac{1}{\Gamma(\beta)}\int_0^\infty y^{\beta-1}e^{-y(\boldsymbol{k}+\boldsymbol{q})^2}dy.\end{aligned} \tag{A.35}$$

Substituting (A.35) into (A.34), we arrive at

$$\int_{\boldsymbol{k}}\frac{1}{\boldsymbol{k}^{2\alpha}(\boldsymbol{k}+\boldsymbol{q})^{2\beta}} = \frac{1}{\Gamma(\alpha)\Gamma(\beta)}\int_0^\infty\int_0^\infty dxdy x^{\alpha-1}y^{\beta-1}\int_{\boldsymbol{k}} e^{-x\boldsymbol{k}^2}e^{-y(\boldsymbol{k}+\boldsymbol{q})^2}. \tag{A.36}$$

Now, we call $x \equiv t(1-a)$ and $y \equiv ta$. The Jacobian of this transformation is $t$. And, in order to keep covering the same domain of integration, we need $t > 0$ and $0 < a < 1$. After this change of variables, the integral over $t$ turns out to be

$$\int_0^\infty t^{\alpha+\beta-1}e^{-t\left((1-a)\boldsymbol{k}^2+a(\boldsymbol{k}+\boldsymbol{q})^2\right)}dt = \frac{\Gamma(\alpha+\beta)}{\left((1-a)\boldsymbol{k}^2+a(\boldsymbol{k}+\boldsymbol{q})^2\right)^{\alpha+\beta}},$$

and we have performed it with the aid of (A.3). After this is done, we find the following integral over $\boldsymbol{k}$,

$$\int_{\boldsymbol{k}}\frac{1}{\left((1-a)\boldsymbol{k}^2+a(\boldsymbol{k}+\boldsymbol{q})^2\right)^{\alpha+\beta}}. \tag{A.37}$$

In order to perform it, we do $\boldsymbol{k} \to \boldsymbol{k} - a\boldsymbol{q}$, so that (A.37) becomes

$$\int_{\boldsymbol{k}}\frac{1}{\left(\boldsymbol{k}^2+a(1-a)\boldsymbol{q}^2\right)^{\alpha+\beta}} = \frac{\Gamma(\alpha+\beta-d/2)}{(4\pi)^{d/2}\Gamma(\alpha+\beta)}\left(a(1-a)\boldsymbol{q}^2\right)^{d/2-\alpha-\beta}, \tag{A.38}$$

where we have performed the integral with the aid of result (A.23). All in all, (A.36) becomes

$$\int_{\boldsymbol{k}}\frac{1}{\boldsymbol{k}^{2\alpha}(\boldsymbol{k}+\boldsymbol{q})^{2\beta}} = \frac{\left(\boldsymbol{q}^2\right)^{d/2-\alpha-\beta}}{(4\pi)^{d/2}}\frac{\Gamma(\alpha+\beta-d/2)}{\Gamma(\alpha)\Gamma(\beta)}\int_0^1 a^{d/2-\alpha-1}(1-a)^{d/2-\beta-1}da. \tag{A.39}$$

But the integral over $a$ in (A.39) is simply the definition (A.4) of the beta function. Using it, we find

$$\int_k \frac{1}{k^{2\alpha}\left(k+q\right)^{2\beta}} = \frac{\left(q^2\right)^{d/2-\alpha-\beta}}{\left(4\pi\right)^{d/2}} \frac{\Gamma\left(\alpha+\beta-d/2\right)}{\Gamma\left(\alpha\right)\Gamma\left(\beta\right)} B\left(d/2-\alpha, d/2-\beta\right). \quad \text{(A.40)}$$

Now, we use (A.9) to write the beta function in (A.40) in terms of gamma functions, so that we finally find

$$\int_k \frac{1}{k^{2\alpha}\left(k+q\right)^{2\beta}} = \frac{\left(q^2\right)^{d/2-\alpha-\beta}}{\left(4\pi\right)^{d/2}} \frac{\Gamma\left(\alpha+\beta-d/2\right)}{\Gamma\left(\alpha\right)\Gamma\left(\beta\right)} \frac{\Gamma\left(d/2-\alpha\right)\Gamma\left(d/2-\beta\right)}{\Gamma\left(d-\alpha-\beta\right)}. \quad \text{(A.41)}$$

## A.7 The scaleless integral

In this section, we compute the following *scaleless integral*,

$$\int_k \frac{1}{\left(k^2\right)^{3-d/2}}. \quad \text{(A.42)}$$

First, we introduce an arbitrary energy scale $\mu$ by rewriting the integrand of (A.42) as

$$\frac{1}{\left(k^2\right)^{3-d/2}} = \frac{1}{\left(k^2\right)^{2-d/2}} \frac{1}{k^2+\mu^2} + \frac{1}{\left(k^2\right)^{3-d/2}} \frac{\mu^2}{k^2+\mu^2}. \quad \text{(A.43)}$$

Integrating over $\boldsymbol{k}$ on both sides of (A.43), we find

$$\int_k \frac{1}{\left(k^2\right)^{3-d/2}} = \int_k \frac{1}{\left(k^2\right)^{2-d/2}} \frac{1}{k^2+\mu^2} + \int_k \frac{1}{\left(k^2\right)^{3-d/2}} \frac{\mu^2}{k^2+\mu^2}. \quad \text{(A.44)}$$

The first integral on the rhs of (A.44) is UV divergent, while the second is IR divergent. Using (A.3), (A.4), (A.9) and (A.18), one can turn (A.44) into

$$\int_k \frac{1}{\left(k^2\right)^{3-d/2}} = \frac{\left(\mu^2\right)^{d-3}}{\left(4\pi\right)^{d/2}\Gamma\left(d/2\right)} \left[\Gamma\left(3-d\right)\Gamma\left(d-2\right)+\Gamma\left(4-d\right)\Gamma\left(d-3\right)\right]. \quad \text{(A.45)}$$

Using the definition of $\epsilon$ given at the beginning of this work, (A.45) becomes

$$\int_k \frac{1}{\left(k^2\right)^{3-d/2}} = \frac{\mu^{2\epsilon}}{\left(4\pi\right)^{\frac{\epsilon+3}{2}}\Gamma\left(\frac{\epsilon+3}{2}\right)} \left[\Gamma\left(-\epsilon\right)\Gamma\left(\epsilon+1\right)+\Gamma\left(1-\epsilon\right)\Gamma\left(\epsilon\right)\right]. \quad \text{(A.46)}$$

Expanding to zeroth order in $\epsilon$ and explicitly indicating the cancellation of divergences happening in (A.46), as well as their origins, we finally find

$$\int_{\boldsymbol{k}} \frac{1}{(\boldsymbol{k}^2)^{3-d/2}} = \frac{\mu^{2\epsilon}}{4\pi^2} \left( \frac{1}{\epsilon_{\text{IR}}} - \frac{1}{\epsilon_{\text{UV}}} \right) . \tag{A.47}$$

# Appendix B

# Propagators and action terms

In this appendix, we present several propagators and action terms used in our calculations.

## B.1 Propagators

Below one finds several propagators used in our computations,

$$\left\langle TH_{\mu\nu}\left(x^0,\mathbf{x}\right)H_{\alpha\beta}\left(y^0,\mathbf{y}\right)\right\rangle_{v^0} = \delta\left(x^0-y^0\right)P_{\mu\nu;\alpha\beta}\int_{\boldsymbol{k}}\frac{i}{-\boldsymbol{k}^2}e^{i\boldsymbol{k}\cdot(\boldsymbol{x}-\boldsymbol{y})}, \tag{B.1}$$

$$\left\langle T\Phi\left(x^0,\boldsymbol{x}\right)\Phi\left(y^0,\boldsymbol{y}\right)\right\rangle_{v^0} = \delta\left(x^0-y^0\right)\int_{\boldsymbol{k}}\frac{i}{-\boldsymbol{k}^2}e^{i\boldsymbol{k}\cdot(\boldsymbol{x}-\boldsymbol{y})}, \tag{B.2}$$

$$\left\langle T\bar{\varphi}\left(x^0,\boldsymbol{x}\right)\bar{\varphi}\left(y^0,\boldsymbol{y}\right)\right\rangle = \int_{\boldsymbol{k}}\frac{d\omega}{2\pi}\frac{i}{\omega^2-\boldsymbol{k}^2}e^{-i\omega\left(x^0-y^0\right)+i\boldsymbol{k}\cdot(\boldsymbol{x}-\boldsymbol{y})}. \tag{B.3}$$

## B.2 Worldline couplings

The following action terms represent couplings of several modes to the point-particles,

$$S_{\mathrm{pp}}^{Hv^0} = \sum_a m_a\int dt_a\frac{H_{00}\left(x_a\right)}{2\Lambda}, \tag{B.4}$$

$$S_{\mathrm{pp}}^{\Phi v^0} = \sum_a \alpha_a m_a\int dt_a\frac{\Phi\left(x_a\right)}{2\Lambda}, \tag{B.5}$$

$$S_{\mathrm{pp}}^{\bar{\varphi}v^0} = \sum_a \alpha_a m_a\int dt_a\frac{\bar{\varphi}\left(x_a\right)}{2\Lambda}, \tag{B.6}$$

$$\Gamma\left[\bar{\varphi}\right] = \frac{1}{2\Lambda}\int dt\sum_{\ell=0}^{\infty}\frac{1}{\ell!}\mathcal{I}^L\left(t\right)\left(\partial_L\bar{\varphi}\right)\left(t,\mathbf{0}\right). \tag{B.7}$$

## B.3 Bulk couplings

Below we present several bulk couplings.

### B.3.1 Cubic non-derivative self-couplings

For the cubic, non-derivative self-interaction, we have the following action terms,

$$S_{\Phi^3} = -\frac{\lambda_3}{3!}\frac{m_{\mathrm{Pl}}^2}{\Lambda}\int dtd^d\boldsymbol{x}\Phi^3, \tag{B.8}$$

$$S_{\Phi^2\bar{\varphi}} = -\frac{\lambda_3}{2}\frac{m_{\mathrm{Pl}}^2}{\Lambda}\int dtd^d\boldsymbol{x}\Phi^2\bar{\varphi}, \tag{B.9}$$

$$S_{\bar{\varphi}^3} = -\frac{\lambda_3}{3!}\frac{m_{\mathrm{Pl}}^2}{\Lambda}\int dtd^d\boldsymbol{x}\bar{\varphi}^3. \tag{B.10}$$

### B.3.2 Cubic self-couplings with derivatives

For the cubic, derivative self-interaction, we have the following action terms,

$$S_{\Phi(\partial_i\Phi)^2} = -\frac{\lambda_{3,2}}{3!}\frac{1}{\Lambda}\int dtd^d\boldsymbol{x}\Phi\left(\partial_i\Phi\right)^2, \tag{B.11}$$

$$S_{(\partial_i\Phi)^2\bar{\varphi}} = -\frac{\lambda_{3,2}}{3!}\frac{1}{\Lambda}\int dtd^d\boldsymbol{x}\left(\partial_i\Phi\right)^2\bar{\varphi}, \tag{B.12}$$

$$S_{\bar{\varphi}(\partial\bar{\varphi})^2} = -\frac{\lambda_{3,2}}{3!}\frac{1}{\Lambda}\int dtd^d\boldsymbol{x}\bar{\varphi}\left(\partial\bar{\varphi}\right)^2. \tag{B.13}$$

### B.3.3 Quartic non-derivative self-couplings

For the quartic, non-derivative self-interaction, we need the following self-couplings,

$$S_{\Phi^4} = -\frac{\lambda_4}{4!}\frac{m_{\mathrm{Pl}}^2}{\Lambda^2}\int dtd^d\boldsymbol{x}\Phi^4, \tag{B.14}$$

$$S_{\Phi^3\bar{\varphi}} = -\frac{\lambda_4}{3!}\frac{m_{\mathrm{Pl}}^2}{\Lambda^2}\int dtd^d\boldsymbol{x}\Phi^3\bar{\varphi}, \tag{B.15}$$

$$S_{\bar{\varphi}^4} = -\frac{\lambda_4}{4!}\frac{m_{\mathrm{Pl}}^2}{\Lambda^2}\int dtd^d\boldsymbol{x}\bar{\varphi}^4. \tag{B.16}$$

# Appendix C

# The scalar potential

In this appendix, we explain in greater detail the motivation behind the scalar potential appearing in (3.2).

## C.1 A starting point

We wanted our scalar potential to be a general polynomial in $\phi$ and $\phi_\mu$, but not in higher derivatives of $\phi$. Since the potential needs to be a scalar and the only indexed quantity available is $\phi_\mu$, we immediately see that $\phi_\mu$ must always appear in covariantly contracted pairs, $g^{\mu\nu}\phi_\mu\phi_\nu$. Thus, our potential must be a polynomial in $\phi$ and $g^{\mu\nu}\phi_\mu\phi_\nu$.

A good starting point is

$$U = \sum_{p=3}^{\infty} \sum_{\substack{q \leq p \\ \text{even}}} \frac{\lambda_{p,q}^{(d)}}{p!} \phi^{p-q} \left(g^{\mu\nu}\phi_\mu\phi_\nu\right)^{q/2}, \tag{C.1}$$

where $\lambda_{p,q}^{(d)}$ denotes the $d$-dimensional self-coupling of the self-interaction involving $p$ fields and $q$ first derivatives. This way, for every number of fields in a given self-interaction, we sum over the possible number of first derivatives. For instance, in a cubic self-interaction, we can have 0 or 2 first derivatives, in a quartic self-interaction, we can have 0, 2 or 4 first derivatives, and so on.

## C.2 Dimensionless self-couplings

In order for the scalar piece of the action to be dimensionless, we need

$$[\phi] = \frac{d-1}{2}, \qquad [U] = d+1. \tag{C.2}$$

Imposing conditions (C.2) on (C.1), we arrive at the following requirement,

$$\left[\lambda^{(d)}_{p,q}\right] = d + 1 - \frac{p}{2}\,(d-1) - q. \tag{C.3}$$

In $d$ spatial dimensions, we also need

$$[\Lambda] = \frac{d-1}{2},$$

from which one can obtain

$$d = 2\,[\Lambda] + 1. \tag{C.4}$$

Substituting (C.4) into (C.3), one sees that

$$\left[\lambda^{(d)}_{p,q}\right] = \left[\Lambda^{2-p}\right] + 2 - q. \tag{C.5}$$

But we also have $[m_{\rm Pl}] = 1$, so that (C.5) can also be written as

$$\left[\lambda^{(d)}_{p,q}\right] = \left[\Lambda^{2-p} m_{\rm Pl}^{2-q}\right].$$

Thus, if we redefine the self-couplings according to

$$\lambda^{(d)}_{p,q} \equiv \lambda_{p,q} \Lambda^{2-p} m_{\rm Pl}^{2-q},$$

then we see that $\lambda_{p,q}$ is *dimensionless*. This has several advantages. First of all, it is much easier to set phenomenological bounds on dimensionless self-couplings. And secondly, this facilitates comparison with GR in the case $q = 2$.

# Bibliography


[1] S. Perlmutter et al. "Discovery of a supernova explosion at half the age of the Universe". In: *Nature* 391.6662 (1998). ISSN: 00280836. DOI: 10.1038/34124.

[2] S. Perlmutter et al. "Measurements of $\Omega$ and $\Lambda$ from 42 High-Redshift Supernovae". In: *The Astrophysical Journal* 517.2 (1999). ISSN: 0004-637X. DOI: 10.1086/307221.

[3] Adam G. Riess et al. "Observational Evidence from Supernovae for an Accelerating Universe and a Cosmological Constant". In: *The Astronomical Journal* 116.3 (1998). ISSN: 00046256. DOI: 10.1086/300499.

[4] Adam G. Riess et al. "BVRI Light Curves for 22 Type Ia Supernovae". In: *The Astronomical Journal* 117.2 (1999). ISSN: 00046256. DOI: 10.1086/300738.

[5] B. Wang, E. Abdalla, F. Atrio-Barandela, and D. Pavón. *Dark matter and dark energy interactions: Theoretical challenges, cosmological implications and observational signatures*. 2016. DOI: 10.1088/0034-4885/79/9/096901.

[6] D. N. Spergel et al. " First-Year Wilkinson Microwave Anisotropy Probe ( WMAP ) Observations: Determination of Cosmological Parameters ". In: *The Astrophysical Journal Supplement Series* 148.1 (2003). ISSN: 0067-0049. DOI: 10.1086/377226.

[7] P. A.R. Ade et al. "Planck 2013 results. I. Overview of products and scientific results". In: *Astronomy and Astrophysics* 571 (2014). ISSN: 14320746. DOI: 10.1051/0004-6361/201321529.

[8] R. Adam et al. "Planck 2015 results: I. Overview of products and scientific results". In: *Astronomy and Astrophysics* 594 (2016). ISSN: 14320746. DOI: 10.1051/0004-6361/201527101.

[9] Daniel J. Eisenstein et al. "Detection of the Baryon Acoustic Peak in the Large-Scale Correlation Function of SDSS Luminous Red Galaxies". In: *The Astrophysical Journal* 633.2 (2005). ISSN: 0004-637X. DOI: 10.1086/466512.

[10] Michele Moresco et al. "Unveiling the Universe with Emerging Cosmological Probes". In: (2022). arXiv: 2201.07241.

[11] Ronald J. Adler, Brendan Casey, and Ovid C. Jacob. "Vacuum catastrophe: An elementary exposition of the cosmological constant problem". In: *American Journal of Physics* 63.7 (1995). ISSN: 0002-9505. DOI: 10.1119/1.17850.

[12] Adrien Kuntz, Federico Piazza, and Filippo Vernizzi. "Effective field theory for gravitational radiation in scalar-tensor gravity". In: *Journal of Cosmology and Astroparticle Physics* 2019.5 (2019). ISSN: 14757516. DOI: 10.1088/1475-7516/2019/05/052.

[13] Sean M. Carroll. *Spacetime and Geometry*. Cambridge University Press, 2019. DOI: 10.1017/9781108770385.

[14] Yasunori Fujii and Kei-ichi Maeda. "The Scalar-Tensor Theory of Gravitation". In: *Classical and Quantum Gravity* 20.20 (2003). ISSN: 0264-9381. DOI: 10.1088/0264-9381/20/20/601.

[15] T. Damour and A. M. Polyakov. "The string dilation and a least coupling principle". In: *Nuclear Physics, Section B* 423.2-3 (1994). ISSN: 05503213. DOI: 10.1016/0550-3213(94)90143-0.

[16] Justin Khoury and Amanda Weltman. "Chameleon fields: Awaiting surprises for tests of gravity in space". In: *Physical Review Letters* 93.17 (2004). ISSN: 00319007. DOI: 10.1103/PhysRevLett.93.171104.

[17] Kurt Hinterbichler and Justin Khoury. "Screening long-range forces through local symmetry restoration". In: *Physical Review Letters* 104.23 (2010). ISSN: 00319007. DOI: 10.1103/PhysRevLett.104.231301.

[18] Paolo Creminelli and Filippo Vernizzi. "Dark Energy after GW170817 and GRB170817A". In: *Physical Review Letters* 119.25 (2017). ISSN: 10797114. DOI: 10.1103/PhysRevLett.119.251302.

[19] Jose María Ezquiaga and Miguel Zumalacárregui. "Dark Energy after GW170817: Dead Ends and the Road Ahead". In: *Physical Review Letters* 119.25 (2017). ISSN: 10797114. DOI: 10.1103/PhysRevLett.119.251304.

[20] T. Baker et al. "Strong Constraints on Cosmological Gravity from GW170817 and GRB 170817A". In: *Physical Review Letters* 119.25 (2017). ISSN: 10797114. DOI: 10.1103/PhysRevLett.119.251301.

[21] Jeremy Sakstein and Bhuvnesh Jain. "Implications of the Neutron Star Merger GW170817 for Cosmological Scalar-Tensor Theories". In: *Physical Review Letters* 119.25 (2017). ISSN: 10797114. DOI: 10.1103/PhysRevLett.119.251303.

[22] Walter D. Goldberger and Ira Z. Rothstein. "Effective field theory of gravity for extended objects". In: *Physical Review D - Particles, Fields, Gravitation and Cosmology* 73.10 (2006). ISSN: 15507998. DOI: 10.1103/PhysRevD.73.104029.

[23] Stefano Foffa, Rafael A. Porto, Ira Rothstein, and Riccardo Sturani. "Conservative dynamics of binary systems to fourth post-Newtonian order in the EFT approach. II. Renormalized Lagrangian". In: *Physical Review D* 100.2 (2019). ISSN: 2470-0010. DOI: 10.1103/physrevd.100.024048.

[24] L. Blanchet and T. Damour. "Radiative gravitational fields in general relativity I. General structure of the field outside the source". In: *Philosophical Transactions of the Royal Society of London. Series A, Mathematical and Physical Sciences* 320.1555 (1986). ISSN: 0080-4614. DOI: 10.1098/rsta.1986.0125.

[25] Michele Maggiore. "Gravitational Waves (Volume I)". In: *Oxford University Press* 53.9 (2007). ISSN: 1098-6596.

[26] Michèle Levi. *Effective field theories of post-Newtonian gravity: A comprehensive review*. 2020. DOI: 10.1088/1361-6633/ab12bc.

[27] Riccardo Sturani. "Fundamental Gravity and Gravitational Waves". In: *Symmetry* 13.12 (2021), p. 2384. DOI: 10.3390/sym13122384.

[28] Rafael A. Porto. *The effective field theorist's approach to gravitational dynamics*. 2016. DOI: 10.1016/j.physrep.2016.04.003.

[29] John F. Donoghue. "General relativity as an effective field theory: The leading quantum corrections". In: *Physical Review D* 50.6 (1994). ISSN: 05562821. DOI: 10.1103/PhysRevD.50.3874.

[30] Andreas Ross. "Multipole expansion at the level of the action". In: *Physical Review D - Particles, Fields, Gravitation and Cosmology* 85.12 (2012). ISSN: 15507998. DOI: 10.1103/PhysRevD.85.125033.

[31] Stefano Foffa and Riccardo Sturani. "Near and far zones in two-body dynamics: An effective field theory perspective". In: *Physical Review D* 104.2 (2021). ISSN: 24700029. DOI: 10.1103/PhysRevD.104.024069.

[32] Philippe Blanchard and Erwin Brüning. *Mathematical Methods in Physics: Distributions, Hilbert Space Operators, Variational Methods, and Applications in Quantum Physics*. 2021.

[33] Michael Peskin and Dan Schroeder. *An Introduction To Quantum Field Theory (Frontiers in Physics)*. CRC Press, 2018.

[34] Clifford M. Will. *The confrontation between general relativity and experiment*. 2014. DOI: 10.12942/lrr-2014-4.

[35] Walter D. Goldberger and Andreas Ross. "Gravitational radiative corrections from effective field theory". In: *Physical Review D - Particles, Fields, Gravitation and Cosmology* 81.12 (2010). ISSN: 15507998. DOI: 10.1103/PhysRevD.81.124015.

[36] Herbert Goldstein, P. Charles Poole, and John L. Safko. *Pearson Education - Classical Mechanics*. 2002.

[37] Junwu Huang et al. "Prospects for axion searches with Advanced LIGO through binary mergers". In: *Physical Review D* 99.6 (2019). ISSN: 24700029. DOI: 10.1103/PhysRevD.99.063013.

[38] The LIGO Scientific Collaboration et al. "Tests of General Relativity with GWTC-3". In: (2021). arXiv: 2112.06861.

[39] J. M. Weisberg and J. H. Taylor. "Relativistic Binary Pulsar B1913+16: Thirty Years of Observations and Analysis". In: (2004). arXiv: 0407149 [astro-ph].